The Dissertation Committee for Yun-Pil Shim

certifies that this is the approved version of the following dissertation:

Pair Condensation in Polarized Fermion Systems

Committee:

Allan H. MacDonald, Supervisor

Willy Fischler

Qian Niu

Chih-Kang Ken Shih

Brian Korgel

Pair Condensation in Polarized Fermion Systems

by

Yun-Pil Shim, B.S.

Dissertation

Presented to the Faculty of the Graduate School of

The University of Texas at Austin

in Partial Fulfillment

of the Requirements

for the Degree of

Doctor of Philosophy

The University of Texas at Austin

December 2006

Acknowledgments

Fist of all, I would like to thank Professor Allan H. MacDonald, my supervisor. He is a great physicist and greater advisor. I have been lucky to have worked with him in the early stage of my career. I learned how to conduct research and how to communicate with other researchers under his guidance during the last six years. He always gave new ideas, showed great patience and encouraged me so that I could go through my graduate studies in Austin. He has been a great role model that I will pursue over my career.

I thank Dr. Lyo for his help when I visited Sandia National Laboratories. He directed me to work on the spin-dependent tunneling problem and gave valuable advice on planning my future.

I am grateful to Professors Willy Fischler, Qian Niu, Chih-Kang Ken Shih and Brian Korgel for reviewing this dissertation as my committee members.

I also would like to thank Becky Drake for her kindness and great help with the administrative work, which has made my life a lot easier. I would like to thank Prof. Rembert Duine for his collaboration on the cold fermion atom systems while he was a postdoctoral researcher here. I would like to thank all the other friends and colleagues in our group. I also have to thank all the friends in physics department.

Special thanks to Bonggu Shim, a long-time friend and former roommate, who took care of me when I first arrived in Austin and helped me a lot during my days here.

I would like to thank my elder brothers, Yoon Kee Shim and Yoon Cheol Shim, who supported my decision to go to USA to study and have always been good friends of mine.

I am also very grateful to my wife Gwon Hui Hwang. She has been a shelter for me whenever I felt depressed and her smile has given me new energy to get back to work.

Finally, I would like to thank my parents, Seung Jin Shim and Yang Ja Lee. They showed constant belief in me even though they were thousands of miles away.

YUN-PIL SHIM

The University of Texas at Austin

December 2006

Pair Condensation in Polarized Fermion Systems

Publication No. _____

Yun-Pil Shim, Ph.D.
The University of Texas at Austin, 2006

Supervisor: Allan H. MacDonald

In this thesis we study the spin or pseudospin singlet pair condensation of two different kinds of polarized fermion systems. Using generalized BCS mean-field theories we study how pairing adapts to unequal spin or pseudospin populations. After briefly reviewing the basic physics of superconductivity in Chapter 2, in Chapter 3 the mean-field theory for electron-hole bilayer systems is derived to describe the condensation of excitons which is analogous to the Cooper pair condensation in superconductors. Self-consistent solution of the exciton system gap equation shows that the excitation energy spectrum is qualitatively the same as in superconductors. In Chapter 4 the role of the spin degree of freedom in the bilayer system is investigated by generalizing the two-component mean-field theory developed in Chapter

3 to four-component cases. The main consequence is that population polarization leads to ferromagnetism. The interplay between exciton condensation and spontaneous spin-order is the most important consequence of the presence of both spin and pseudospin degrees of freedom in excitonic condensates. In a sense that we explain in this Chapter, both normal and condensed fluids are present in the ferromagnetic excitonic state. Using the Rashba spin-orbit interaction model derived in the appendix, we show that an external electric field can alter the characteristics of the ferromagnetic condensate phase. The spin splitting by the spin-orbit interaction and its different spin state structures lead to qualitatively different magnetic properties for electron and hole layers. In Chapter 5 we turn our attention to a second class of polarized fermion systems that is of great current interest. A fully quantum mechanical treatment of a rotating fermion atom cloud is developed and implicit equations determining the critical temperatures for all center-of-mass Landau level pairings are obtained. In Chapter 6 the condition for the realization of higher center-of-mass Landau level pairing, which corresponds to FFLO state in spin split superconductors, is determined by calculating the critical temperatures for all possible pairing channels. It is shown that FFLO states can be realized in the strong interaction and low rotation frequency regimes in parameter space, where the pairing energy can survive the high polarization.

Contents

List of Figures

xvi

Chapter 1

Introduction

Since the observation of superconductivity [1] and the successful microscopic explanation of the phenomena [2], pair condensation has been one of the most active topics of condensed matter physics. In superconductors, electrons form a bound pair due to the effective attractive interaction through the retarded electron-phonon interaction. The pairing mechanism in high T_c superconductors, however, is not so clear. The mechanism is believed to be electron-electron interactions but not certain yet. For recent reviews on this intriguing topic, see [3], [4]. In conventional superconductors with local interactions, electrons form spin-singlet pairs composed of opposite spins due to the antisymmetry of fermions. Other pairings are also possible. In superfluid ^{3}He, the pairs have p-wave and spin-triplet symmetry due to the hard core repulsion. In systems where superconducting order and ferromagnetic order coexist, the exchange field of the magnetic moments act as pair breakers since it tends to put the electron spins in the same direction. It is thought [5], however, that near the quantum critical point of the ferromagnetism, quantum spin fluctuations can lead to spin-triplet pairing where electrons with the same spin form pairs. In this thesis we consider opposite (pseudo)spin pairing which is the appropriate pairing mechanism for the systems we will consider as will be discussed later.

The Cooper pairing can occur regardless of the interaction strength because of the background Fermi sea [6]. This pairing mechanism can be applied to any fermion system as long as the effective interaction is attractive. Pairing with zero total momentum is usually the lowest energy pairing when the Fermi surfaces of the two components are identical. If there is population difference between the constituents, the pairing mechanism is expected to be different depending on how many fermion components are in the system. These population polarized systems are the main topic of this thesis. Population polarized two-component fermion systems tend toward finite pair momentum condensates. In superconductors, electron spin-polarization can be induced by the application of an external field or by proximity coupling to a ferromagnet. Finite-momentum Cooper pair condensates in spin-polarized superconductors, Fulde-Ferrell-Larkin-Ovchinnikov (FFLO) states, were first proposed in the early 1960's [7, 8]. One important consequence of finite-momentum pairing in an isolated superconductor is a spatially inhomogeneous order parameter. There have been many efforts in various solid state systems to detect this exotic state, including recent ones [9, 10], but its definitive identification has remained elusive. If there is a degeneracy for each pairing component, each component can adjust itself to regain the Fermi surface matching by spontaneously breaking the degeneracy. This leads to the ferromagnetism for spin degenerate systems. In this thesis we study two different types of polarized fermion systems: electron-hole semiconductor bilayer systems and cold fermion atom systems.

Electrons and holes (or absence of electrons normally near the top of the valence band of a semiconductor) have natural attractive Coulomb interaction which makes the system a good candidate for the fermion pair condensation. An exciton is an elementary excitation of semiconductors in which an electron and a hole form a bound state. Like Cooper pairs, excitons can condense under appropriate circumstances. The broken symmetry associated with exciton condensation is spontaneous

phase coherence between conduction and valence band states in a semiconductor. Excitonic condensation is one of the most sought-for fermion pair condensates and has been looked for since first predicted in early 1960's [11, 12, 13, 14, 15]. The traditional method of creating excitons is by optically exciting valence band electrons in semiconductors. The main obstacle for realization of the exciton condensate has been the finite life time of excitons due to optical recombination of excited excitons accompanied by the emission of a photon. It was proposed [16, 17] some time ago that the exciton life-time can be substantially increased by spatially separating electrons and holes in a bilayer configuration. Progress in fabrication techniques in semiconductors made it feasible to realize bilayer electron-hole systems with great flexibility. When the distance between the two layers is smaller than the average distance between particles in one layer, it undergoes excitonic condensation [18]. There have been many experimental works which have attempted to verify exciton condensation by photoluminescence measurements [19, 20, 21, 22, 23, 24, 25] in coupled quantum well structures where holes are created optically, then separated by external electric fields.

If electrons and holes could be created in equilibrium they could be studied using transport properties. The essential technical ability required for transport measurements related to exciton condensation is to make separate contacts with each layer [26]. Coherent transport behavior in electron-electron bilayers [27, 28], rather than electron-hole bilayers, in strong magnetic field such that the total filling factor is one can be attributed to the excitonic condensation. The theory looks more like the standard theory of exciton condensation if a particle-hole transformation is made for a Landau level in one of the two layers [29]. Another essential advantage of bilayer systems with independent contacts is that we can create electron-hole systems electrically by controlling the gate voltage without optically exciting the system. In this way, we can even create density polarized electron-hole systems

3

which is one of the main topics of this thesis. Since both conduction and valence bands are spin degenerate, it has been expected that the population polarization between electrons and holes can lead to a ferromagnetic phase [30, 31].

While sufficiently clean, low density, electron-hole bilayers have not yet been realized in solid state systems, experimental progress [32, 33, 34, 35] in fermion atom systems provides a new kind of polarized fermion system, which has given rise to a new strategy for realizing the FFLO state or the related Sarma state [36] and has stimulated a great deal of theoretical activity [37, 38, 39, 40, 41, 42, 43, 44, 45, 46, 47, 48, 49, 50, 51]. The tunability of the interaction between atoms via a Feshbach resonance [52, 53] has made it possible to increase the strength of fermion pairing and has even made the BEC-BCS crossover [54, 55, 56] experimentally accessible. On the Bose-Einstein condensate (BEC) side of a Feshbach resonance fermionic atoms form bosonic molecules which condense at low temperatures. On the Bardeen-Cooper-Schrieffer (BCS) side, the effective attractive interaction between fermion atoms leads to BCS-type pairing. In between lies the so-called unitarity limit [57] in which no weakly-interacting particle description applies. The change from the BEC side to the BCS side is a smooth crossover and there are no phase transitions between the BCS weak-coupling paired state and the molecular paired state. The same smooth crossover is expected to occur in excitons as the ratio of the electron-hole interaction strength to the Fermi energy changes.

Easy control over the population of two hyperfine states in a trapped atom cloud makes cold-atom systems a promising candidate for FFLO state realization. The FFLO state competes [37, 38, 39, 40, 41, 42, 43, 44, 45, 46, 47, 48, 49, 50, 51] with a number of other states, including in cold atom systems states with phase separated regions that are respectively unpolarized and unpaired. The FFLO state is expected to occur on the BCS side of the BEC-BCS crossover, at temperatures and pressures close to the normal/superfluid phase boundary. Population imbalance in cold atoms

plays essentially the same role as a Zeeman or exchange field in superconductors since pairing is dependent on energy measured from the Fermi energy for each species of fermion. While the Zeeman field in superconductors enforces a chemical potential difference, it is really a population difference that is enforced in cold atoms. In both cases the Fermi radius of the majority species exceeds the Fermi radius of the minority species and pairs at the Fermi energy necessarily have non-zero total momentum.

In this thesis a generalized mean-field theory for the polarized fermion systems is presented. After a brief review of the BCS theory and phenomenological Ginzburg-Landau (GL) theory of superconductivity in Chap. 2, we generalize the BCS theory to derive a mean-field Hamiltonian for the bilayer electron-hole systems in Chap. 3. We carefully consider the electrostatic interactions between the electrons and holes as well as the outside charge distribution, that maintains the overall charge neutrality in polarized systems. In Chap. 4, we apply the mean-field theory including the spin degree of freedom. The mean-field solution of polarized electron-hole systems are shown to be ferromagnetic as expected. In two-dimensional quantum well structures, the spin-orbit (SO) interaction that arises due to the structural inversion asymmetry, Rashba SO interaction [58, 59], can play an important role. We introduce this Rashba SO interaction and present its effects on the ferromagnetic exciton condensate. Since the SO interaction breaks the isotropic spin rotational symmetry, it leads to qualitatively different ferromagnetic ground states. In Chap. 5, we apply the mean-field theory to the cold fermion atom systems. We develop a mean-field theory for rotating atom clouds since rotation is essential for the realization of the vortex lattice structures which is one of the most definitive experimental evidence for the superfluidity. In rotating systems, we can work in a co-rotating frame with effective orbital magnetic field. We derive an implicit equation for the critical temperature including the Landau quantization effect due to the effective

magnetic field. The non-zero pairing momentum in FFLO states then corresponds to higher center-of-mass(COM) Landau level (LL) and the implicit T_c equation gives the critical temperature for each COM LL pairing. Using the T_c equation developed in Chap. 5, we determine the phase in the parameter space spanned by rotation frequency, interaction strength and the polarization in Chap. 6. Finally a brief summary and some suggestions for promising future work are given in Chap. 7.

Chapter 2

BCS Theory and Ginzburg-Landau Theory of Superconductivity

2.1 Introduction

Classic superconductivity is perhaps the best understood example of fermion pair condensation. The hallmark properties of superconductors are perfect conductivity and perfect diamagnetism, which was explained fully microscopically by Bardeen, Cooper and Schrieffer(BCS) [2]. The microscopic BCS theory is most easily applicable for the case of constant order parameter Δ. For spatially inhomogeneous states like type II superconductors, however, the application of BCS theory becomes complex. Ginzburg-Landau(GL) theory [60] gives a good alternative for such cases. The phenomenological GL theory was originally derived, with the assistance of a large dose of physical intuition, even before the microscopic BCS theory was in place. Later, it was shown that it can be derived from the microscopic theory as a limiting case [61]. The GL theory is applicable when the temperature is close to T_c and

the spatial variations of the pseudowavefucntion ψ and the vector potential $\mathbf{A}$ are not too rapid. In sec. 2.2, we introduce the basic phenomenology of superconductivity using the London equations and derive the BCS theory using the canonical transformation approach in Sec. 2.3. In Sec. 2.4 we derive the BCS gap equation and numerically calculate the temperature dependence of the gap. In Sec. 2.5, we review the phenomenological GL theory In Sec. 2.6, we explain the appearance of vortices in type II superconductors and discuss the vortex lattice states that form when many vortices are present. For general introductions to superconductivity, see [62], [63], [64].

2.2 Phenomenology

When we cool down a metallic sample such as aluminum, lead or tin below a critical temperature T_c the electrical resistance suddenly drops to zero. This perfect conductivity can be demonstrated by persistent current in superconducting rings which can flow without measurable decay for years. While this phenomenon is the most obvious characteristic of superconductors, Meissner and Ochsenfeld [65] demonstrated that all magnetic flux is expelled from bulk superconductors below T_c, which implies that superconductors are perfect diamagnets too. These two basic properties can be described by two phenomenological equations that govern the microscopic electric and magnetic fields [66], which are called London equations.

$$\frac{\partial \mathbf{J}_s}{\partial t} = \frac{n_s e^2}{m}\mathbf{E} \tag{2.1}$$

$$\boldsymbol{\nabla} \times \mathbf{J}_s = -\frac{n_s e^2}{mc}\mathbf{B} \ . \tag{2.2}$$

Here n_s is the superconducting electron density and electron charge is $-e$. These equations can be understood as follows (see, for example, [64]). The first London equation [Eq. (2.1)] is simply Newton's law $\mathbf{F} = m\mathbf{a}$ for a free electron system

8

without scattering mechanism.

$$(-e)\mathbf{E} = m\dot{\mathbf{v}}_s = -\frac{m}{n_s e}\frac{\partial \mathbf{J_s}}{\partial t} \tag{2.3}$$

$$\Rightarrow \quad \frac{\partial \mathbf{J_s}}{\partial t} = \frac{n_s e^2}{m}\mathbf{E} \ . \tag{2.4}$$

This describes the perfect conductivity. Takin the curl of the above equation and using one of Maxwell equations,

$$\boldsymbol{\nabla} \times \mathbf{E} = -\frac{1}{c}\frac{\partial \mathbf{B}}{\partial t} \ , \tag{2.5}$$

we obtain after integrating over time,

$$\boldsymbol{\nabla} \times \mathbf{J_s} = -\frac{n_s e^2}{mc}(\mathbf{B} - \mathbf{B_0}) \tag{2.6}$$

where $\mathbf{B_0}$ is a constant of integration. London proposed [67] that Meissner effect could be explained by setting $\mathbf{B_0}$ to zero obtaining the second London equation [Eq. (2.2)]. The second London equation explains the Meissner effect, which can be seen by taking the curl of one of the Maxwell equation,

$$\boldsymbol{\nabla} \times \boldsymbol{\nabla} \times \mathbf{B} = \frac{4\pi}{c}\boldsymbol{\nabla} \times \mathbf{J}_s$$

$$\Rightarrow \quad \nabla^2 \mathbf{B} = \frac{1}{\lambda_L^2}\mathbf{B} \ , \tag{2.7}$$

where $\lambda_L = (mc^2/4\pi n_s e^2)^{1/2}$ is the London penetration depth. If we apply Eq. (2.7) to a plane boundary at $z = 0$, the normal component of the magnetic field vanishes at the boundary and the parallel component decays exponentially over the length

scale λ_L,

$$B_z = 0 \tag{2.8}$$

$$B_\parallel(z) = B_\parallel(0)e^{-z/\lambda_L} , \tag{2.9}$$

which explains the Meissner effect.

These two London equations can be understood from quantum mechanical point of view. Since the average of the momentum in the absence of an applied field is zero for the ground state, arguing that the same holds for the canonical momentum $\mathbf{p} = m\mathbf{v}_s - e/c\mathbf{A}$ in the presence of an applied field, we have

$$\langle \mathbf{v}_s \rangle = \frac{e}{mc}\mathbf{A} . \tag{2.10}$$

Then the current is

$$\mathbf{J}_s = n_s(-e)\langle \mathbf{v}_s \rangle = -\frac{n_s e^2}{mc}\mathbf{A} . \tag{2.11}$$

Takin time derivative of both sides leads to the first London equation [Eq. (2.1)] and taking the curl of both sides we obtainthe second London equation [Eq. (2.2)]. The more general phenomenological Landau-Ginzburg theory will be discussed in Sec 2.5.

2.3 Bogoliubov Transformation and the BCS Ground State

As first demonstrated by Cooper [6], the Fermi sea of electrons is unstable against the formation of bound pairs called Cooper pairs, as long as the effective interaction between electrons is attractive. In classical superconductors, electron-phonon interactions give rise to this attractive effective interaction. For translationally invariant systems, pairing between two electrons with opposite momenta and spins

10

leads to the lowest energy of the system and these pairs are strongly correlated via the Pauli exclusion principle. The ground state is then a phase-coherent superposition of many-body states where Bloch states with opposite momenta and spins are either both occupied or both unoccupied. Because the radius of each pair is usually much larger than the average distance between electrons, the total Hamiltonian of the system can be simplified using a mean-field approximation,

$$c_{\mathbf{k}\uparrow}^{\dagger}c_{-\mathbf{k}\downarrow}^{\dagger} = \langle c_{\mathbf{k}\uparrow}^{\dagger}c_{-\mathbf{k}\downarrow}^{\dagger}\rangle + \left(c_{\mathbf{k}\uparrow}^{\dagger}c_{-\mathbf{k}\downarrow}^{\dagger} - \langle c_{\mathbf{k}\uparrow}^{\dagger}c_{-\mathbf{k}\downarrow}^{\dagger}\rangle\right) \ , \tag{2.12}$$

with the assumption that the fluctuation around the expectation value is very small so that we can keep only up to the first order terms of the fluctuation. Then the Hamiltonian becomes

$$\widehat{H}_{BCS} = \sum_{\mathbf{k},\sigma} \xi_{\mathbf{k}\sigma}c_{\mathbf{k}\sigma}^{\dagger}c_{\mathbf{k}\sigma} - \sum_{\mathbf{k}} \left(\Delta_{\mathbf{k}}c_{\mathbf{k}\uparrow}^{\dagger}c_{-\mathbf{k}\downarrow}^{\dagger} + \Delta_{\mathbf{k}}^{*}c_{-\mathbf{k}\downarrow}c_{\mathbf{k}\uparrow} - \Delta_{\mathbf{k}}\langle c_{\mathbf{k}\uparrow}^{\dagger}c_{-\mathbf{k}\downarrow}^{\dagger}\rangle\right) \ , \tag{2.13}$$

where

$$\Delta_{\mathbf{k}} = -\sum_{\mathbf{k}'} V(\mathbf{k},\mathbf{k}')\langle c_{-\mathbf{k}'\downarrow}c_{\mathbf{k}'\uparrow}\rangle \tag{2.14}$$

$$\xi_{\mathbf{k}\sigma} = \varepsilon_{\mathbf{k}\sigma} - \mu \ , \tag{2.15}$$

and $\varepsilon_{\mathbf{k}\sigma}$ is the band energy of the Bloch state $|\mathbf{k},\sigma\rangle$ and μ is the chemical potential. In the normal state, the order parameter $\Delta_{\mathbf{k}}$ vanishes since the expectation value $\langle c_{-\mathbf{k}'\downarrow}c_{\mathbf{k}'\uparrow}\rangle$ averages to zero. In the Nambu-Gorkov representation [68, 69],

$$\widehat{H}_{BCS} = E_0 + \sum_{\mathbf{k}} \left(\begin{array}{cc} c_{\mathbf{k}\uparrow}^{\dagger} & c_{-\mathbf{k}\downarrow} \end{array}\right) \left(\begin{array}{cc} \xi_{\mathbf{k}\uparrow} & -\Delta_{\mathbf{k}} \\ -\Delta_{\mathbf{k}}^{*} & \xi_{-\mathbf{k}\downarrow} \end{array}\right) \left(\begin{array}{c} c_{\mathbf{k}\uparrow} \\ c_{-\mathbf{k}\downarrow}^{\dagger} \end{array}\right) \tag{2.16}$$

where

$$E_0 = \sum_{\mathbf{k}} \left(\xi_{-\mathbf{k}\downarrow} + \Delta_{\mathbf{k}} \langle c_{\mathbf{k}\uparrow}^{\dagger} c_{-\mathbf{k}\downarrow}^{\dagger} \rangle \right) \ . \tag{2.17}$$

Now we introduce new Fermi operators $\alpha_{\mathbf{k}}$ and $\beta_{\mathbf{k}}$ such that

$$\begin{pmatrix} c_{\mathbf{k}\uparrow} \\ c_{-\mathbf{k}\downarrow}^{\dagger} \end{pmatrix} = \begin{pmatrix} u_{\mathbf{k}}^* & v_{\mathbf{k}} \\ -v_{\mathbf{k}}^* & u_{\mathbf{k}} \end{pmatrix} \begin{pmatrix} \alpha_{\mathbf{k}} \\ \beta_{\mathbf{k}}^{\dagger} \end{pmatrix} \equiv \mathbf{U} \begin{pmatrix} \alpha_{\mathbf{k}} \\ \beta_{\mathbf{k}}^{\dagger} \end{pmatrix} \ . \tag{2.18}$$

The new Fermi operators should satisfy the fermion commutation relations

$$\{\alpha_{\mathbf{k}}^{\dagger}, \alpha_{\mathbf{k}}\} = |u_{\mathbf{k}}|^2 + |v_{\mathbf{k}}|^2 = 1 \tag{2.19}$$

$$\{\beta_{\mathbf{k}}^{\dagger}, \beta_{\mathbf{k}}\} = |v_{\mathbf{k}}|^2 + |u_{\mathbf{k}}|^2 = 1 \tag{2.20}$$

$$\{\alpha_{\mathbf{k}}^{\dagger}, \beta_{\mathbf{k}}\} = \{\beta_{\mathbf{k}}^{\dagger}, \alpha_{\mathbf{k}}\} = 0 \tag{2.21}$$

$$\{\alpha_{\mathbf{k}}^{\dagger}, \beta_{\mathbf{k}}^{\dagger}\} = \{\alpha_{\mathbf{k}}, \beta_{\mathbf{k}}\} = 0 \ . \tag{2.22}$$

We choose $u_{\mathbf{k}}$ and $v_{\mathbf{k}}$ so that the Hamiltonian is diagonal in terms of the new operators $\alpha_{\mathbf{k}}$ and $\beta_{\mathbf{k}}$.

$$\begin{aligned} \widehat{H}_{BCS} &= E_0 + \sum_{\mathbf{k}} \begin{pmatrix} \alpha_{\mathbf{k}}^{\dagger} & \beta_{\mathbf{k}} \end{pmatrix} \mathbf{U}^{\dagger} \begin{pmatrix} \xi_{\mathbf{k}\uparrow} & -\Delta_{\mathbf{k}} \\ -\Delta_{\mathbf{k}}^* & \xi_{-\mathbf{k}\downarrow} \end{pmatrix} \mathbf{U} \begin{pmatrix} \alpha_{\mathbf{k}} \\ \beta_{\mathbf{k}}^{\dagger} \end{pmatrix} \\ &= E_0 + \sum_{\mathbf{k}} \begin{pmatrix} \alpha_{\mathbf{k}}^{\dagger} & \beta_{\mathbf{k}} \end{pmatrix} \begin{pmatrix} E_{1\mathbf{k}} & 0 \\ 0 & E_{2\mathbf{k}} \end{pmatrix} \begin{pmatrix} \alpha_{\mathbf{k}} \\ \beta_{\mathbf{k}}^{\dagger} \end{pmatrix} \end{aligned} \tag{2.23}$$

where

$$E_{1\mathbf{k}} = \sqrt{\xi_{\mathbf{k}}^2 + |\Delta_{\mathbf{k}}|^2} \equiv E_{\mathbf{k}} \tag{2.24}$$

$$E_{2\mathbf{k}} = -\sqrt{\xi_{\mathbf{k}}^2 + |\Delta_{\mathbf{k}}|^2} = -E_{\mathbf{k}} \tag{2.25}$$

$$|u_{\mathbf{k}}|^2 = \frac{1}{2}\left(1 + \frac{\xi_{\mathbf{k}}}{E_{\mathbf{k}}}\right) \tag{2.26}$$

$$|v_{\mathbf{k}}|^2 = \frac{1}{2}\left(1 - \frac{\xi_{\mathbf{k}}}{E_{\mathbf{k}}}\right) \tag{2.27}$$

$$u_{\mathbf{k}}^* v_{\mathbf{k}} = \frac{\Delta_{\mathbf{k}}}{2E_{\mathbf{k}}} . \tag{2.28}$$

We assume that the Bloch state band energy is degenerate, $\xi_{\mathbf{k}\uparrow} = \xi_{-\mathbf{k}\downarrow} \equiv \xi_{\mathbf{k}}$. The Hamiltonian then reduces to

$$\widehat{H}_{BCS} = E_0 - \sum_{\mathbf{k}} E_{\mathbf{k}} + \sum_{\mathbf{k}} E_{\mathbf{k}}\left(\alpha_{\mathbf{k}}^\dagger \alpha_{\mathbf{k}} + \beta_{\mathbf{k}}^\dagger \beta_{\mathbf{k}}\right) . \tag{2.29}$$

The first two constant terms give the condensation energy of the system at zero temperature and the last term describes the quasi-particle excitation of the system. The two species of quasi-particles have the same positive excitation energy $E_{\mathbf{k}}$. The ground state $|\Psi_G\rangle$ is, therefore, the vacuum state for the quasi-particle operators,

$$\langle\Psi_G|\alpha_{\mathbf{k}}^\dagger \alpha_{\mathbf{k}}|\Psi_G\rangle = \langle\Psi_G|\beta_{\mathbf{k}}^\dagger \beta_{\mathbf{k}}|\Psi_G\rangle = 0 . \tag{2.30}$$

(In electron-hole systems where the band energies of conduction and valence bands are different due to the different effective masses, the quasi-particle excitation energies are also different. This property will play a central role in the excitonic condensation as will be discussed later.) The ground state that satisfies Eq. (2.30) can be obtained as follows. Define $|\Phi_F\rangle$ to be a state that all the Bloch states are completely occupied,

$$|\Phi_F\rangle \equiv \prod_{\mathbf{k}} c_{\mathbf{k}\uparrow}^\dagger c_{-\mathbf{k}\downarrow}^\dagger |0\rangle \tag{2.31}$$

13

where $|0\rangle$ is the electron vacuum state. Then the BCS ground state can be obtained by annihilating all the quasi-particles present in $|\Phi_F\rangle$.

$$\begin{aligned}
|\Psi_G\rangle &= \prod_{\mathbf{k}} \alpha_{\mathbf{k}} \beta_{\mathbf{k}} |\Phi_F\rangle \\
&= \prod_{\mathbf{k}} \left(u_{\mathbf{k}} c_{\mathbf{k}\uparrow} - v_{\mathbf{k}} c_{-\mathbf{k}\downarrow}^{\dagger} \right) \left(v_{\mathbf{k}} c_{\mathbf{k}\uparrow}^{\dagger} + u_{\mathbf{k}} c_{-\mathbf{k}\downarrow} \right) c_{\mathbf{k}\uparrow}^{\dagger} c_{-\mathbf{k}\downarrow}^{\dagger} |0\rangle \\
&= -\prod_{\mathbf{k}} u_{\mathbf{k}} \left(u_{\mathbf{k}} + v_{\mathbf{k}} c_{\mathbf{k}\uparrow}^{\dagger} c_{-\mathbf{k}\downarrow}^{\dagger} \right) |0\rangle \ . \quad (2.32)
\end{aligned}$$

After applying the normalization condition $\langle \Psi_G | \Psi_G \rangle = 1$, we obtain

$$|\Psi_G\rangle = \prod_{\mathbf{k}} \left(u_{\mathbf{k}} + v_{\mathbf{k}} c_{\mathbf{k}\uparrow}^{\dagger} c_{-\mathbf{k}\downarrow}^{\dagger} \right) |0\rangle \ . \quad (2.33)$$

2.4 Gap Equation and Critical Temperature

BCS theory is a self-consistent mean-field theory. The self-consistency is encoded in the definition of the order parameter $\Delta_{\mathbf{k}}$, which depends on the solution of the problem.

$$\begin{aligned}
\Delta_{\mathbf{k}} &= -\sum_{\mathbf{k}'} V(\mathbf{k}, \mathbf{k}') \langle c_{-\mathbf{k}'\downarrow} c_{\mathbf{k}'\uparrow} \rangle \\
&= -\sum_{\mathbf{k}'} V(\mathbf{k}, \mathbf{k}') \langle \left(-v_{\mathbf{k}'} \alpha_{\mathbf{k}'}^{\dagger} + u_{\mathbf{k}'}^{*} \beta_{\mathbf{k}'} \right) \left(u_{\mathbf{k}'}^{*} \alpha_{\mathbf{k}'} + v_{\mathbf{k}'} \beta_{\mathbf{k}'}^{\dagger} \right) \rangle \\
&= -\sum_{\mathbf{k}'} V(\mathbf{k}, \mathbf{k}') \left(-v_{\mathbf{k}'} u_{\mathbf{k}'}^{*} \langle \alpha_{\mathbf{k}'}^{\dagger} \alpha_{\mathbf{k}'} \rangle + u_{\mathbf{k}'}^{*} v_{\mathbf{k}'} \langle \beta_{\mathbf{k}'} \beta_{\mathbf{k}'}^{\dagger} \rangle \right) \\
&= -\sum_{\mathbf{k}'} V(\mathbf{k}, \mathbf{k}') u_{\mathbf{k}'}^{*} v_{\mathbf{k}'} \left(1 - \langle \alpha_{\mathbf{k}'}^{\dagger} \alpha_{\mathbf{k}'} \rangle - \langle \beta_{\mathbf{k}'}^{\dagger} \beta_{\mathbf{k}'} \rangle \right) \\
&= -\sum_{\mathbf{k}'} V(\mathbf{k}, \mathbf{k}') \frac{\Delta_{\mathbf{k}'}}{2E_{\mathbf{k}'}} \left(1 - \langle \alpha_{\mathbf{k}'}^{\dagger} \alpha_{\mathbf{k}'} \rangle - \langle \beta_{\mathbf{k}'}^{\dagger} \beta_{\mathbf{k}'} \rangle \right) \ . \quad (2.34)
\end{aligned}$$

This is the self-consistent gap equation. The trivial solution $\Delta_{\mathbf{k}} = 0$ corresponds to the normal Fermi gas and we expect nontrivial solution with lower energy for

attractive interactions. If we adopt the simple model invented by BCS in their seminal articles,

$$V(\mathbf{k}, \mathbf{k}') = \begin{cases} -V_0 & \text{if } |\xi_{\mathbf{k}}| \text{ and } |\xi_{\mathbf{k}'}| \leq \hbar\omega_c \\ 0 & \text{otherwise} \end{cases} \tag{2.35}$$

where ω_c is the cut-off frequency, the solution of the gap equation at $T = 0$ is

$$\Delta_{\mathbf{k}} = \begin{cases} \Delta_0 & \text{for } |\xi_{\mathbf{k}}| < \hbar\omega_c \\ 0 & \text{for } |\xi_{\mathbf{k}}| > \hbar\omega_c \end{cases}, \tag{2.36}$$

where Δ_0 satisfies

$$1 = \sum_{\mathbf{k}}' \frac{V_0}{2\sqrt{\xi_{\mathbf{k}}^2 + \Delta_0^2}} \tag{2.37}$$

and $\sum_{\mathbf{k}}'$ indicates that the summation is over $\mathbf{k}$ that satisfies $|\xi_{\mathbf{k}}| < \hbar\omega_c$. Here the overall phase of Δ_0 is set such that Δ_0 is real and positive. Changing the summation into an integration, we obtain

$$\frac{1}{V_0} = \int_{-\hbar\omega_c}^{\hbar\omega_c} d\xi \frac{N(\xi)}{2\sqrt{\xi^2 + \Delta_0^2}} \tag{2.38}$$

where $N(\xi)$ is the density of states for electrons of one spin orientation. Assuming $N(\xi)$ is slowly varying over the range of $|\xi| < \hbar\omega_c$,

$$\begin{aligned} \frac{1}{N(0)V_0} &= \int_0^{\hbar\omega_c} d\xi \frac{1}{\sqrt{\xi^2 + \Delta_0^2}} \\ &= \ln \frac{\hbar\omega_c + \sqrt{(\hbar\omega_c)^2 + \Delta_0^2}}{\Delta_0}, \end{aligned} \tag{2.39}$$

where $N(0)$ is the density of states at the Fermi level. Thus we find the gap Δ_0 at zero temperature

$$\Delta_0 = \frac{\hbar\omega_c}{\sinh(1/N(0)V_0)} \simeq 2\hbar\omega_c e^{-1/N(0)V_0} \tag{2.40}$$

15

where the last step is for weak-coupling limit $N(0)V_0 \ll 1$. At finite temperatures, the expectation value of the quasi-particle number operators in Eq. (2.34) is given by the Fermi function

$$\langle \alpha_{\mathbf{k}}^{\dagger} \alpha_{\mathbf{k}} \rangle = \langle \beta_{\mathbf{k}}^{\dagger} \beta_{\mathbf{k}} \rangle = \frac{1}{e^{\beta E_{\mathbf{k}}} + 1} = f(E_{\mathbf{k}}) \tag{2.41}$$

where $\beta = 1/k_B T$ and using the same BCS effective interaction [Eq. (2.35)], the gap equation becomes

$$\Delta_{\mathbf{k}} = \begin{cases} V_0 \sum_{\mathbf{k}'}' \frac{\Delta_{\mathbf{k}'}}{2E_{\mathbf{k}'}} \left(1 - 2f(E_{\mathbf{k}'})\right) & \text{for } |\xi_{\mathbf{k}}| < \hbar\omega_c \\ 0 & \text{for } |\xi_{\mathbf{k}}| > \hbar\omega_c \end{cases} . \tag{2.42}$$

Because the right-hand-side does not depend on $\mathbf{k}$, $\Delta_{\mathbf{k}}$ is constant. Then

$$\Delta_{\mathbf{k}} = \begin{cases} \Delta & \text{for } |\xi_{\mathbf{k}}| < \hbar\omega_c \\ 0 & \text{for } |\xi_{\mathbf{k}}| > \hbar\omega_c \end{cases} , \tag{2.43}$$

where Δ satisfies an implicit equation

$$\frac{1}{V_0} = \frac{1}{2} \sum_{\mathbf{k}}' \frac{\tanh(\beta E_{\mathbf{k}}/2)}{E_{\mathbf{k}}} \tag{2.44}$$

$$\Rightarrow \frac{1}{N(0)V_0} = \int_0^{\hbar\omega_c} d\xi \frac{\tanh(\frac{\beta}{2}\sqrt{\xi^2 + \Delta^2})}{\sqrt{\xi^2 + \Delta^2}} . \tag{2.45}$$

The critical temperature T_c is determined by setting $\Delta(T) \to 0$.

$$\frac{1}{N(0)V_0} = \int_0^{\beta_c \hbar\omega_c} dx \frac{\tanh x}{x} = \ln\left(\frac{2e^{\gamma}}{\pi}\beta_c \hbar\omega_c\right) \tag{2.46}$$

where $\gamma = 0.577...$ is Euler's constant. Therefore, the critical temperature

$$k_B T_c = \beta_c^{-1} = 1.13\hbar\omega_c e^{-1/N(0)V_0} = 0.565\Delta_0 \tag{2.47}$$

16
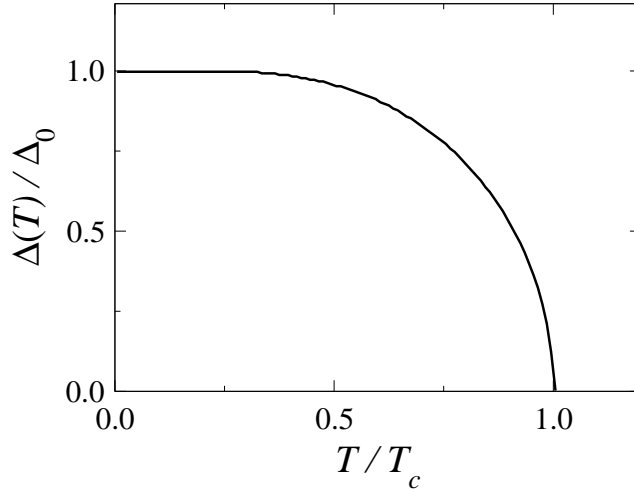
Figure 2.1: BCS gap $\Delta(T)$ at finite temperatures, numerically evaluated by solving the gap equation Eq. (2.45).

is of the same order as the zero-temperature gap Δ_0. The similarity of critical temperatures and zero temperature gaps is a hallmark of mean-field theories of order-disorder phase transitions. At finite temperatures, the gap $\Delta(T)$ can be calculated by solving the gap equation Eq. (2.45) numerically. The result is shown in Fig. 2.1. At low temperatures, $\Delta(T)$ is almost constant because the hyperbolic tangent in Eq. (2.45) is almost unity since $e^{-\Delta/k_B T} \simeq 0$. Near T_c, $\Delta(T)/\Delta_0 \propto (1 - T/T_c)^{1/2}$.

2.5   GL Free Energy and Differential Equations

The basic postulates of GL theory are that there is a small and slowly varying complex order parameter $\psi(\mathbf{r})$ such that $|\psi(\mathbf{r})|^2$ is the local density of the superconducting electrons, $n_s(\mathbf{r})$. The free energy density then can be expanded in powers of $|\psi|^2$ and $|\nabla\psi|^2$,

$$f = f_{n0} + \alpha|\psi|^2 + \frac{\beta}{2}|\psi|^4 + \frac{1}{2m^*}\left|\left(\frac{\hbar}{i}\boldsymbol{\nabla} + \frac{e^*}{c}\mathbf{A}\right)\psi\right|^2 + \frac{H^2}{8\pi} \qquad (2.48)$$

17

where $\mathbf{A}$ is the vector potential. The effective charge e^* of the superconducting particle is easily identified as $2e$ of the Cooper pair, while the effective mass depends on the crystal structures and the interaction between electrons and phonons. e^* was originally set equal to e and only the subsequent microscopic theory made it clear that e^* should be $2e$. The size of the 'superconducting' flux quantum proves experimentally that this parameter should be $2e$ as will be discussed in the next section. In the absence of external fields and gradients of the pseudowavefunction, we have

$$f_s - f_n = \alpha|\psi|^2 + \frac{\beta}{2}|\psi|^4 \ . \tag{2.49}$$

Note that β must be positive since otherwise the lowest free energy would occur for arbitrarily large $|\psi|^2$. If α is also positive, the lowest free energy occurs at $|\psi|^2{=}0$, corresponding to the normal state. If α is negative, the minimum occurs when

$$|\psi|^2 = |\psi_\infty|^2 \equiv -\frac{\alpha}{\beta} \tag{2.50}$$

where $|\psi_\infty|^2$ is $|\psi|^2$ value in infinitely deep interior of the superconductor.

By carrying out functional derivative of Eq. (2.48) with respect to $\psi = |\psi|e^{i\varphi}$ and $\mathbf{A}$, we obtain GL differential equations

$$\alpha\psi + \beta|\psi|^2\psi + \frac{1}{2m*}\left(\frac{\hbar}{i}\boldsymbol{\nabla} + \frac{e^*}{c}\mathbf{A}\right)^2\psi = 0 \tag{2.51}$$

$$\mathbf{J} = \frac{c}{4\pi}\boldsymbol{\nabla}\times\mathbf{H} = -\frac{e^*}{m^*}\left(\hbar\boldsymbol{\nabla}\varphi + \frac{e^*}{c}\mathbf{A}\right)|\psi|^2 = -e^*n_s\mathbf{v}_s \tag{2.52}$$

where

$$\mathbf{v}_s = \frac{1}{m^*}\left(\hbar\boldsymbol{\nabla}\varphi + \frac{e^*}{c}\mathbf{A}\right) \tag{2.53}$$

is the supercurrent velocity. Taking the time derivative and the curl of Eq. (2.52) recovers the first [Eq. (2.1)] and the second [Eq. (2.2)] London equations respectively.

There are two length scales for superconductors, the coherence length and

the penetration depth. The coherence length is the length scale over which the order parameter changes in space while the penetration depth is the length scale that the magnetic field penetrates into the superconductor. In the absence of external fields we can take ψ to be real and in one-dimension Eq. (2.51) becomes,

$$\frac{\hbar^2}{2m^*|\alpha|}\frac{d^2f}{dx^2} + f - f^3 = 0 \tag{2.54}$$

where $f = \psi/\psi_\infty$. Therefore the characteristic length scale for order parameter variation is

$$\xi = \frac{\hbar}{\sqrt{2m^*|\alpha|}} \tag{2.55}$$

which is called GL coherence length. An expression for the penetration depth in terms of the Landau parameters α and β can be obtained by substituting Eq. (2.52) into the London equation Eq. (2.2) for constant n_s. Using $\boldsymbol{\nabla} \times \boldsymbol{\nabla}\varphi = 0$ we obtain for the penetration depth

$$\lambda_{\text{eff}}^2 = \frac{m^*c^2}{4\pi|\psi|^2 e^{*2}} = \frac{m^*c^2\beta}{4\pi|\alpha|e^{*2}} \ . \tag{2.56}$$

The GL parameter κ which is defined as the ratio of the two length scales

$$\kappa = \frac{\lambda_{\text{eff}}}{\xi} = \frac{m^*c}{e^*\hbar}\sqrt{\frac{\beta}{2\pi}} \tag{2.57}$$

determines whether the superconductor is type I or type II. There are many examples of both types of superconductors.

2.6 Vortex Lattices

The Helmholtz free energy of the normal state occupying volume V in the presence of the field is

$$F_n = V f_{n0} + V \frac{H^2}{8\pi} + V_{\text{ext}} \frac{H^2}{8\pi} \qquad (2.58)$$

where f_{n0} is the free energy density of the normal state in the absence of the field and V_{ext} is the volume of the space outside the sample. For superconductors, since the field is zero inside the sample,

$$F_s = V f_{s0} + V_{\text{ext}} \frac{H^2}{8\pi} \qquad (2.59)$$

where f_{s0} is the free energy density in the absence of the field. In the presence of an external field, if we choose the external field $\mathbf{H}$ as the independent variable the appropriate thermodynamic potential is the Gibbs free energy whose density is given by

$$g = f - \frac{\mathbf{B} \cdot \mathbf{H}}{4\pi} \ . \qquad (2.60)$$

Then the Gibbs free energy of the normal state and the superconducting state are

$$G_n = V f_{n0} - V \frac{H^2}{8\pi} - V_{\text{ext}} \frac{H^2}{8\pi} \qquad (2.61)$$

$$G_s = V f_{s0} - V_{\text{ext}} \frac{H^2}{8\pi} \qquad (2.62)$$

because $B = H$ in the normal state and outside the sample. The critical field H_c is defined as the field where the Gibbs free energies of the normal and superconducting states are the same. This leads to

$$f_{n0} - f_{s0} = \frac{H_c^2}{8\pi} \ . \qquad (2.63)$$

Using this relation combined with Eq. (2.49) and Eq. (2.50), we obtain

$$H_c^2 = \frac{4\pi\alpha^2}{\beta} \ .$$

(2.64)

The superconducting order parameter cannot remain constant if field penetrates into a superconductor. The critical field defined above was for a first order phase transition between superconducting and normal states assuming no field penetration. If field does penetrate, the superconducting state can no longer be constant. A second critical field can be defined by assuming a continuous phase transition between superconducting and normal states in which flux penetration is allowed. Near the second critical field H_{c2} where the order parameter ψ is very small, we can keep only the first order terms from Eq. (2.51)

$$\frac{1}{2m*}\left(\frac{\hbar}{i}\boldsymbol{\nabla} + \frac{e^*}{c}\mathbf{A}\right)^2 \psi = -\alpha\psi \ .$$

(2.65)

This equation has a nontrivial solution only if $-\alpha$ is larger than the lowest eigenvalue $\hbar\omega_c/2$ where $\omega_c = 2eH_{c2}/mc$. Therefore the critical field H_{c2} is defined by

$$H_{c2} = \frac{mc|\alpha|}{e\hbar} \ .$$

(2.66)

The ratio between these two critical field is

$$\frac{H_{c2}}{H_c} = \sqrt{2}\kappa \ .$$

(2.67)

If $\kappa < 1/\sqrt{2}$ (type I), H_{c2} lies below H_c and has no physical meaning. On the other hand if $\kappa > 1/\sqrt{2}$ (type II), H_{c2} is larger than H_c and between these two critical fields, it is energetically unfavorable to expel all magnetic flux while favorable to be in the superconducting state. This corresponds to the negative surface energy between the superconduting and the normal region. In a type II superconductor in the field

21
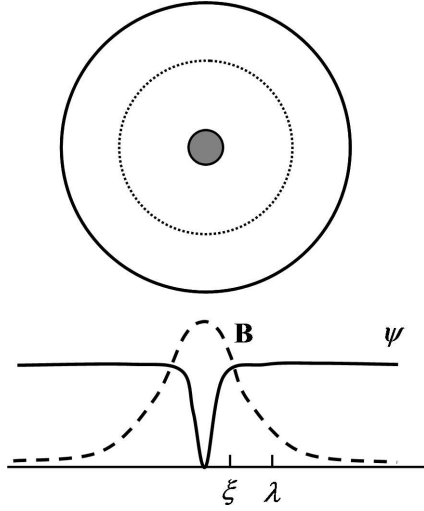
Figure 2.2: Illustration of a single vortex in a type II superconductor. Shaded region presents the vortex core where the superconducting order parameter vanishes. The outside region is superconducting and the order parameter is almost constant. The integration of $\boldsymbol{\nabla}\varphi$ over the dotted contour which is deep in the superconducting region must be a multiple of 2π. This property implies that the magnetic flux that penetrates through the superconductor in the neighborhood of the vortex must be a multiple of the quantum of magnetic flux.

range $H_c < H < H_{c2}$, the magnetic flux penetrates through the superconductor and it forms as much surface as possible to minimize the energy. The magnetic flux therefore split into the smallest possible unit in the superconductor, which leads to the vortex lattice state where a flux quantum penetrates through a single vortex.

A single vortex is illustrated in Fig. 2.2. There is a vortex core region of the size of about the coherence length where the order parameter vanishes in the center. The magnetic flux penetrates through this core region. Outside of the core region is the superconducting region where the order parameter is almost constant. The minimum possible flux for a single vortex can be determined by demanding the single-valued condition on the phase of the order parameter. If we integrate the gradient of the phase along a contour around the vortex whose radius is larger than

the penetration depth [dotted contour in Fig. 2.2],

$$
\begin{aligned}
2n\pi &= \oint d\mathbf{l} \cdot \boldsymbol{\nabla}\varphi = -\frac{e^*}{\hbar c} \oint d\mathbf{l} \cdot \mathbf{A} \\
&= -\frac{e^*}{\hbar c} \int d\mathbf{a} \cdot \mathbf{B} = -\frac{e^*}{\hbar c}\Phi \ ,
\end{aligned}
\tag{2.68}
$$

which leads to the condition on the flux

$$
\Phi = \frac{hc}{2e}n = \frac{n}{2}\Phi_0
\tag{2.69}
$$

where n is any integer and $\Phi_0 = hc/e$ is the quantum of magnetic flux. The factor $1/2$ proves experimentally [70, 71] that superconductivity is a condensate of electron pairs. Therefore, the smallest magnetic flux in a vortex is $\Phi_0/2$. If the total magnetic flux Φ is much larger than the flux quantum Φ_0, the vortices naturally form a lattice configuration which has lower energy than the random configuration [72]. The most favorable lattice structure was found to be the triangular lattice [73].

Chapter 3

Mean-Field Theory of Fermion Pair Condensation in Electron-Hole Bilayers

3.1 Introduction

We consider a double-quantum-well structure composed of two GaAs quantum wells separated by an GaAlAs spacer. The difference between the fundamental energy gaps of GaAs and GaAlAs leads to potential profiles for the conduction and valence bands which can be treated as confining potentials. A gate voltage is applied in the perpendicular direction to the layers so that the valence band maximum can move higher than the conduction band minimum, leading to a spatially separated electron and hole gas system. In addition to making electron-hole systems stable, the external field also affects [74, 75, 76, 77] the Rashba spin-orbit interaction [58, 59], which arises from the structural inversion asymmetry in quantum wells. The Rashba SO interaction plays an important role in the ferromagnetic phase expected to accompany excitonic condensation as will be discussed in the next chapter. We

assume that there is external charge distributed outside of the bilayer system that determines the external electric fields E_L and E_R and that the hole layer contains uniform positive charges with charge density of en_0 (see Fig. 3.1). Treating E_L and E_R as experimentally controllable parameters rather than the electron and hole densities, does a better job of representing real experimental condition. Once we fix the external charge densities ρ_L and ρ_R, the density difference between electron and hole $\Delta n = n_c - n_h$ is determined by overall charge neutrality, but n_c and n_h are only self-consistently determined after we solve the problem. If E_L and E_R are the same, $\rho_L + \rho_R = 0$ and therefore $n_c = n_h$, while if $E_L - E_R \neq 0$, then $\rho_L + \rho_R \neq 0$ and $\Delta n = -(\rho_A + \rho_B)/e = (\rho_L + \rho_R)/e$. Therefore, by controlling the external charge densities ρ_A and ρ_B or equivalently, the external electric fields E_L and E_R, we can create density polarized electron-hole bilayer systems. Tuning the difference between electron and hole populations will come for free as an experimental tuning parameter in these experiments. This population polarization leads to interesting new physics that will be discussed in the next chapter.

In this chapter, we generalize the BCS theory to more general fermion systems with more general attractive interactions, particularly to electron-hole systems with natural attractive Coulomb interaction between electrons and holes. We consider only a single conduction band and a single valence band in this chapter. For population unpolarized systems, the spin degree of freedom does not change the results of this chapter except for the spin-degeneracy of each bands. In Sec. 3.2, we derive the mean-field Hamiltonian and the formal expression for the total energy for the bilayer system. When all electrons are in the same layer, the charge density is uniform and we can neglect all the direct Coulomb interactions. In bilayer systems where charges are spatially separated, however, the Hartree energy that comes from the direct Coulomb interactions must be included explicitly. This is quite a tricky issue that is often treated incorrectly. In Sec. 3.3, we discuss how we treat the di-
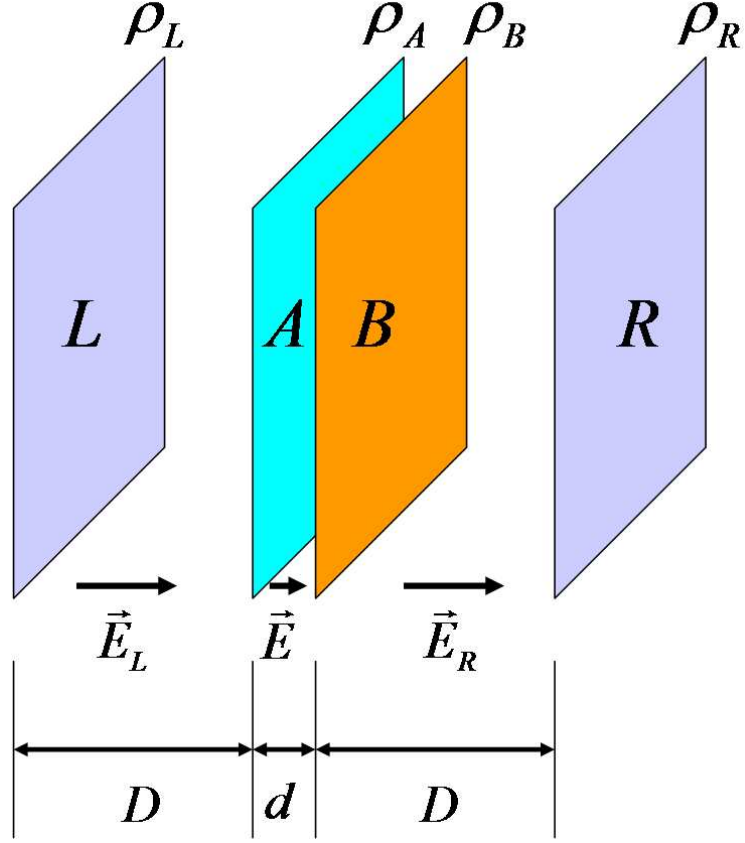
Figure 3.1: Cartoon depicting the bilayer system including the external charge distribution which gives rise to the external electric field. Layer A is the electron layer and layer B is the hole layer. Layers L and R contain the external charge distribution. The overall charge is neutral so that $\rho_L + \rho_A + \rho_B + \rho_R = 0$. ρ_L and ρ_R are purely external charge and lead to gate external fields $\mathbf{E}_L$ and $\mathbf{E}_R$. $\rho_A = -en_c$ is contributed by the conduction band electrons and $\rho_B = -en_v + en_0 = en_h$ is the total charge density that comes from the valence band electrons and the background positive charge in layer B. The electric field outside of the whole system is zero because of overall charge neutrality.

rect Coulomb interaction and the electrostatic energy due to the external charges. Using the mean-field Hamiltonian, we derive a BCS-like gap equation in Sec. 3.4, and present some numerical results for this 2-band model.

3.2 Mean-Field Hamiltonian for Excitonic Bilayer Systems

The total Hamiltonian of the bilayer system that has one conduction band and one valence band is

$$\widehat{H} = E_{ES}^{\text{ext}} + \sum_{a\mathbf{k}} \left(\varepsilon_{a\mathbf{k}}^{(0)} + V_a^{\text{ext}} \right) c_{a\mathbf{k}}^\dagger c_{a\mathbf{k}} + \frac{1}{2\Omega} \sum_{\substack{\mathbf{k}\mathbf{k}'\mathbf{q} \\ aa'}} V^{aa'}(\mathbf{q}) c_{a\mathbf{k}}^\dagger c_{a'\mathbf{k}'}^\dagger c_{a'\mathbf{k}'+\mathbf{q}} c_{a\mathbf{k}-\mathbf{q}} \quad (3.1)$$

where a's are the band indices for conduction band c in layer A and valence band v in layer B, $\mathbf{k}$ is the two-dimensional wave vector, Ω is area of each layer and $V^{aa'}(\mathbf{q})$ is the Fourier transform of the Coulomb interaction between electrons in band a and band a'. E_{ES}^{ext} is the electrostatic energy that comes from the Coulomb interaction between the outside charge distribution and the positive background charge in layer B, and V_a^{ext} is the electric field the electrons in band a feel due to the outside charge and the background charge in layer B. The bare band energies $\varepsilon_{a\mathbf{k}}^{(0)}$'s are assumed to be parabolic for both conduction and valence bands,

$$\varepsilon_{c\mathbf{k}}^{(0)} = \frac{\hbar k^2}{2m_c} \qquad (3.2)$$

$$\varepsilon_{v\mathbf{k}}^{(0)} = -\frac{\hbar k^2}{2m_v} - E_g \ , \qquad (3.3)$$

with the fundamental band gap E_g. V_a^{ext} does not depend on $\mathbf{k}$ and only depends on the z-coordinate of the layers. We neglect the small overlap of electron and hole wavefunctions so that the interaction V conserves band indices. Using the mean-

field approximation allowing inter-band coherence, the two-body interaction part of the total Hamiltonian leads to the Hartree field and the exchange field.

$$\widehat{H}_{MF} = E_{ES}^{\text{ext}} + E_0 + \sum_{a\mathbf{k}} \left(\varepsilon_{a\mathbf{k}}^{(0)} + V_a^{\text{ext}} + \varepsilon_a^h + \varepsilon_{a\mathbf{k}}^{ex} \right) c_{a\mathbf{k}}^\dagger c_{a\mathbf{k}} - \sum_{\mathbf{k}} \left(\Delta_{\mathbf{k}} c_{c\mathbf{k}}^\dagger c_{v\mathbf{k}} + h.c. \right)$$
(3.4)

where

$$E_0 = -\frac{1}{2} \sum_{a\mathbf{k}} \left(\varepsilon_a^h + \varepsilon_{a\mathbf{k}}^{ex} \right) \langle c_{a\mathbf{k}}^\dagger c_{a\mathbf{k}} \rangle + \frac{1}{2} \sum_{\mathbf{k}} \left(\Delta_{\mathbf{k}} \langle c_{c\mathbf{k}}^\dagger c_{v\mathbf{k}} \rangle + c.c. \right) \qquad (3.5)$$

$$\varepsilon_a^h = \frac{1}{\Omega} V^{aa'}(0) \sum_{a'\mathbf{k}} \langle c_{a'\mathbf{k}}^\dagger c_{a'\mathbf{k}} \rangle \qquad (3.6)$$

$$\varepsilon_{a\mathbf{k}}^{ex} = -\frac{1}{\Omega} \sum_{\mathbf{k}'} V^{aa}(\mathbf{k} - \mathbf{k}') \langle c_{a\mathbf{k}'}^\dagger c_{a\mathbf{k}'} \rangle \qquad (3.7)$$

$$\Delta_{\mathbf{k}} = \frac{1}{\Omega} \sum_{\mathbf{k}'} V^{cv}(\mathbf{k} - \mathbf{k}') \langle c_{v\mathbf{k}'}^\dagger c_{c\mathbf{k}'} \rangle \ . \qquad (3.8)$$

Here ε_a^h is the Hartree field, $\varepsilon_{a\mathbf{k}}^{ex}$ is the intra-band exchange field and $\Delta_{\mathbf{k}}$ is the inter-band exchange field. The constant E_0 is included to avoid double counting of two-body interaction when we calculate the total energy. In bulk systems where the total charge density is uniform, the Hartree term ε_a^h is exactly cancelled by the background positive ions. In bilayer systems where electrons and holes are spatially separated, the net electrostatic potential energy is not cancelled and the Hartree term must be calculated self-consistently including all the electrostatic potentials from the electrons and holes. This Hartree term for bilayer systems will be explicitly calculated in the next section. Introducing the density matrix

$$\rho^{a'a}(\mathbf{k}) \equiv \langle c_{a\mathbf{k}}^\dagger c_{a'\mathbf{k}} \rangle \ , \qquad (3.9)$$

28

Eq. (3.5) $\sim$ Eq. (3.8) can be rewritten as

$$E_0 = -\frac{1}{2}\sum_{a\mathbf{k}}\left(\varepsilon_a^h + \varepsilon_{a\mathbf{k}}^{ex}\right)\rho^{aa}(\mathbf{k}) + \frac{1}{2}\sum_{\mathbf{k}}\left(\Delta_{\mathbf{k}}\rho^{vc}(\mathbf{k}) + c.c.\right) \tag{3.10}$$

$$\varepsilon_a^h = \frac{1}{\Omega}V^{aa'}(0)\sum_{a'\mathbf{k}}\rho^{a'a'}(\mathbf{k}) \tag{3.11}$$

$$\varepsilon_{a\mathbf{k}}^{ex} = -\frac{1}{\Omega}\sum_{\mathbf{k}'}V^{aa}(\mathbf{k}-\mathbf{k}')\rho^{aa}(\mathbf{k}') \tag{3.12}$$

$$\Delta_{\mathbf{k}} = \frac{1}{\Omega}\sum_{\mathbf{k}'}V^{cv}(\mathbf{k}-\mathbf{k}')\rho^{cv}(\mathbf{k}') \ , \tag{3.13}$$

We allow the inter-layer coherence which leads to non-vanishing expectation values of $\langle c_{v\mathbf{k}'}^{\dagger} c_{c\mathbf{k}'}\rangle$, and $\Delta_{\mathbf{k}}$ is the resulting inter-layer momentum-dependent exchange interaction term. The exchange term for the valence band diverges in general because we assume that the valence band energy goes to the negative infinity for large k. This problem can be removed by noticing that the experimentally measured valence band effective mass presumably includes all the interaction effects in a normal state with empty conduction band and full valence band, which we will define as $|\Phi_0\rangle$. Thus

$$-\frac{\hbar k^2}{2m_v^*} = -\frac{\hbar k^2}{2m_v} - \frac{1}{\Omega}\sum_{\mathbf{k}'}V^{vv}(\mathbf{k}-\mathbf{k}')\rho_0^{vv}(\mathbf{k}')$$

$$= -\frac{\hbar k^2}{2m_v} - \frac{1}{\Omega}\sum_{\mathbf{k}'}V^{vv}(\mathbf{k}-\mathbf{k}') \tag{3.14}$$

where ρ_0 is the density matrix when the system is in state $|\Phi_0\rangle$,

$$\rho_0^{aa'}(\mathbf{k}) = \begin{cases} 1 & a = v, a' = v \\ 0 & \text{otherwise} \end{cases} . \tag{3.15}$$

It follows that

$$\varepsilon_{v\mathbf{k}}^{(0)} + \varepsilon_{v\mathbf{k}}^{ex} = -\frac{\hbar k^2}{2m_v^*} - E_g - \frac{1}{\Omega} \sum_{\mathbf{k}'} V^{vv}(\mathbf{k} - \mathbf{k}') \left(\rho^{vv}(\mathbf{k}') - 1 \right) \qquad (3.16)$$

which remains finite.

The total energy of the ground state $|\Psi_G\rangle$ can be calculated as the expectation value of the mean-field Hamiltonian,

$$\begin{aligned} E_{\text{tot}}[\Psi_G] &\equiv \langle \Psi_G | \widehat{H}_{MF} | \Psi_G \rangle \\ &= \sum_{a\mathbf{k}} \left(\varepsilon_{a\mathbf{k}}^{(0)} + \frac{1}{2} \varepsilon_{a\mathbf{k}}^{ex} \right) \rho^{aa}(\mathbf{k}) - \frac{1}{2} \sum_{a\mathbf{k}} \left(\Delta_{\mathbf{k}} \rho^{vc}(\mathbf{k}) + c.c. \right) + E_{ES} \,, \end{aligned}$$

$$(3.17)$$

where

$$E_{ES} = E_{ES}^{\text{ext}} + \sum_{a\mathbf{k}} \left(V_a^{\text{ext}} + \frac{1}{2} \varepsilon_a^h \right) \rho^{aa}(\mathbf{k}) \qquad (3.18)$$

is the electrostatic energy that comes from the direct Coulomb interaction of total charge distribution and will be calculated in the next section. The first term in Eq. (3.17) in general diverges again because the valence band energy goes to negative infinity for large $\mathbf{k}$ where the occupancy is always very close to 1. To remove this unphysical divergence, we introduce a new density matrix

$$\widetilde{\rho}^{aa'}(\mathbf{k}) \equiv \rho^{aa'}(\mathbf{k}) - \rho_0^{aa'}(\mathbf{k}) \qquad (3.19)$$

which goes to zero at large $\mathbf{k}$ because we subtract the density matrix of the no-carrier $|\Phi_0\rangle$ state. Let us define a new band energy and a new exchange energy that

correspond to this new density matrix:

$$\widetilde{\varepsilon}^{(0)}_{c\mathbf{k}} = \frac{\hbar k^2}{2m_c} \tag{3.20}$$

$$\widetilde{\varepsilon}^{(0)}_{v\mathbf{k}} = -\frac{\hbar k^2}{2m_v^*} - E_g \tag{3.21}$$

$$\widetilde{\varepsilon}^{ex}_{a\mathbf{k}} = -\frac{1}{\Omega} \sum_{\mathbf{k'}} V^{aa}(\mathbf{k} - \mathbf{k'}) \widetilde{\rho}^{aa}(\mathbf{k'}) \ . \tag{3.22}$$

Note that

$$\varepsilon^{(0)}_{a\mathbf{k}} + \varepsilon^{ex}_{a\mathbf{k}} = \widetilde{\varepsilon}^{(0)}_{a\mathbf{k}} + \widetilde{\varepsilon}^{ex}_{a\mathbf{k}} \tag{3.23}$$

does not change with the new choice of the new density matrix. Then the total energy minus the electrostatic energy becomes

$$
\begin{aligned}
&E_{\text{tot}}[\Psi_G] - E_{ES} \\
= \ & \sum_{a\mathbf{k}} \left(\varepsilon^{(0)}_{a\mathbf{k}} + \varepsilon^{ex}_{a\mathbf{k}} \right) \rho^{aa}(\mathbf{k}) - \frac{1}{2} \sum_{a\mathbf{k}} \varepsilon^{ex}_{a\mathbf{k}} \rho^{aa}(\mathbf{k}) - \frac{1}{2} \sum_{a\mathbf{k}} \left(\Delta_{\mathbf{k}} \rho^{vc}(\mathbf{k}) + c.c. \right) \\
= \ & \sum_{a\mathbf{k}} \left(\widetilde{\varepsilon}^{(0)}_{a\mathbf{k}} + \frac{1}{2} \widetilde{\varepsilon}^{ex}_{a\mathbf{k}} \right) \widetilde{\rho}^{aa}(\mathbf{k}) - \frac{1}{2} \sum_{a\mathbf{k}} \left(\Delta_{\mathbf{k}} \rho^{vc}(\mathbf{k}) + c.c. \right) + E_{\text{tot}}[\Phi_0] \tag{3.24}
\end{aligned}
$$

where

$$E_{\text{tot}}[\Phi_0] = \sum_{a\mathbf{k}} \widetilde{\varepsilon}^{(0)}_{a\mathbf{k}} \rho^{aa}_0(\mathbf{k}) + \frac{1}{2\Omega} \sum_{\mathbf{k'}} V^{aa}(\mathbf{k} - \mathbf{k'}) \rho^{aa}_0(\mathbf{k}) \rho^{aa}_0(\mathbf{k'}) \tag{3.25}$$

is the total energy of Φ_0. Then the divergence can be removed by subtracting $E_{\text{tot}}[\Phi_0]$ from the total energy. Therefore we have

$$
\begin{aligned}
&E_{\text{tot}}[\Psi_G] - E_{\text{tot}}[\Phi_0] \\
= \ & \sum_{a\mathbf{k}} \left(\widetilde{\varepsilon}^{(0)}_{a\mathbf{k}} + \frac{1}{2} \widetilde{\varepsilon}^{ex}_{a\mathbf{k}} \right) \widetilde{\rho}^{aa}(\mathbf{k}) - \frac{1}{2} \sum_{a\mathbf{k}} \left(\Delta_{\mathbf{k}} \rho^{vc}(\mathbf{k}) + c.c. \right) + E_{ES} \tag{3.26}
\end{aligned}
$$

which has finite value.

31

3.3 Calculation of Hartree Potential and Electrostatic Energy in Bilayer Systems

The Hartree potential defined as

$$\varepsilon_a^h = \frac{1}{\Omega} V^{aa'}(0) \sum_{a'\mathbf{k}} \rho^{a'a'}(\mathbf{k}) \tag{3.27}$$

gives

$$
\begin{aligned}
\varepsilon_c^h &= \lim_{q \to 0} \frac{2\pi e^2}{\epsilon q} \left(n_c + n_v e^{-qd} \right) \\
&= \lim_{q \to 0} \frac{2\pi e^2}{\epsilon q} \left(n_c - n_h e^{-qd} + n_0 e^{-qd} \right) \\
\varepsilon_v^h &= \lim_{q \to 0} \frac{2\pi e^2}{\epsilon q} \left(n_v + n_c e^{-qd} \right) \\
&= \lim_{q \to 0} \frac{2\pi e^2}{\epsilon q} \left(n_0 - n_h + n_c e^{-qd} \right)
\end{aligned}
\tag{3.28, 3.29}
$$

for the Coulomb interaction with dielectric constant ϵ where $n_c(n_v)$ is the electron density of conduction(valence) band, $n_h = n_0 - n_v$ is the hole density and n_0 is the total number of states per unit area in the valence band. This Hartree term is not well defined because $V^{aa'}(\mathbf{q})$ goes to infinity as q goes to zero. To remove this divergence, we have to include the Coulomb interaction with the background positive ions that maintain the overall charge neutrality. The external field V_a^{ext} which consists of the direct Coulomb interactions from ρ_L, ρ_R and the background charge en_0 in the hole layer can be formally written as

$$V_c^{\text{ext}} = -\lim_{q \to 0} \frac{2\pi e^2}{\epsilon q} \left(\frac{\rho_L}{e} e^{-qD} + \frac{\rho_R}{e} e^{-q(D+d)} + n_0 e^{-qD} \right) \tag{3.30}$$

$$V_v^{\text{ext}} = -\lim_{q \to 0} \frac{2\pi e^2}{\epsilon q} \left(\frac{\rho_L}{e} e^{-q(D+d)} + \frac{\rho_R}{e} e^{-qD} + n_0 \right) . \tag{3.31}$$

Then the total electrostatic field for the conduction band electrons is

$$
\begin{aligned}
\varepsilon_c^h + V_c^{\text{ext}} &= \lim_{q \to 0} \frac{2\pi e^2}{\epsilon q} \left(n_c - n_h e^{-qd} - n_L e^{-qD} - n_R e^{-q(D+d)} \right) \\
&= \frac{2\pi e^2}{\epsilon} \left(n_h d + n_L D + n_R(D+d) \right) \\
&= \frac{2\pi e^2 n_c d}{\epsilon} + \frac{2\pi e^2}{\epsilon} \left((n_c - n_h)(D-d) + n_R d \right) \\
&\equiv \frac{2\pi e^2 n_c d}{\epsilon} + \varepsilon_0
\end{aligned}
\tag{3.32}
$$

and for the valence band electrons,

$$
\begin{aligned}
\varepsilon_v^h + V_v^{\text{ext}} &= \lim_{q \to 0} \frac{2\pi e^2}{\epsilon q} \left(-n_h + n_c e^{-qd} - n_L e^{-q(D+d)} - n_R e^{-qD} \right) \\
&= \frac{2\pi e^2}{\epsilon} \left(-n_c d + n_L(D+d) + n_R D \right) \\
&= -\frac{2\pi e^2 n_h d}{\epsilon} + \frac{2\pi e^2}{\epsilon} \left((n_c - n_h)(D-d) + n_L d \right) \\
&= -\frac{2\pi e^2 n_h d}{\epsilon} + \varepsilon_0 + \frac{2\pi e^2}{\epsilon}(n_L - n_R)d \\
&\equiv -\frac{2\pi e^2 n_h d}{\epsilon} + \varepsilon_0 + \varepsilon_{v0} \ .
\end{aligned}
\tag{3.33}
$$

With fixed ρ_L and ρ_R, ε_0 is just a constant energy shift of both bands so we can set $\varepsilon_0 = 0$ and ε_{v0} determines the relative position of the conduction band minimum and the valence band maximum. Then we can define new Hartree potentials and external fields as

$$
\widetilde{\varepsilon}_c^h = \frac{2\pi e^2 n_c d}{\epsilon} \tag{3.34}
$$

$$
\widetilde{\varepsilon}_v^h = -\frac{2\pi e^2 n_h d}{\epsilon} \tag{3.35}
$$

$$
\widetilde{V}_c^{\text{ext}} = 0 \tag{3.36}
$$

$$
\widetilde{V}_v^{\text{ext}} = \varepsilon_{v0} \ . \tag{3.37}
$$

33

The total electrostatic energy E_{ES} includes the Coulomb interaction among charges in layer L, layer R and the positive background charge in layer B as well as the electrostatic energy of the electrons in both layers A and B.

$$\frac{E_{ES}}{\Omega} = \left(V_c^{\text{ext}} + \frac{1}{2}\varepsilon_c^h \right) n_c + \left(V_v^{\text{ext}} + \frac{1}{2}\varepsilon_c^v \right) n_c + \frac{E_{ES}^{\text{ext}}}{\Omega} \tag{3.38}$$

where

$$\frac{E_{ES}^{\text{ext}}}{\Omega} = \lim_{q \to 0} \frac{2\pi e^2}{\epsilon q} \left(\frac{n_L^2 + n_R^2 + n_0^2}{2} + n_L n_R e^{-q(2D+d)} + n_L n_0 e^{-q(D+d)} + n_R n_0 e^{-qD} \right) \tag{3.39}$$

and $n_L = \rho_L/e$, $n_R = \rho_R/e$. After some algebra we obtain

$$\begin{aligned} \frac{E_{ES}}{\Omega} &= \frac{1}{2}\frac{2\pi e^2 d}{\epsilon}\left(n_c^2 + n_h^2 \right) + \varepsilon_0(n_c - n_h) + \varepsilon_{v0}(-n_h) \\ &+ \frac{2\pi e^2 d}{\epsilon}\left(d\left(\frac{(n_c - n_h)^2}{2} - n_L n_R \right) - 2D n_L n_R \right) . \end{aligned} \tag{3.40}$$

With fixed ρ_L and ρ_R, and setting $\varepsilon_0 = 0$,

$$\frac{E_{ES}}{\Omega} = \frac{1}{2}\left(\widetilde{\varepsilon}_c^h n_c - \widetilde{\varepsilon}_v^h n_h \right) + \widetilde{V}_v^{\text{ext}}(-n_h) + \text{const.} \tag{3.41}$$

which can be obtained up to a constant by replacing ε_a^h, V_a^{ext} and ρ^{aa} in Eq. (3.18) with new ones in Eq. (3.34) $\sim$ Eq. (3.37),

$$E_{ES} = \sum_{a\mathbf{k}} \left(\widetilde{V}_a^{\text{ext}} + \frac{1}{2}\widetilde{\varepsilon}_a^h \right) \widetilde{\rho}^{aa}(\mathbf{k}) . \tag{3.42}$$

The total electrostatic energy can be calculated alternatively by solving the Poisson equation for the charge distribution in Fig. 3.1. Using Gauss theorem, we find the

electric field

$$
\begin{align}
E_L &= \frac{4\pi e}{\epsilon} n_L \tag{3.43} \\
E &= \frac{4\pi e}{\epsilon}(n_L - n_c) \tag{3.44} \\
E_R &= \frac{4\pi e}{\epsilon}(n_L - n_c + n_h) \; . \tag{3.45}
\end{align}
$$

We can see the difference of the electrostatic field in the conduction and the valence bands is the same with the difference in the Hartree field and the external field in Eq. (3.34) $\sim$ Eq. (3.37),

$$
\left(\widetilde{\varepsilon}_v^h + \widetilde{V}_v^{\text{ext}} \right) - \left(\widetilde{\varepsilon}_v^c + \widetilde{V}_c^{\text{ext}} \right) = \frac{4\pi e^2 d}{\epsilon}(n_L - n_c) = eEd \; . \tag{3.46}
$$

The total electrostatic energy is given by the integration

$$
\begin{align}
\frac{E_{ES}}{\Omega} &= \frac{1}{\Omega}\int d^3 \mathrm{r}\, \frac{1}{8\pi}\epsilon |\mathbf{E}|^2 \notag \\
&= \frac{2\pi e^2}{\epsilon}\left(d(n_L - n_c)^2 + D(n_L^2 + n_R^2) \right) \tag{3.47}
\end{align}
$$

which can be shown to be equal to Eq. (3.40) up to a constant.

3.4   Gap Equation

In this section we derive the gap equation for the bilayer system with equal densities of electrons and holes. The mean-field Hamiltonian in matrix form is,

$$
\widehat{H}_{MF} = \sum_{\mathbf{k}} \begin{pmatrix} c_{c\mathbf{k}}^\dagger & c_{v\mathbf{k}}^\dagger \end{pmatrix} \begin{pmatrix} \varepsilon_{c\mathbf{k}} & -\Delta_{\mathbf{k}} \\ -\Delta_{\mathbf{k}}^* & \varepsilon_{v\mathbf{k}} \end{pmatrix} \begin{pmatrix} c_{c\mathbf{k}} \\ c_{v\mathbf{k}} \end{pmatrix} \tag{3.48}
$$

where

$$
\varepsilon_{a\mathbf{k}} = \widetilde{\varepsilon}_{a\mathbf{k}}^{(0)} + \widetilde{V}_a^{\text{ext}} + \widetilde{\varepsilon}_a^h + \widetilde{\varepsilon}_{a\mathbf{k}}^{ex} \tag{3.49}
$$

35

with the definitions of new variables in the previous section. We can diagonalize the Hamiltonian $\widehat{H}_{MF}$ by introducing the new Fermi quasi-particle operators using a Bogoliubov transformation:

$$\widehat{H}_{MF} = \sum_{\mathbf{k}} \left(\begin{array}{cc} \alpha_{\mathbf{k}}^{\dagger} & \beta_{\mathbf{k}}^{\dagger} \end{array} \right) \left(\begin{array}{cc} \varepsilon_{\mathbf{k}}^{(1)} & 0 \\ 0 & \varepsilon_{\mathbf{k}}^{(2)} \end{array} \right) \left(\begin{array}{c} \alpha_{\mathbf{k}} \\ \beta_{\mathbf{k}} \end{array} \right) \tag{3.50}$$

where

$$\left(\begin{array}{c} \alpha_{\mathbf{k}} \\ \beta_{\mathbf{k}} \end{array} \right) = \left(\begin{array}{cc} u_{\mathbf{k}} & -v_{\mathbf{k}} \\ v_{\mathbf{k}}^* & u_{\mathbf{k}}^* \end{array} \right) \left(\begin{array}{c} c_{c\mathbf{k}} \\ c_{v\mathbf{k}} \end{array} \right) \tag{3.51}$$

$$\varepsilon_{\mathbf{k}}^{(1,2)} = \frac{1}{2}(\varepsilon_{c\mathbf{k}} + \varepsilon_{v\mathbf{k}}) \pm \sqrt{\varepsilon_{\mathbf{k}}^2 + |\Delta_{\mathbf{k}}|^2} \tag{3.52}$$

$$|u_{\mathbf{k}}|^2 = \frac{1}{2}\left(1 + \frac{\varepsilon_{\mathbf{k}}}{\sqrt{\varepsilon_{\mathbf{k}}^2 + |\Delta_{\mathbf{k}}|^2}} \right) \tag{3.53}$$

$$|v_{\mathbf{k}}|^2 = \frac{1}{2}\left(1 - \frac{\varepsilon_{\mathbf{k}}}{\sqrt{\varepsilon_{\mathbf{k}}^2 + |\Delta_{\mathbf{k}}|^2}} \right) \tag{3.54}$$

$$u_{\mathbf{k}}^* v_{\mathbf{k}} = \frac{\Delta_{\mathbf{k}}}{2\sqrt{\varepsilon_{\mathbf{k}}^2 + |\Delta_{\mathbf{k}}|^2}} \tag{3.55}$$

$$\varepsilon_{\mathbf{k}} = \frac{1}{2}\left(\varepsilon_{c\mathbf{k}} - \varepsilon_{v\mathbf{k}} \right) , \tag{3.56}$$

and the ground state is given by

$$|\Psi_G\rangle = \prod_{\mathbf{k}} \beta_{\mathbf{k}}^{\dagger}|0\rangle = \prod_{\mathbf{k}} \left(v_{\mathbf{k}} c_{c\mathbf{k}}^{\dagger} + u_{\mathbf{k}} c_{v\mathbf{k}}^{\dagger} \right) |0\rangle , \tag{3.57}$$

where $|0\rangle$ is the vacuum states. This canonical transformation is analogous to the canonical transformation of the BCS theory if we perform the electron-hole transformation to the valence band electrons. In conduction-valence band picture, these new fermion operators correspond to the superposition of the conduction band states

and valence band states that diagonalize the self-consistent mean-field Hamiltonian. In this language our mean-field calculation is just standard Hartree-Fock theory in which special care is required in how the electrostatic energy is treated to extract the finite energy of an electrically neutral system in a consistent way. We will consistently use conduction-valence band picture of electrons rather than the electron-hole picture throughout all the calculations for bilayer systems because it is easier to avoid confusions about how the cancelling Coulombic divergences are handled. The self-consistent gap equation at zero temperature is obtained from the definition of the inter-band exchange field,

$$
\begin{aligned}
\Delta_{\mathbf{k}} &= \frac{1}{\Omega} \sum_{\mathbf{k}'} V^{cv}(\mathbf{k} - \mathbf{k}') \langle c_{v\mathbf{k}'}^{\dagger} c_{c\mathbf{k}'} \rangle \\
&= \frac{1}{\Omega} \sum_{\mathbf{k}'} V^{cv}(\mathbf{k} - \mathbf{k}') u_{\mathbf{k}'}^{*} v_{\mathbf{k}'} \\
&= \frac{1}{\Omega} \sum_{\mathbf{k}'} V^{cv}(\mathbf{k} - \mathbf{k}') \frac{\Delta_{\mathbf{k}'}}{2\sqrt{\varepsilon_{\mathbf{k}'}^{2} + |\Delta_{\mathbf{k}'}|^{2}}} \ .
\end{aligned}
\tag{3.58}
$$

The total energy of the ground state is given by Eq. (3.26) and Eq. (3.42), with

$$
\widetilde{\rho}^{a'a}(\mathbf{k}) = \langle \Psi_G | c_{a\mathbf{k}}^{\dagger} c_{a'\mathbf{k}} | \Psi_G \rangle - \rho_0^{a'a}(\mathbf{k}) \ .
\tag{3.59}
$$

We numerically solve the gap equation [Eq. (3.58)] self-consistently for a system with an equal density of electrons and holes. The effective masses are $m_c = 0.067m_0$ and $m_v^* = 0.11m_0$. The inter-layer distance $d = 100\text{Å}$ and the dielectric constant $\epsilon = 13$ in the calculation. We choose the density difference $\Delta n = n_c - n_h$ and the initial band overlap $\mu_0 = \varepsilon_{v0} - E_g$ as two controllable parameters and set $\Delta n = 0$ for the following calculations. There is close analogy to the BCS theory for a superconductor and we obtain a similar energy spectrum with a gap [Fig.3.2]. The gap function $\Delta_{\mathbf{k}}$ has a maximum around the Fermi wave vector and it decreases as density increases [Fig.3.3]. At very high densities, the ground state converges to the
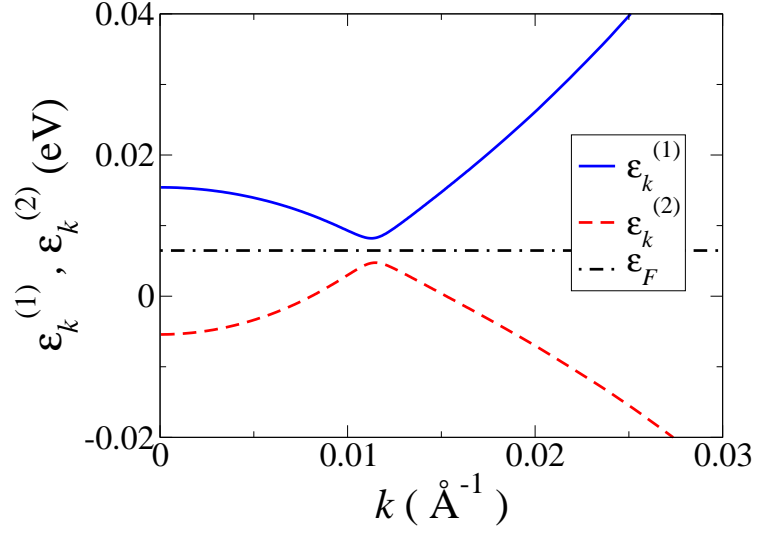
Figure 3.2: Excitation energy $\varepsilon_{\mathbf{k}}^{(1,2)}$ of a 2-band excitonic condensate. $\mu_0 = 10\text{meV}$ and $n_c - n_h = 0$. The calculated densities are $n_c = n_h = 1.0 \times 10^{11}\text{cm}^{-2}$. ε_F is the Fermi energy.
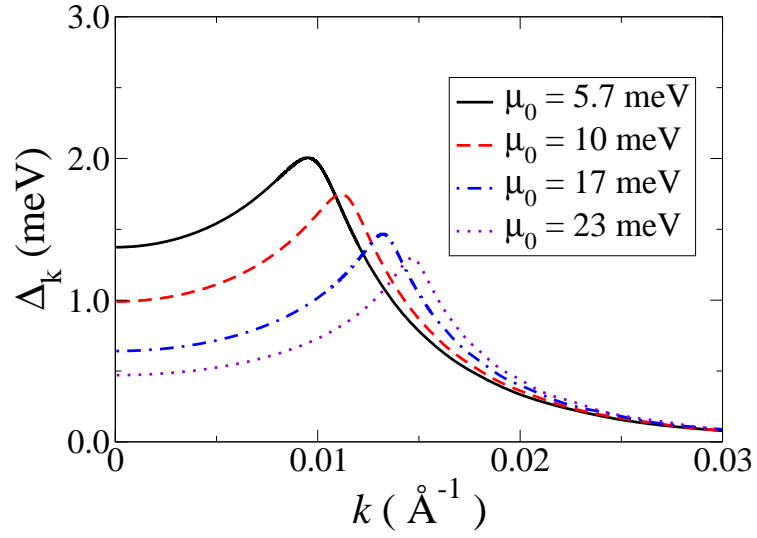
Figure 3.3: $\Delta_{\mathbf{k}}$ in the 2-band model for various μ_0 values. The calculated densities are $n = 0.8 \times 10^{11}\text{cm}^{-2}$, $1.0 \times 10^{11}\text{cm}^{-2}$, $1.4 \times 10^{11}\text{cm}^{-2}$ and $1.7 \times 10^{11}\text{cm}^{-2}$ for $\mu_0 = 5.7\text{meV}$ to 23meV, respectively.

electron-hole plasma state and the gap goes to zero. These results agree with the previous work by Zhu *et al* [78]. Even though the attractive interaction is now the Coulomb interaction rather than the BCS-like short range interaction[Eq. (2.35)], the gap function shows similar behavior, which implies that the pairing is most significant for electrons and holes near the Fermi surface.

Chapter 4

Ferromagnetic Excitonic Condensation

4.1 Introduction

In this chapter, we restore the spin degree of freedom in the bilayer systems to study its effects on excitonic condensation. In population polarized systems this additional degree of freedom plays an important role in realizing the ferromagnetic phase. The experimental observation of weak ferromagnetism in lightly doped divalent hexaborides [79] gave rise to some new interest in the ferromagnetic exciton condensate as a possible explanation for the experiment [80, 81, 82]. This ferromagnetism is driven by the condensation and has some unique symmetry properties related to the approximate spin-rotational symmetry of the microscopic Hamiltonian. The Rashba SO interaction that is caused by structural inversion asymmetry breaks this spin-rotational symmetry of the system and leads to more complicated magnetic symmetries.

In Sec. 4.2 we derive the mean-field Hamiltonian for the bilayer electron-hole system with spin degrees of freedom and discuss the validity of the mean-field theory

40

for different density regimes.. We then apply the mean-field theory to systems with an equal density of electrons and holes, allowing spin-polarization of each layer. In Sec. 4.3 we show that the ferromagnetic state can occur for population polarized condensate systems where electron and hole densities are different. In Sec. 4.4, we introduce the Rashba spin-orbit interaction and describe the effects of the Rashba interaction on the ferromagnetic exciton condensate in Sec. 4.5.

4.2   Mean-Field Hamiltonian

When we allow different number of spin-up and spin-down electrons in a two-dimensional system, the mean-field calculation generally overestimates the tendency towards spontaneous spin polarization [83]. At low densities the total energy of a completely spin-polarized state can be smaller than the energy of the spin-unpolarized paramagnetic state since the exchange energy dominates the kinetic energy. In the Hartree-Fock approximation the total energy of a two-dimensional electron system in a narrow quantum well is given by

$$\frac{E_{\text{tot}}(\chi)}{N_{\text{tot}}} = \frac{\varepsilon_{F0}}{4} \left((1+\chi)^2 + (1-\chi)^2 - \frac{16}{3\pi} \frac{1}{k_{F0}a_0} \left((1+\chi)^{3/2} + (1-\chi)^{3/2} \right) \right) \quad (4.1)$$

where N_{tot} is the total number of electrons in the system, ε_{F0} and k_{F0} are the Fermi energy and the Fermi wavevector of the unpolarized system, $a_0 = \epsilon\hbar^2/me^2$ and $\chi = (N_\uparrow - N_\downarrow)/N_{\text{tot}}$. ϵ is the dielectric constant. This mean-field total energy describes how the energy depends on the spin-polarization and the total density of the system. Fig. 4.1 shows the total energy as a function of the spin-polarization χ for various densities. At high densities[Fig. 4.1(a)], the kinetic energy is dominant and the spin-unpolarized state is the ground state and the only stable state against small spin-polarization. As we decrease the density, completely spin-polarized states begin to be energetically favored at the critical density[Fig. 4.1(c)] where $E_{\text{tot}}(\chi =$

41
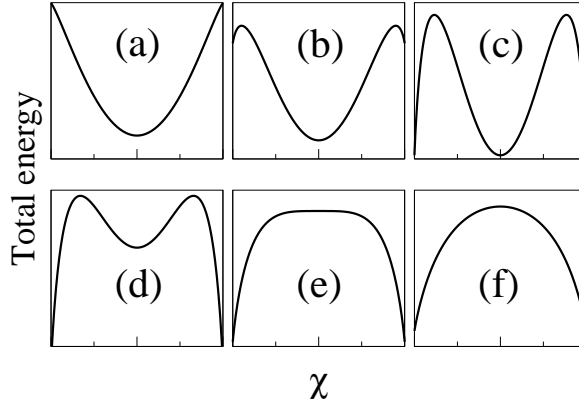
Figure 4.1: Total energy of the two-dimensional electron gas as a function of the spin-polarization χ for various densities under mean-field approximation. (a) is for $k_{F0}a_0$=1.0, (b) 0.75, (c) 0.7032, (d) 0.68, (e) 0.637 and (f) 0.55. (c) is where the completely spin-polarized state begins to have lower energy than the spin-unpolarized state. The critical density is determined by $k_{F0}a_0=16(\sqrt{2}-1)/3\pi$. (e) is where the paramagnetic state becomes unstable against a small polarization. The density is determined by $k_{F0}a_0=2/\pi$.

$1) = E_{\text{tot}}(\chi = 0)$, but the spin-unpolarized state is still stable against small spin-polarization until the density further decreases to Fig. 4.1(e) where $\partial^2 E_{\text{tot}}(\chi = 0)/\partial\chi^2$ begins to be negative. It is worth to note that the self-consistent mean-field solutions can be obtained for any locally stable state. Self-consistent solutions of the mean-field equations do not always yield the mean-field theory ground state. Therefore, it can describe the behavior of the spin-unpolarized states for wider range of densities, even below the critical density where the spin-polarized state is the ground state in the mean-field approximation. We expect this argument also applies to bilayer systems. For GaAs quantum wells which we use as our model system throughout the calculations, the effective masses are $m_c = 0.067m_0$ and $m_v^* = 0.11m_0$ where m_0 is the bare electron mass, and the dielectric constant $\epsilon = 13$. Then the critical densities for the conduction band electron gas is $n_c \simeq 7.5 \times 10^{10}\text{cm}^{-2}$ and for the heavy hole gas, $n_h \simeq 2.1 \times 10^{11}\text{cm}^{-2}$, but the instability

of the spin-unpolarized state begins at $n_c \simeq 6.1 \times 10^{10} \text{cm}^{-2}$ and $n_v \simeq 1.7 \times 10^{11} \text{cm}^{-2}$ respectively. If the density is larger than the density where the instability occurs, the mean-field calculation should describe, at least qualitatively, the behavior of the spin-unpolarized states, not the behavior of the spin-polarized states, unless we begin our iteration with a state with a large spin-polarization.

We now restore the spin degrees of freedom of the bilayer system from the previous chapter. All operators get additional spin index σ and then the total Hamiltonian is

$$
\begin{aligned}
\widehat{H} &= E_{ES}^{\text{ext}} + \sum_{a\sigma\mathbf{k}} \left(\varepsilon_{a\mathbf{k}}^{(0)} + V_a^{\text{ext}} \right) c_{a\sigma\mathbf{k}}^{\dagger} c_{a\sigma\mathbf{k}} \\
&\quad + \frac{1}{2\Omega} \sum_{\substack{\mathbf{kk'q} \\ aa'\sigma\sigma'}} V(\mathbf{q}) c_{a\sigma\mathbf{k}}^{\dagger} c_{a'\sigma'\mathbf{k'}}^{\dagger} c_{a'\sigma'\mathbf{k'}+\mathbf{q}} c_{a\sigma\mathbf{k}-\mathbf{q}} \; .
\end{aligned}
\tag{4.2}
$$

Using the mean-field approximation we obtain,

$$
\begin{aligned}
\widehat{H}_{MF} &= E_{ES}^{\text{ext}} + E_0 + \sum_{a\sigma\mathbf{k}} \left(\varepsilon_{a\mathbf{k}}^{(0)} + V_a^{\text{ext}} + \varepsilon_a^h + \mathrm{h}_{a\mathbf{k}}^{(0)} \right) c_{a\sigma\mathbf{k}}^{\dagger} c_{a\sigma\mathbf{k}} \\
&\quad + \sum_{a\sigma\sigma'\mathbf{k}} \left(\mathbf{h}_{a\mathbf{k}} \cdot \boldsymbol{\tau}_{\sigma\sigma'} \right) c_{a\sigma\mathbf{k}}^{\dagger} c_{a\sigma'\mathbf{k}} - \sum_{\sigma\sigma'\mathbf{k}} \left(\Delta_{\mathbf{k}}^{\sigma\sigma'} c_{c\sigma\mathbf{k}}^{\dagger} c_{v\sigma'\mathbf{k}} + h.c. \right)
\end{aligned}
\tag{4.3}
$$

where

$$
\begin{aligned}
E_0 &= -\frac{1}{2} \sum_{a\sigma\mathbf{k}} \left(\varepsilon_a^h + \mathrm{h}_{a\mathbf{k}}^{(0)} \right) \rho_{\sigma\sigma}^{aa}(\mathbf{k}) - \frac{1}{2} \sum_{a\sigma\sigma'\mathbf{k}} \left(\mathbf{h}_{a\mathbf{k}} \cdot \boldsymbol{\tau}_{\sigma\sigma'} \right) \rho_{\sigma'\sigma}^{aa}(\mathbf{k}) \\
&\quad + \frac{1}{2} \sum_{\sigma\sigma'\mathbf{k}} \left(\Delta_{\mathbf{k}}^{\sigma\sigma'} \rho_{\sigma'\sigma}^{vc}(\mathbf{k}) + c.c \right)
\end{aligned}
\tag{4.4}
$$

is the constant term that takes care of the double counting and

$$\varepsilon_a^h = \frac{1}{\Omega} V^{aa'}(0) \sum_{a'\sigma\mathbf{k}} \rho_{\sigma\sigma}^{a'a'}(\mathbf{k}) \tag{4.5}$$

$$\mathrm{h}_{a\mathbf{k}}^{(0)} = -\frac{1}{\Omega} \sum_{\sigma\mathbf{k}'} V^{aa}(\mathbf{k} - \mathbf{k}')\rho_{\sigma\sigma}^{aa}(\mathbf{k}') \tag{4.6}$$

$$\mathbf{h}_{a\mathbf{k}} = -\frac{1}{2\Omega} \sum_{\sigma\sigma'\mathbf{k}'} V^{aa}(\mathbf{k} - \mathbf{k}')\rho_{\sigma\sigma'}^{aa}(\mathbf{k}')\boldsymbol{\tau}_{\sigma'\sigma} \tag{4.7}$$

$$\Delta_\mathbf{k}^{\sigma\sigma'} = \frac{1}{\Omega} \sum_{\mathbf{k}'} V^{cv}(\mathbf{k} - \mathbf{k}')\rho_{\sigma\sigma'}^{cv}(\mathbf{k}') \tag{4.8}$$

$$\rho_{\sigma\sigma'}^{aa'}(\mathbf{k}) = \langle c_{a'\sigma'\mathbf{k}}^\dagger c_{a\sigma\mathbf{k}} \rangle . \tag{4.9}$$

Here $h_{a\mathbf{k}}^{(0)}$ is the spin-independent part of the intra-band exchange interaction, $\mathbf{h}_{a\mathbf{k}}$ is the intra-band exchange spin-splitting field and $\boldsymbol{\tau}$ is a vector whose components are Pauli spin matrices. As in the previous chapter where we use new density operators to remove the unphysical divergence that originates from the negative infinite valence band energy for large k, we define new density operators

$$\widetilde{\rho}_{\sigma\sigma'}^{aa'}(\mathbf{k}) = \rho_{\sigma\sigma'}^{aa'}(\mathbf{k}) - \langle c_{a'\sigma'\mathbf{k}}^\dagger c_{a\sigma\mathbf{k}} \rangle_0 \tag{4.10}$$

where $\langle ... \rangle_0$ means the expectation value with respect to the state

$$|\Phi_0\rangle \equiv \prod_{\sigma\mathbf{k}} c_{v\sigma\mathbf{k}}^\dagger |0\rangle , \tag{4.11}$$

where all the valence band states are occupied and all the conduction band states

are empty. Then we solve the mean-field Hamiltonian

$$\widehat{H}_{MF} = \left(\begin{array}{cccc} c^\dagger_{c\uparrow\mathbf{k}} & c^\dagger_{c\downarrow\mathbf{k}} & c^\dagger_{v\uparrow\mathbf{k}} & c^\dagger_{v\downarrow\mathbf{k}} \end{array}\right) \mathbf{H} \left(\begin{array}{c} c_{c\uparrow\mathbf{k}} \\ c_{c\downarrow\mathbf{k}} \\ c_{v\uparrow\mathbf{k}} \\ c_{v\downarrow\mathbf{k}} \end{array}\right) \tag{4.12}$$

where

$$\mathbf{H} = \left(\begin{array}{cccc} \varepsilon_{c\mathbf{k}} + \widetilde{\mathrm{h}}^z_{c\mathbf{k}} & \widetilde{\mathrm{h}}^x_{c\mathbf{k}} - i\widetilde{\mathrm{h}}^y_{c\mathbf{k}} & -\Delta^{\uparrow\uparrow}_{\mathbf{k}} & -\Delta^{\uparrow\downarrow}_{\mathbf{k}} \\ \widetilde{\mathrm{h}}^x_{c\mathbf{k}} + i\widetilde{\mathrm{h}}^y_{c\mathbf{k}} & \varepsilon_{c\mathbf{k}} - \widetilde{\mathrm{h}}^z_{c\mathbf{k}} & -\Delta^{\downarrow\uparrow}_{\mathbf{k}} & -\Delta^{\downarrow\downarrow}_{\mathbf{k}} \\ -\Delta^{*\uparrow\uparrow}_{\mathbf{k}} & -\Delta^{*\downarrow\uparrow}_{\mathbf{k}} & \varepsilon_{v\mathbf{k}} + \widetilde{\mathrm{h}}^z_{v\mathbf{k}} & \widetilde{\mathrm{h}}^x_{v\mathbf{k}} - i\widetilde{\mathrm{h}}^y_{v\mathbf{k}} \\ -\Delta^{*\uparrow\downarrow}_{\mathbf{k}} & -\Delta^{*\downarrow\downarrow}_{\mathbf{k}} & \widetilde{\mathrm{h}}^x_{v\mathbf{k}} + i\widetilde{\mathrm{h}}^y_{v\mathbf{k}} & \varepsilon_{v\mathbf{k}} - \widetilde{\mathrm{h}}^z_{v\mathbf{k}} \end{array}\right) \tag{4.13}$$

is a matrix representation of the mean-field Hamiltonian. The entries that appear in Eq. (4.13) are defined by the following expressions:

$$\varepsilon_{a\mathbf{k}} = \widetilde{\varepsilon}^{(0)}_{a\mathbf{k}} + \widetilde{V}^{\text{ext}}_a + \widetilde{\varepsilon}^h_a + \widetilde{\mathrm{h}}^{(0)}_{a\mathbf{k}} \tag{4.14}$$

$$\widetilde{V}^{\text{ext}}_c = 0 \tag{4.15}$$

$$\widetilde{V}^{\text{ext}}_v = \varepsilon_{v0} \tag{4.16}$$

$$\widetilde{\varepsilon}^h_c = \frac{2\pi e^2 n_c d}{\epsilon} \tag{4.17}$$

$$\widetilde{\varepsilon}^h_v = -\frac{2\pi e^2 n_h d}{\epsilon} \tag{4.18}$$

$$\widetilde{\varepsilon}^{(0)}_{c\mathbf{k}} = \frac{\hbar k^2}{2m_c} \tag{4.19}$$

$$\widetilde{\varepsilon}^{(0)}_{v\mathbf{k}} = -\frac{\hbar k^2}{2m^*_v} - E_g \tag{4.20}$$

$$\widetilde{\mathrm{h}}^{(0)}_{a\mathbf{k}} = -\frac{1}{\Omega} \sum_{\sigma\mathbf{k}'} V^{aa}(\mathbf{k} - \mathbf{k}') \widetilde{\rho}^{aa}_{\sigma\sigma}(\mathbf{k}') \tag{4.21}$$

$$\widetilde{\mathbf{h}}_{a\mathbf{k}} = -\frac{1}{\Omega} \sum_{\sigma\sigma'\mathbf{k}'} V^{aa}(\mathbf{k} - \mathbf{k}') \widetilde{\rho}^{aa}_{\sigma\sigma'}(\mathbf{k}') \boldsymbol{\tau}_{\sigma\sigma'} \; . \tag{4.22}$$

The total energy of the ground state Ψ_G is given by

$$
\begin{aligned}
E_{\text{tot}}[\Psi_G] &- E_{\text{tot}}[\Phi_0] \\
&= E_{ES} + \sum_{a\sigma\mathbf{k}} \left(\widetilde{\varepsilon}_{a\mathbf{k}}^{(0)} + \frac{1}{2}\widetilde{\mathrm{h}}_{a\mathbf{k}}^{(0)} \right) \widetilde{\rho}_{\sigma\sigma}^{aa}(\mathbf{k}) \\
&+ \frac{1}{2} \sum_{a\sigma\sigma'\mathbf{k}} \left(\widetilde{\mathbf{h}}_{a\mathbf{k}} \cdot \boldsymbol{\tau}_{\sigma\sigma'} \right) \widetilde{\rho}_{\sigma'\sigma}^{aa}(\mathbf{k}) - \frac{1}{2} \sum_{\sigma\sigma'\mathbf{k}} \left(\Delta_{\mathbf{k}}^{\sigma\sigma'} \widetilde{\rho}_{\sigma'\sigma}^{vc}(\mathbf{k}) + c.c \right)
\end{aligned}
\tag{4.23}
$$

where the electrostatic energy is

$$
E_{ES} = \sum_{a\sigma\mathbf{k}} \left(\widetilde{V}_a^{\text{ext}} + \frac{1}{2}\widetilde{\varepsilon}_a^h \right) \widetilde{\rho}_{\sigma\sigma}^{aa}(\mathbf{k}) \ ,
\tag{4.24}
$$

as derived in the previous chapter.

Unlike the 2-band model, the diagonalization of this $4{\times}4$ matrix is not trivial. We numerically diagonalize this matrix self-consistently, which is equivalent to solving a generalized Hartree-Fock equation of the system allowing coherence between conduction and valence bands, as well as the spontaneous intra-band spin polarization. We use $\mu_0 = \varepsilon_{v0} - E_g$ and $\Delta n = n_c - n_h$ as two parameters for the numerical calculations. We choose the inter-layer distance $d = 100$Å. With same number of electrons and holes the essential physics does not change except that we get doubly degenerate bands (The effective magnetic field due to the intra-band exchange term $\widetilde{\mathbf{h}}_{a\mathbf{k}}$ disappears in this case). Fig. 4.2 shows the eigenvalues of the Hartree-Fock matrix which are the quasi-particle excitation energies. Each quasi-particle band is doubly degenerate as expected. Note that the hole density n_h is below the critical density where the hole gas would be completely spin-polarized. One reason the spin-polarization does not occur is the stability of the spin-unpolarized state as mentioned before, and another reason is the coherence between the conduction and valence bands favors spin-unpolarized states because the Fermi surfaces are equal for spin-unpolarized systems while they would be drastically different for
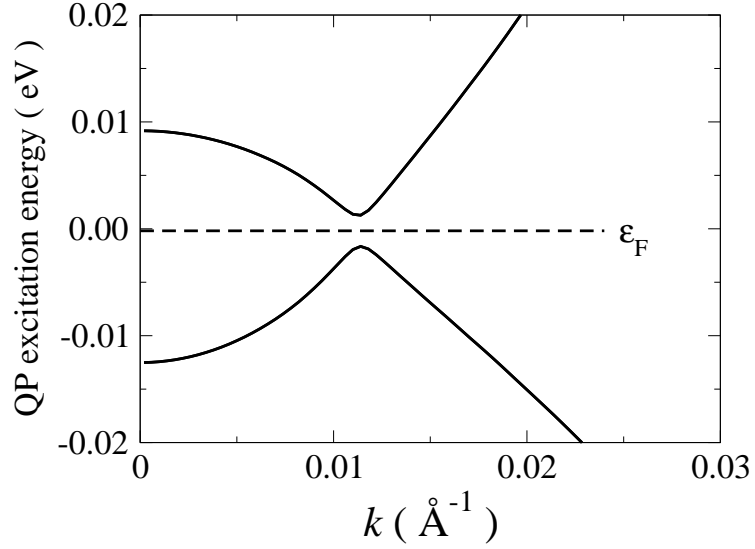
Figure 4.2: Quasi-particle excitation energy for an excitonic condensate state with $\mu_0 = 25\text{meV}$ and $\Delta n = 0$. The calculated densities are $n_c = n_h = 2.04 \times 10^{11}\text{cm}^{-2}$.

the spin-unpolarized electron gas and the spin-polarized hole gas, hence making the condensation more difficult.

4.3   Ferromagnetism of Population Polarized States

If we have different densities of electrons and holes, the Fermi surfaces of the conduction band and the valence band have different Fermi wave vectors and we have two competing effects due to this mismatch. First, the inter-band coherence favors both bands having exactly the same Fermi surfaces to maximize the energy gain by the condensation. Fermi surface matching can be restored for one conduction-valence band pair by splitting the spin-degenerate bands so that one conduction-valence band pair forms a condensed state and the other pair remains in the normal state. On the other hand, this spin-polarization causes the kinetic energy to increase. Therefore, for not so large population polarizations, we expect to have spontaneous

spin polarization which leads to a ferromagnetic excitonic condensate state. See Fig. 4.3 for an illustrative explanation. Fig. 4.4 shows the quasi-particle excitation energy spectrum for a system with number polarization for $\mu_0 = 25\text{meV}$ and $\Delta n = 5.0 \times 10^{10}\text{cm}^{-2}$. The splitting of the spin degeneracy indeed occurs and one pair of bands shows an energy gap due to the condensation and the other pair shows no such energy gap which indicates they are in the normal state. Since the valence band effective mass is larger than the conduction band effective mass, the splitting in the valence band is much larger than that of the conduction band to minimize the kinetic energy cost.

In bulk samples, there is a small overlap of electron and hole wave functions which is usually neglected(dominant term approximation). If this small overlap cannot be neglected, it gives nonzero electron-hole exchange interactions. When these exchange interactions are ignored, the Hamiltonian is invariant under independent spin-rotations in the two bands. When they are included it is invariant only under simultaneous spin-rotations and it favors spin triplet states [84]. In bilayer systems, the overlap is exponentially small and we can neglect it for large enough inter-layer distances or for high enough barriers between the two layers. Since we neglect the small overlap the interaction conserves the band indices. Therefore the system has the spin-rotational symmetry for each band and this SU(2)×SU(2) symmetry leads to the degeneracy of spin singlet and triplet states. The terms in the Hamiltonian that break this continuous symmetry are extremely small compared to the bulk case. Thus we have infinitely degenerate ground states which differ only in the direction of the spontaneous magnetization of each layer. This family of ground states have the same magnitude of magnetization for each layer but total magnetization magnitudes are in general different depending on the configuration of the magnetization directions of each layer. The intra-layer interaction $\widetilde{\mathbf{h}}_{a\mathbf{k}}$ plays an important role here to stabilize the ferromagnetic state since it favors spin polarized state. As mentioned
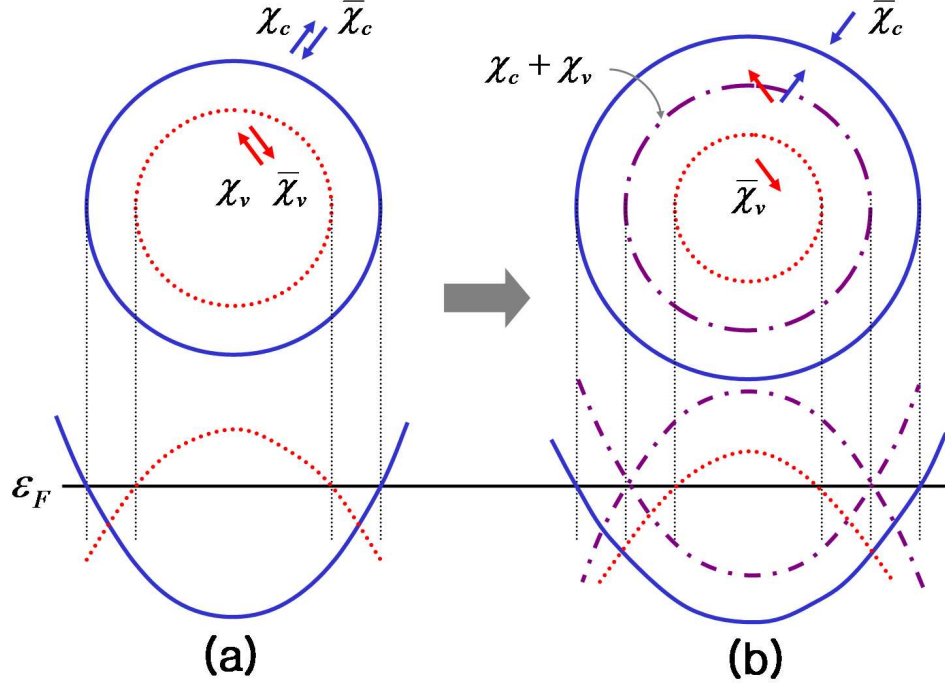
Figure 4.3: Schematic diagram of the Fermi surfaces and the energy bands for the spontaneous spin splitting in ferromagnetic exciton condensates. (a) For different number of electrons and holes, the conduction band Fermi surface(solid blue circle) does not coincide with the valence band Fermi surface (dotted red circle). (b) Conduction band electrons with spin χ_c flip to spin state $\bar{\chi}_c$ so the Fermi surface of χ_c electrons shrinks and the Fermi surface of $\bar{\chi}_c$ electrons expands. Similarly, χ_v valence band electrons flip to $\bar{\chi}_v$ state so that the Fermi surface of the χ_v electrons increases until it matches the χ_c Fermi surface. The $\chi_c$conduction band and χ_v valence band electrons (dot-dashed violet circle in the middle) then condense to form excitonic condensates while the $\bar{\chi}_c$ and $\bar{\chi}_v$ electrons remain in the normal state. The spin repopulation necessary to achieve Fermi surface nesting leads to ferromagnetism, i.e. to spontaneous spin polarization.
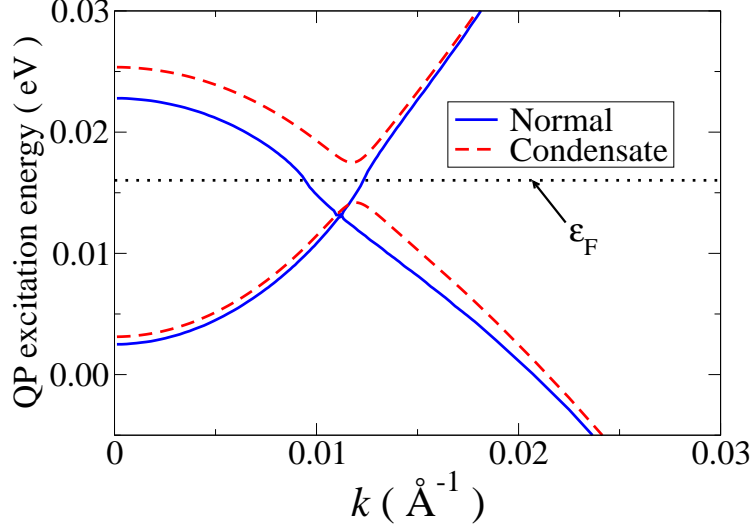
Figure 4.4: Quasi-particle excitation energy for a ferromagnetic condensate state with $\mu_0 = 25$meV and $\Delta n = n_c - n_h = 5.0 \times 10^{10}$cm^{-2}. The calculated densities are $n_c = 2.33 \times 10^{11}$cm^{-2} and $n_h = 1.83 \times 10^{11}$cm^{-2}.

previously the mean-field theory overestimates the stability of the ferromagnetic state for the normal electron systems. This is true in bilayer electron-hole systems as well. It is problematic particularly in very low density regimes, but it is likely not as large an issue in the density regimes we consider here. To verify that really only one pair of bands forms a condensate and the other pair remains normal, we change the spin basis states from spin-up and spin-down to χ_c and $\bar{\chi}_c$ for the conduction bands and χ_v and $\bar{\chi}_v$ for the valence bands. These new quantization directions can be determined by the total magnetization of each layer, because the magnetization and the spin direction of the electrons participating in the condensation are the same. Let the magnetization for the conduction (valence) band has polar angle θ_c (θ_v) and azimuthal angle ϕ_c (ϕ_v). We define a unitary operator $U_a^\dagger$ that connects the two spin bases,

$$\begin{pmatrix} c_{a\chi_a} \\ c_{a\bar{\chi}_a} \end{pmatrix} = U_a^\dagger \begin{pmatrix} c_{a\uparrow} \\ c_{a\downarrow} \end{pmatrix} \tag{4.25}$$

where

$$U_a^\dagger = \begin{pmatrix} \cos\frac{\theta_a}{2} & \sin\frac{\theta_a}{2}e^{-i\phi_a} \\ \sin\frac{\theta_a}{2} & -\cos\frac{\theta_a}{2}e^{-i\phi_a} \end{pmatrix} \tag{4.26}$$

for $a=c,v$. The order parameters in the new basis are

$$
\begin{aligned}
\Delta_\mathbf{k}^{\alpha_c\alpha_v} &= \frac{1}{\Omega}\sum_{\mathbf{k}'}V^{cv}(\mathbf{k}-\mathbf{k}')\langle c_{v\alpha_v\mathbf{k}'}^\dagger c_{c\alpha_c\mathbf{k}'}\rangle \\
&= \frac{1}{\Omega}\sum_{\mathbf{k}'}V^{cv}(\mathbf{k}-\mathbf{k}')\left(U_v^\dagger\right)_{\alpha_v\sigma_v}^* \left(U_c^\dagger\right)_{\alpha_c\sigma_c}\langle c_{v\sigma_v\mathbf{k}'}^\dagger c_{c\sigma_c\mathbf{k}'}\rangle \\
&= \left(U_c^\dagger\right)_{\alpha_c\sigma_c}\Delta_\mathbf{k}^{\sigma_c\sigma_v}\left(U_v\right)_{\sigma_v\alpha_v}
\end{aligned}
\tag{4.27}
$$

where α_a is χ_a or $\bar{\chi}_a$ and σ_a is spin up or down. Hence we obtain,

$$\begin{pmatrix} \Delta_\mathbf{k}^{\chi_c\chi_v} & \Delta_\mathbf{k}^{\chi_c\bar{\chi}_v} \\ \Delta_\mathbf{k}^{\bar{\chi}_c\chi_v} & \Delta_\mathbf{k}^{\bar{\chi}_c\bar{\chi}_v} \end{pmatrix} = U_c^\dagger \begin{pmatrix} \Delta_\mathbf{k}^{\uparrow\uparrow} & \Delta_\mathbf{k}^{\uparrow\downarrow} \\ \Delta_\mathbf{k}^{\downarrow\uparrow} & \Delta_\mathbf{k}^{\downarrow\downarrow} \end{pmatrix} U_v \ . \tag{4.28}$$

Only $\Delta^{\chi_c\chi_v}$ is nonzero and all the other order parameters are zero[Fig. 4.5] in the new basis, which verifies that only χ_c and χ_v spin bands form a condensate. The Hamiltonian can now be separated into normal part and condensation part.

$$\widehat{H}_{MF} = \widehat{H}_N + \widehat{H}_C \tag{4.29}$$

where

$$\widehat{H}_N = \sum_\mathbf{k}\left(c_{c\bar{\chi}_c\mathbf{k}}^\dagger \ c_{v\bar{\chi}_v\mathbf{k}}^\dagger\right)\begin{pmatrix} \varepsilon_{c\mathbf{k}}-\widetilde{\mathrm{h}}_{c\mathbf{k}}^{\chi_c} & 0 \\ 0 & \varepsilon_{v\mathbf{k}}-\widetilde{\mathrm{h}}_{v\mathbf{k}}^{\chi_v} \end{pmatrix}\begin{pmatrix} c_{c\bar{\chi}_c\mathbf{k}} \\ c_{v\bar{\chi}_v\mathbf{k}} \end{pmatrix} \tag{4.30}$$

$$\widehat{H}_C = \sum_\mathbf{k}\left(c_{c\chi_c\mathbf{k}}^\dagger \ c_{v\chi_v\mathbf{k}}^\dagger\right)\begin{pmatrix} \varepsilon_{c\mathbf{k}}+\widetilde{\mathrm{h}}_{c\mathbf{k}}^{\chi_c} & -\Delta_\mathbf{k} \\ -\Delta_\mathbf{k}^* & \varepsilon_{v\mathbf{k}}+\widetilde{\mathrm{h}}_{v\mathbf{k}}^{\chi_v} \end{pmatrix}\begin{pmatrix} c_{c\chi_c\mathbf{k}} \\ c_{v\chi_v\mathbf{k}} \end{pmatrix} , \tag{4.31}$$

and $\widetilde{\mathrm{h}}_{a\mathbf{k}}^{\chi_a}$ is the χ_a-parallel component of the intra-layer exchange field in the new
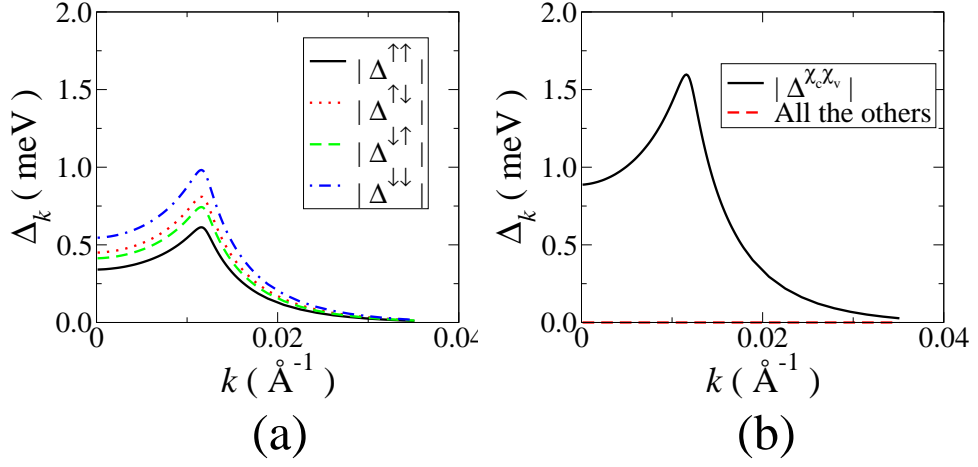
Figure 4.5: The magnitudes of $\Delta_{\mathbf{k}}$ in different spin bases. (a) is in the spin up and down basis and (b) is in the new basis where the spin quantization direction is chosen to be parallel to the calculated total magnetization of each layer. In the new basis, the only non-vanishing Δ is $\Delta^{\chi_c \chi_v}$.

spin basis, which is the only non-vanishing component of the exchange field. The condensate part can be diagonalized using the Bogoliubov transformation as in the 2-band model studied in the previous chapter, which leads to the eigenstates

$$|1\mathbf{k}\rangle = |c\bar{\chi}_c\mathbf{k}\rangle \tag{4.32}$$

$$|2\mathbf{k}\rangle = |v\bar{\chi}_v\mathbf{k}\rangle \tag{4.33}$$

$$|3\mathbf{k}\rangle = u_{\mathbf{k}}^*|c\chi_c\mathbf{k}\rangle - v_{\mathbf{k}}^*|v\chi_v\mathbf{k}\rangle \tag{4.34}$$

$$|4\mathbf{k}\rangle = v_{\mathbf{k}}|c\chi_c\mathbf{k}\rangle + u_{\mathbf{k}}|v\chi_v\mathbf{k}\rangle \tag{4.35}$$

with eigenvalues

$$\varepsilon_{1\mathbf{k}} = \varepsilon_{c\mathbf{k}} - \widetilde{h}_{c\mathbf{k}}^{\chi_c} \tag{4.36}$$

$$\varepsilon_{2\mathbf{k}} = \varepsilon_{v\mathbf{k}} - \widetilde{h}_{v\mathbf{k}}^{\chi_v} \tag{4.37}$$

$$\varepsilon_{3\mathbf{k}} = E_{\mathbf{k}}^{(1)} \tag{4.38}$$

$$\varepsilon_{4\mathbf{k}} = E_{\mathbf{k}}^{(2)} \tag{4.39}$$

where

$$E_{\mathbf{k}}^{(1,2)} = \frac{1}{2}\left(\varepsilon_{c\mathbf{k}} + \varepsilon_{v\mathbf{k}} + \widetilde{h}_{c\mathbf{k}}^{\chi_c} + \widetilde{h}_{v\mathbf{k}}^{\chi_v}\right) \pm \sqrt{\varepsilon_{\mathbf{k}}^2 + |\Delta_{\mathbf{k}}|^2} \tag{4.40}$$

$$\varepsilon_{\mathbf{k}} = \frac{1}{2}\left(\varepsilon_{c\mathbf{k}} - \varepsilon_{v\mathbf{k}} + \widetilde{h}_{c\mathbf{k}}^{\chi_c} - \widetilde{h}_{v\mathbf{k}}^{\chi_v}\right) \tag{4.41}$$

and

$$|u_{\mathbf{k}}|^2 = \frac{1}{2}\left(1 + \frac{\varepsilon_{\mathbf{k}}}{\sqrt{\varepsilon_{\mathbf{k}}^2 + |\Delta_{\mathbf{k}}|^2}}\right) \tag{4.42}$$

$$|v_{\mathbf{k}}|^2 = \frac{1}{2}\left(1 - \frac{\varepsilon_{\mathbf{k}}}{\sqrt{\varepsilon_{\mathbf{k}}^2 + |\Delta_{\mathbf{k}}|^2}}\right) \tag{4.43}$$

$$u_{\mathbf{k}}^* v_{\mathbf{k}} = \frac{\Delta_{\mathbf{k}}}{2\sqrt{\varepsilon_{\mathbf{k}}^2 + |\Delta_{\mathbf{k}}|^2}} . \tag{4.44}$$

The ground state $|\Psi_G\rangle$ is given by

$$|\Psi_G\rangle = \prod_{k<k_{Fc}} c_{1\mathbf{k}}^\dagger \prod_{k>k_{Fv}} c_{2\mathbf{k}}^\dagger \prod_{\mathbf{k}} c_{4\mathbf{k}}^\dagger |0\rangle \tag{4.45}$$

where $|0\rangle$ is the vacuum state with no electrons and k_{Fc} (k_{Fv}) is the fermi wavevector for the normal conduction(valence) band.

When the density difference is very small, the pair of bands with different

53

Fermi surfaces can also form a condensate and the spin repopulation would be readjust to minimize the total energy. On the other hand if the density difference is very large, the kinetic energy cost accompanying the spin repopulation will be larger than the condensation energy gain. Then there will be no condensation at all and the system will remain in the normal paramagnetic state. In between we have the mixed state where one pair of bands forms a condensate and the other pair remains normal.

4.4   Rashba SO Interaction

In 2D layers, the Rashba SO interaction appears due to the structural inversion asymmetry of the confining potential. The strength of the SO coupling can be tuned by applying an external electric field perpendicular to the layers [74, 75, 76, 77]. The Rashba Hamiltonian can be derived using Löwdin perturbation theory [85, 86] up to the third order [87] (see Appendix A for an explicit derivation of the Rashba Hamiltonian). The effective Rashba SO interactions for the conduction band and the heavy hole valence band are respectively

$$
\begin{aligned}
\widehat{H}_c^R &= \alpha \mathbf{k} \times \hat{z} \cdot \vec{\tau} \\
&= \alpha \begin{pmatrix} 0 & ike^{-i\phi_{\mathbf{k}}} \\ -ike^{i\phi_{\mathbf{k}}} & 0 \end{pmatrix} \\
&= \mathbf{h}_{\mathbf{ck}}^R \cdot \boldsymbol{\tau}
\end{aligned}
\tag{4.46}
$$

and

$$
\begin{aligned}
\widehat{H}_{hh}^R &= i\beta(\tau_+ k_-^3 + \tau_- k_+^3) \\
&= \beta \begin{pmatrix} 0 & ik^3 e^{-i3\phi_{\mathbf{k}}} \\ -ik^3 e^{i3\phi_{\mathbf{k}}} & 0 \end{pmatrix} \\
&= \mathbf{h}_{v\mathbf{k}}^R \cdot \boldsymbol{\tau}
\end{aligned}
\tag{4.47}
$$

where τ's are the Pauli matrices, $\tau_\pm = 1/2(\tau_x \pm i\tau_y)$, $k_\pm = k_x \pm ik_y$ and $\tan\phi_{\mathbf{k}} = k_y/k_x$. The effective magnetic fields due to the Rashba SO interaction are defined by

$$
\mathbf{h}_{c\mathbf{k}}^R = \alpha\left(k_y\hat{\mathbf{x}} - k_x\hat{\mathbf{y}}\right)
\tag{4.48}
$$

$$
\mathbf{h}_{v\mathbf{k}}^R = \beta k^3\left(\sin 3\phi_{\mathbf{k}}\hat{\mathbf{x}} - \cos 3\phi_{\mathbf{k}}\hat{\mathbf{y}}\right)
\tag{4.49}
$$

which changes direction in spin-space as the direction changes in momentum space (see Fig. 4.6(a) and Fig. 4.7(a)). For the conduction band, the energy dispersion gets an additional linear term $\varepsilon_{c\mathbf{k}}^{(\pm)} = \varepsilon_{c\mathbf{k}}^{(0)} \pm \alpha k$ and the corresponding spin states are

$$
|c\mathbf{k}\pm\rangle = \frac{1}{\sqrt{2}}\left(|c\mathbf{k}\uparrow\rangle \mp ie^{i\phi_{\mathbf{k}}}|c\mathbf{k}\downarrow\rangle\right)
\tag{4.50}
$$

which are shown in Fig. 4.6(b). For the heavy hole valence band, we get an additional term proportional to k^3, $\varepsilon_{v\mathbf{k}}^{(\pm)} = \varepsilon_{c\mathbf{k}}^{(0)} \pm \beta k^3$ and the corresponding spin states are

$$
|v\mathbf{k}\pm\rangle = \frac{1}{\sqrt{2}}\left(|v\mathbf{k}\uparrow\rangle \mp ie^{3i\phi_{\mathbf{k}}}|v\mathbf{k}\downarrow\rangle\right)
\tag{4.51}
$$

which are shown in Fig. 4.7(b).

Unlike the electron gas without Rashba SO interactions, the ground state of the free electron gas does not solve the Hartree-Fock equation of the system with Rashba SO interaction. The spin states for each $\mathbf{k}$ is determined by the total effective
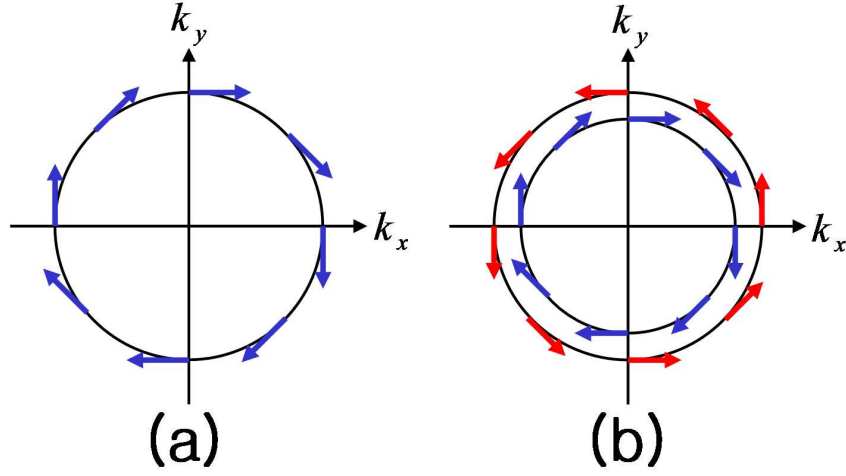
Figure 4.6: (a) Rashba SO effective magnetic field $\mathbf{h}_{c\mathbf{k}}^R$ and (b) the spin states for the conduction band. The spin direction is $\phi_{\mathbf{k}} - \pi/2$ for $|c\mathbf{k}+\rangle$(inner circle and blue arrows) and $\phi_{\mathbf{k}} + \pi/2$ for $|c\mathbf{k}-\rangle$(outer circle and red arrows).
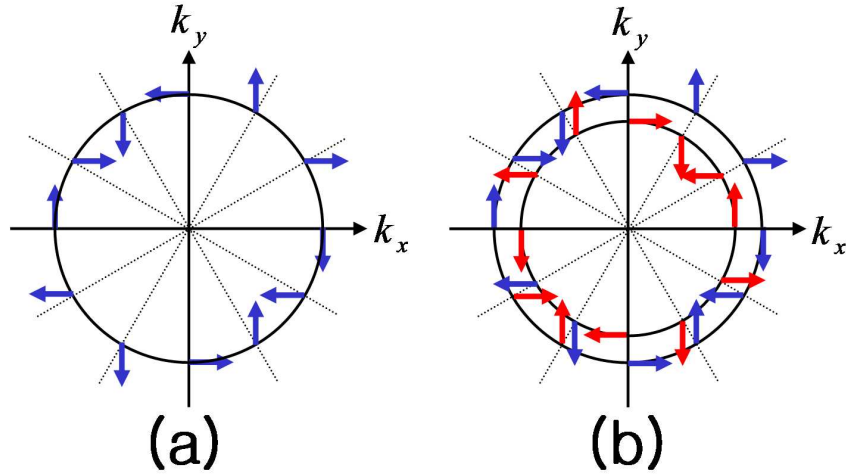
Figure 4.7: (a) Rashba SO effective magnetic field $\mathbf{h}_{v\mathbf{k}}^R$ and (b) the spin states for the heavy hole valence band. The spin direction is $3\phi_{\mathbf{k}} - \pi/2$ for $|v\mathbf{k}+\rangle$(outer circle and blue arrows) and $3\phi_{\mathbf{k}} + \pi/2$ for $|v\mathbf{k}-\rangle$(inner circle and red arrows).

magnetic field $\mathbf{h}_{a\mathbf{k}}^{\text{eff}}$ consisting of the intra-band exchange field $\widetilde{\mathbf{h}}_{a\mathbf{k}}$ and the Rashba SO field $\mathbf{h}_a^R$. For higher energy band with energy $\varepsilon_{a\mathbf{k}}^{(+)} = \varepsilon_{a\mathbf{k}} + |\mathbf{h}_{a\mathbf{k}}^{\text{eff}}|$, the spin state is parallel to the total effective magnetic field and for lower energy band with energy $\varepsilon_{a\mathbf{k}}^{(-)} = \varepsilon_{a\mathbf{k}} - |\mathbf{h}_{a\mathbf{k}}^{\text{eff}}|$, the spin state is antiparallel to the total effective magnetic field. The self-consistency conditions for the intra-band exchange field then lead to

$$\widetilde{\mathbf{h}}_{a\mathbf{k}} = -\frac{1}{2\Omega} \sum_{\mathbf{k}'} V\left(\mathbf{k} - \mathbf{k}'\right) \frac{\mathbf{h}_{a\mathbf{k}'}^{\text{eff}}}{|\mathbf{h}_{a\mathbf{k}'}^{\text{eff}}|} \left(\widetilde{\rho}_{++}^{aa} - \widetilde{\rho}_{--}^{aa}\right) \ , \tag{4.52}$$

where the spinor of the state $|a\mathbf{k}\pm\rangle$ is parallel(+) or antiparallel(-) to the total effective field $\mathbf{h}_{a\mathbf{k}}^{\text{eff}}$, not just the Rashba field. The total spin $\mathbf{S}_a$ of band a is given by

$$\mathbf{S}_a = \frac{1}{2} \sum_{\mathbf{k}} \frac{\mathbf{h}_{a\mathbf{k}}^{\text{eff}}}{|\mathbf{h}_{a\mathbf{k}}^{\text{eff}}|} \left(\widetilde{\rho}_{++}^{aa}(\mathbf{k}') - \widetilde{\rho}_{--}^{aa}(\mathbf{k}')\right) \ . \tag{4.53}$$

4.5 Effects of SO Interaction on Ferromagnetic Exciton Condensates

The Rashba SO Hamiltonian breaks the spin-rotational symmetry around an arbitrary axis, but keeps the symmetry of simultaneous spin and orbital rotations around z-direction and the inversion symmetry $z \to -z$. Thus we expect the total spin of the ferromagnetic exciton condensate has a fixed polar angle θ_a or $\pi - \theta_a$ but the total energy is the same for states with different azimuthal angle ϕ_a. In addition the conduction band magnetization and the valence band magnetization are no longer independent. In spin-degenerate systems, we can increase the Fermi surface of one spin species and decrease the other by simply repopulating the spins as described previously. In systems with Rashba SO interactions, there are two kinds of mechanisms to deform the Fermi surfaces. If $\theta_a = 0$ or π, the ground state has the rotational symmetry around the z-direction because we have only two directions($\pm\hat{\mathbf{z}}$) and all physical quantities have rotational symmetry around the z-direction. In this

case the Fermi surfaces can only change their radii just like the spin-degenerate systems. On the other hand, if $\theta_a \neq 0$ or π, the Fermi surfaces deform their shapes in addition to changing their radii. By deforming the Fermi surfaces, a pair of Fermi surfaces, one from the conduction band and one from the valence band, can have some regions in $\mathbf{k}$ space in which the two surfaces are closer and some regions where they are more widely separated than the undeformed surfaces. Condensation then occurs mainly in the region in which the two surfaces are close together. To clarify the physics, we consider systems with the Rashba SO interaction only in one layer.

Fig. 4.8 shows a result for a case where $\theta_c \simeq 0$ with $\alpha \neq 0$ and $\beta = 0$. Since $\beta = 0$, the magnetization direction of the valence band layer is arbitrary. We show the constant-energy surfaces[Fig. 4.8(b) and (c)] in momentum space to verify that the surfaces are rotationally symmetric. All the constant-energy surfaces are concentric circles which implies the density matrices depend only on the magnitude of $\mathbf{k}$. Then the intra-band exchange field for the conduction band $\widetilde{\mathbf{h}}_{c\mathbf{k}}$ whose in-plane components are constant times the Rashba field $\mathbf{h}_{c\mathbf{k}}^R$ solves the self-consistency equation Eq. (4.52). The total effective field of the conduction band has a form

$$\mathbf{h}_{c\mathbf{k}}^{\text{eff}} = \mathrm{h}_\perp(k) \left(\sin \phi_{\mathbf{k}} \hat{\mathbf{x}} - \cos \phi_{\mathbf{k}} \hat{\mathbf{y}} \right) + \mathrm{h}_z(k) \hat{\mathbf{z}} \ . \tag{4.54}$$

Then the in-plane components of the total spin [Eq. (4.53)] vanishes and we get total magnetization along the z-direction. Similarly for the case $\alpha = 0$ and $\beta \neq 0$ [Fig. 4.9], we get concentric constant-energy surfaces and the total effective field of the valence band has a form

$$\mathbf{h}_{v\mathbf{k}}^{\text{eff}} = \mathrm{h}_\perp(k) \left(\sin 3\phi_{\mathbf{k}} \hat{\mathbf{x}} - \cos 3\phi_{\mathbf{k}} \hat{\mathbf{y}} \right) + \mathrm{h}_z(k) \hat{\mathbf{z}} \ . \tag{4.55}$$

and again, the in-plane components of the total spin [Eq. (4.53)] vanishes and we get total magnetization along the z-direction. For these uniaxial cases, we calculate

Figure 4.8: (a) Quasi-particle excitation energy for a ferromagnetic condensate state with Rashba SO interaction in the conduction band with coefficient $\alpha = 0.05\,\text{eV\AA}$ and no SO interaction in the valence band $\beta = 0$. System parameters are $\mu_0 = 30\text{meV}$ and $\Delta n = n_c - n_h = 4.0 \times 10^{10}\text{cm}^{-2}$. The calculated densities are $n_c = 2.59 \times 10^{11}\text{cm}^{-2}$ and $n_h = 2.19 \times 10^{11}\text{cm}^{-2}$. The direction of the total spin of the conduction band layer is $\theta_c = 0.04\pi$ and $\phi_c = 1.72\pi$. (b) and (c) are constant-energy surfaces in momentum space, corresponding to the energies shown in (a). (b) is for 0.025 eV (red dot-dashed line in (a)) and (c) is for 0.012 eV (blue dotted line in (a)).

Figure 4.9: (a) Quasi-particle excitation energy for a ferromagnetic condensate state with Rashba SO interaction in the valence band with coefficient $\beta = 500\,\mathrm{eV\mathring{A}^3}$ and no SO interaction in the conduction band $\alpha = 0$. System parameters are $\mu_0 = 30\mathrm{meV}$ and $\Delta n = n_c - n_h = -4.0 \times 10^{10}\mathrm{cm}^{-2}$. The calculated densities are $n_c = 2.24 \times 10^{11}\mathrm{cm}^{-2}$ and $n_h = 2.64 \times 10^{11}\mathrm{cm}^{-2}$. The direction of the total spin of the conduction band layer is $\theta_v = 0.99\pi$ and $\phi_v = 0.85\pi$. (b) and (c) are constant-energy surfaces in momentum space. (b) is for 0.023 eV and (c) is for 0.01 eV.
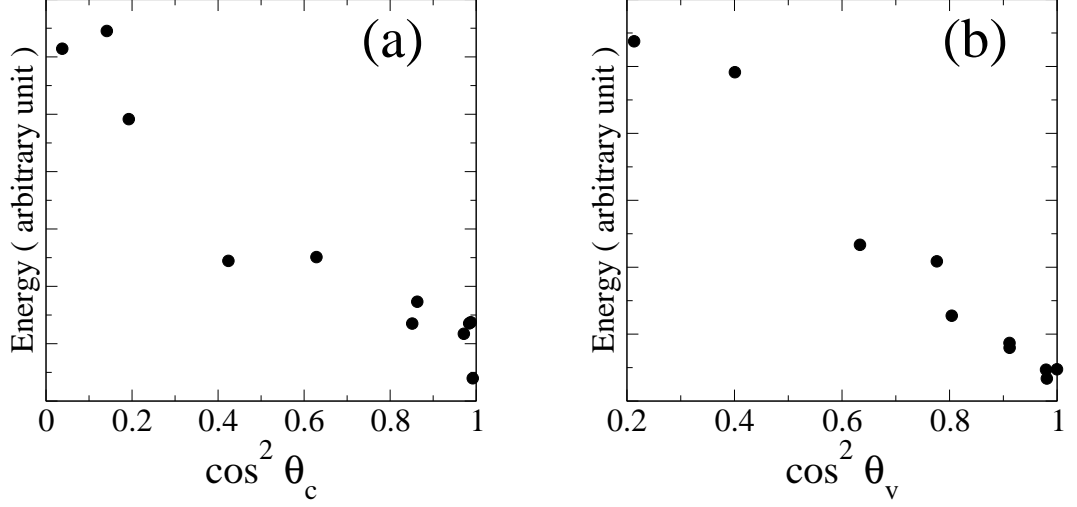
Figure 4.10: Magnetic anisotropy of uniaxial systems. μ_0=30meV and Δn=5.0 × 10^{10}cm^{-2}. (a)$\alpha = 0.05\,\mathrm{eV\AA}$, $\beta = 0$, (b)$\alpha = 0$, $\beta = 700\,\mathrm{eV\AA}^3$.

the total energy of the system for different magnetization angles θ_a. We apply external magnetic field to change the magnetization direction, then subtract the magnetization energy $\mathbf{M}\cdot\mathbf{H}_{\mathrm{ext}}$ from the total energy. Fig. 4.10 shows the numerically evaluated total energy for (a)$\alpha \neq 0$, $\beta = 0$ and (b)$\alpha = 0$, $\beta \neq 0$, as a function of $\cos^2\theta_a$ for uniaxial cases. It shows that the total energy of the uniaxial system is roughly proportional to $\cos^2\theta_a$. Because the magnetic anisotropy energy is very small that Fig. 4.10 looks somewhat noisy. We can derive this linear behavior by doing perturbation theory treating the Rashba SO interaction as a perturbation. The zeroth order ground state is given by Eq.(4.45). We calculate the perturbed energy for each $\mathbf{k}$ using the states Eq. (4.32) $\sim$ Eq. (4.35) as the unperturbed states. The total perturbed energy is evaluated by summing the corrections for each $\mathbf{k}$ up to the Fermi energy of the unperturbed ground state, assuming that the Fermi energy does not change much by the Rashba SO interaction. The first order correction

vanishes and up to the second order we obtain

$$E_{\text{tot}} = E_{\text{tot}}^{(0)} + \delta E + A\alpha^2 \cos^2 \theta_c + B\beta^2 \cos^2 \theta_v \qquad (4.56)$$

where δE is the energy correction that does not depend on the magnetization angles and A, B are constants. Depending on the signs of A and B, the system can have an easy axis($\theta_a = 0$ or π) or an easy plane($\theta_a = \pi/2$). In the easy plane case the dependence of energy on $\cos^2 \theta_a$ should also be linear, but the slope should change sign.

In cases where the total spin has nonzero in-plane components, the total energy is independent of the azimuthal angel. For a given spontaneously chosen azimuthal angle the 2D band structure is anisotropic. This broken XY symmetry leads to intricate and quite interesting properties of quasi-particles. Fig. 4.11 shows a case with $\alpha \neq 0$ and $\beta = 0$ where the total spin of the conduction band has $\theta_c = 0.45\pi$. The quasi-particle excitation energy dispersions are not rotationally symmetric for the conduction band as can be seen in Fig. 4.11(b) and (c). The constant-energy surfaces for the conduction band shifts so that the two bands are closer in one direction and farther apart in the opposite direction in $\mathbf{k}$ space. This corresponds to the intra-band field that points in the same direction as the Rashba field but the magnitude of the intra-band field is not just a function of k but also depends on $\phi_{\mathbf{k}}$. To get nonzero in-plane components of the total spin along the ϕ_c direction, the total effective magnetic field is stronger when the azimuthal angle of the spin states of the majority species($|c\mathbf{k}-\rangle$ for the conduction band) is ϕ_c and weaker when the azimuthal angle the spin states of the minority species($|c\mathbf{k}+\rangle$ for the conduction band) is ϕ_c. The constant-energy surfaces are farther in the direction where the effective field is stronger and closer where the effective field is weaker since the energy difference between the two spin bands is the magnitude of the effective magnetic field. Therefore, we obtainthe condition for the closer(farther) constant-
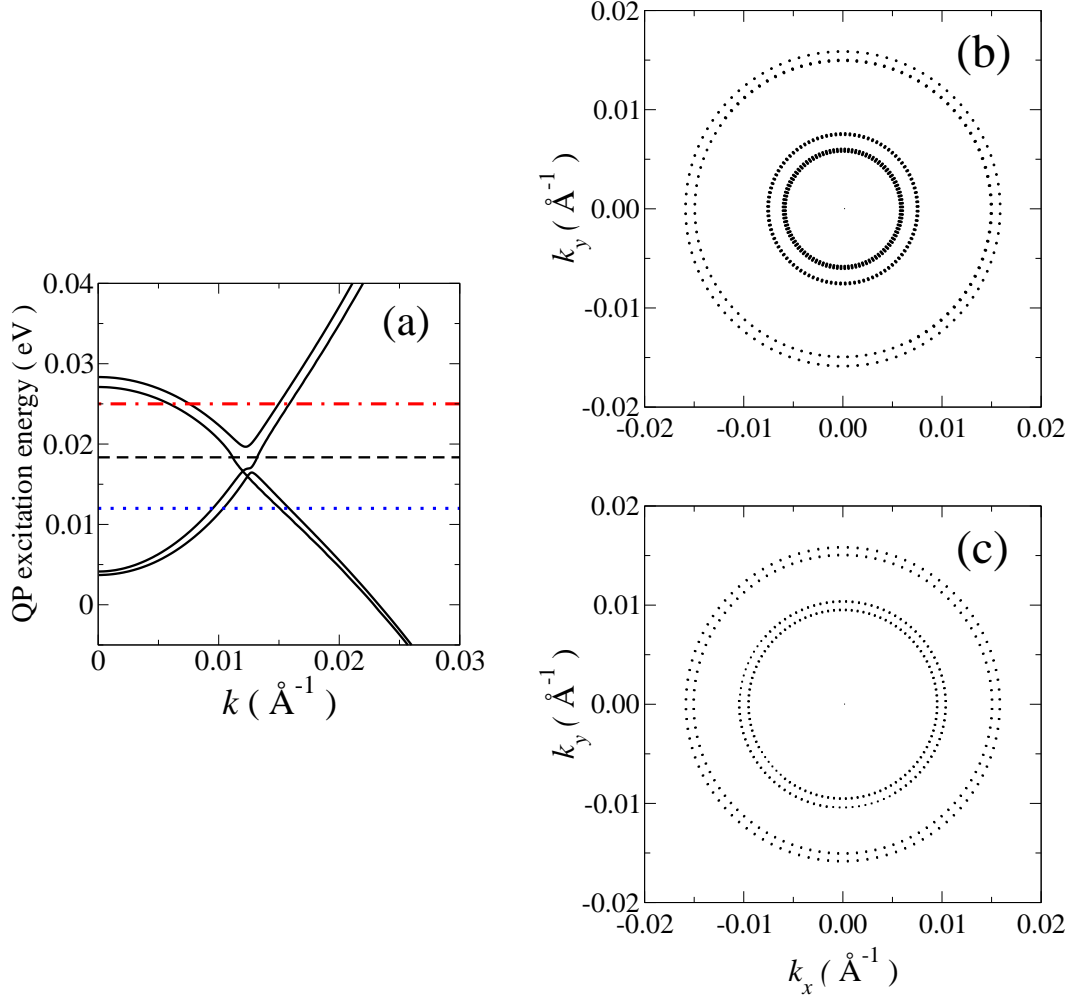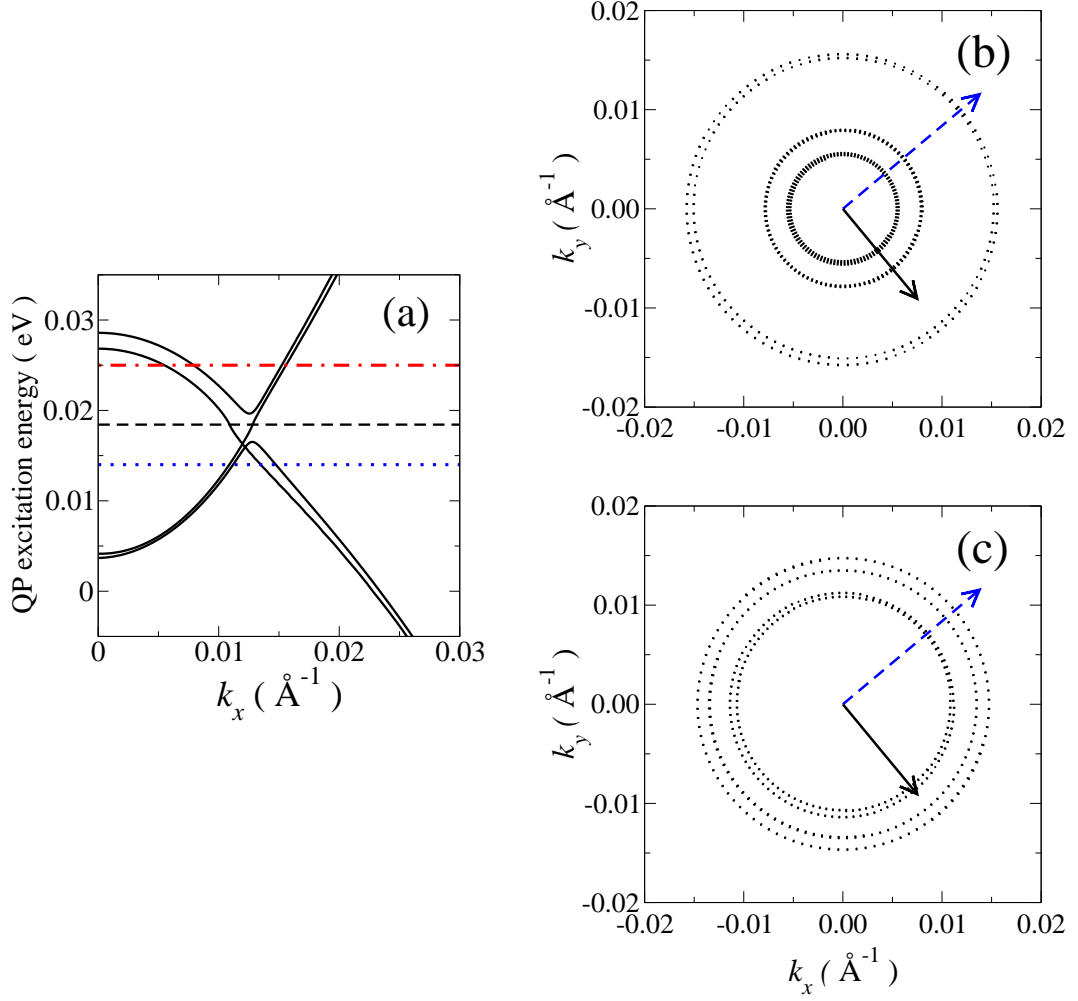
Figure 4.11: (a) Quasi-particle excitation energy for a ferromagnetic conden-
sate state with Rashba SO interaction in the conduction band with coefficient
$\alpha = 0.03\,\mathrm{eV\mathring{A}}$ and no SO interaction in the valence band $\beta = 0$. System parameters
are $\mu_0 = 30\mathrm{meV}$ and $\Delta n = n_c - n_h = 4.0 \times 10^{10}\mathrm{cm}^{-2}$. The calculated densities
are $n_c = 2.59 \times 10^{11}\mathrm{cm}^{-2}$ and $n_h = 2.19 \times 10^{11}\mathrm{cm}^{-2}$. The direction of the total
spin of the conduction band layer is $\theta_c = 0.45\pi$ and $\phi_c = 1.72\pi$. (b) and (c) are
constant-energy surfaces in momentum space. (b) is for 0.025 eV and (c) is for 0.014
eV. The black solid arrow depicts the direction of the total spin in the conduction
layer and the blue dashed arrow depicts the direction of $\phi_{\mathbf{k}} = \phi_c + \pi/2$.
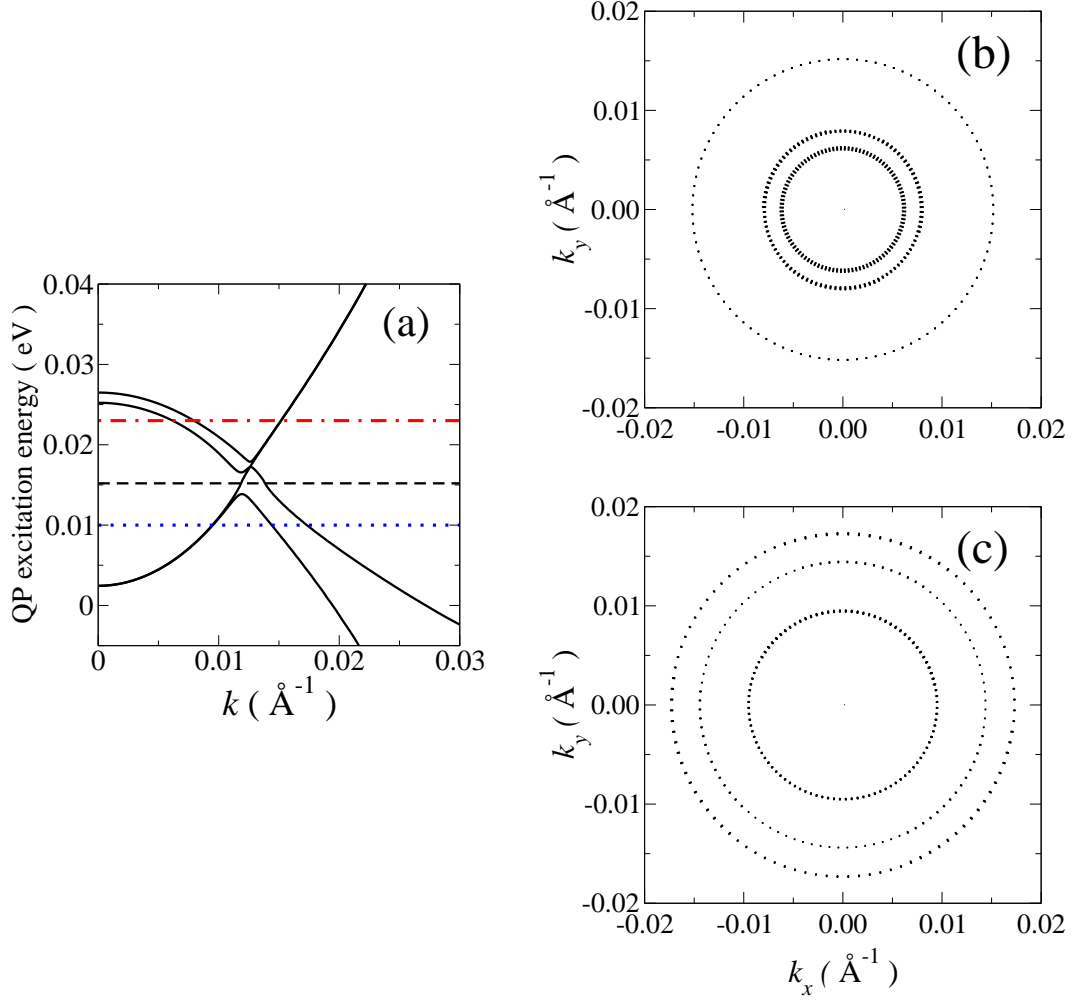
63
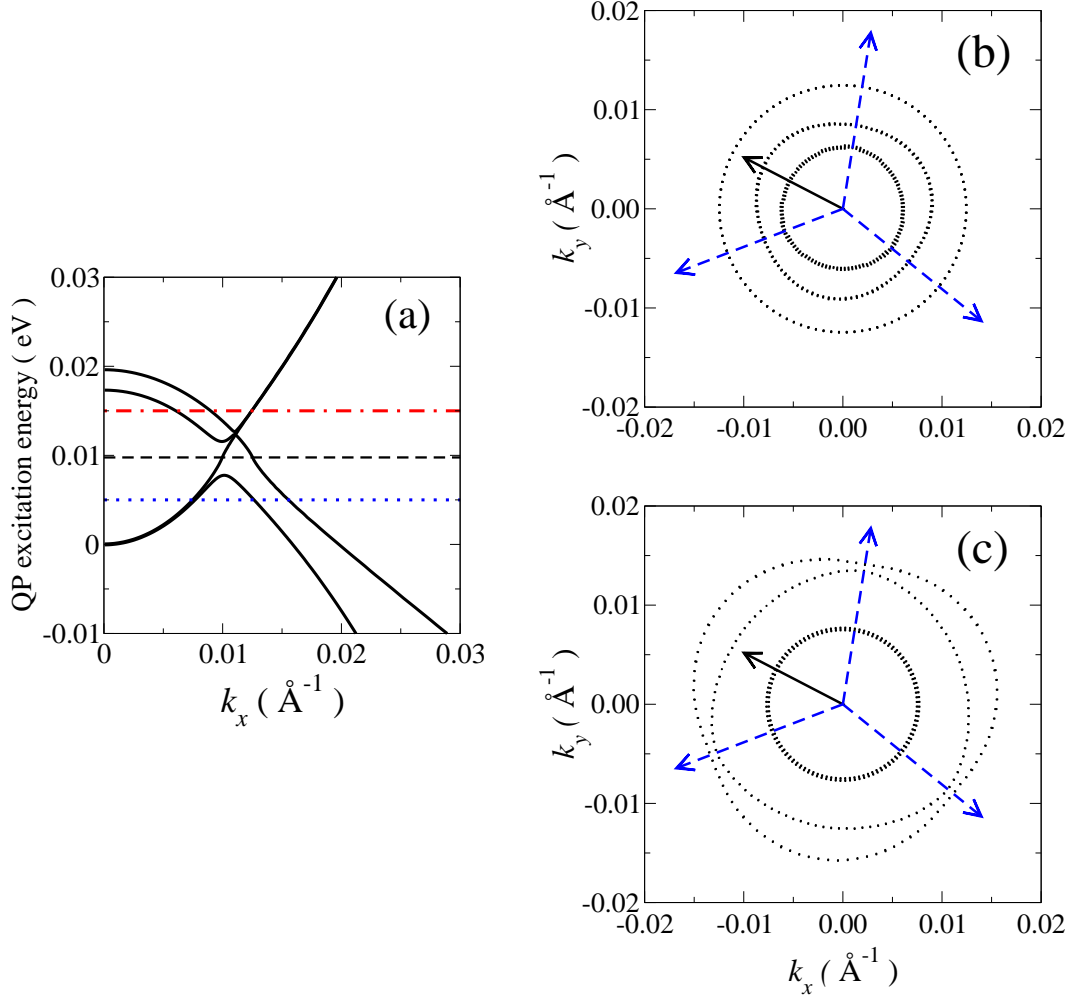
Figure 4.12: (a) Quasi-particle excitation energy for a ferromagnetic condensate state with Rashba SO interaction in the valence band with coefficient $\beta = 400\,\mathrm{eV\mathring{A}^3}$ and no SO interaction in the conduction band $\alpha = 0$. System parameters are $\mu_0 = 20\mathrm{meV}$ and $\Delta n = n_c - n_h = -4.0 \times 10^{10}\mathrm{cm}^{-2}$. The calculated densities are $n_c = 1.59 \times 10^{11}\mathrm{cm}^{-2}$ and $n_h = 1.99 \times 10^{11}\mathrm{cm}^{-2}$. The direction of the total spin of the valence band layer is $\theta_v = 0.63\pi$ and $\phi_v = 0.85\pi$. (b) and (c) are constant-energy surfaces in momentum space. (A) is for 0.015 eV and (B) is for 0.005 eV. The black solid arrow depicts the direction of the total spin in the valence band layer and the blue dashed arrows depict the direction $\phi_{\mathbf{k}} = \phi_v/3 + \pi/6 + 2n\pi/3$ for integer n.

energy surfaces

$$\begin{cases} \phi_c = \phi_{\mathbf{k}} - \frac{\pi}{2}; & \text{closer} \\ \phi_c = \phi_{\mathbf{k}} + \frac{\pi}{2}; & \text{farther} \end{cases} . \tag{4.57}$$

The blue dashed arrow in Fig. 4.11(b) and (c) shows the $\phi_{\mathbf{k}}$ that satisfy the closer condition, which agrees with the numerically calculated constant-energy surfaces.

Fig. 4.12 shows a case with $\alpha = 0$ and $\beta \neq 0$ where $\theta_v = 0.63\pi$. For the valence band, the majority species has spin state $|v\mathbf{k}-\rangle$ and minority species has $|v\mathbf{k}+\rangle$ because the valence band has opposite energy dispersion curve compared to the conduction band. So the majority band has spin states that points to $3\phi_{\mathbf{k}} + \pi/2$ and the minority species has spin states that point to $3\phi_{\mathbf{k}} - \pi/2$. Thus there are 3 closer directions and 3 farther directions that satisfy

$$\begin{cases} \phi_v + 2n\pi = 3\phi_{\mathbf{k}} - \frac{\pi}{2}; & \text{closer} \\ \phi_v + 2n\pi = 3\phi_{\mathbf{k}} + \frac{\pi}{2}; & \text{farther} \end{cases} . \tag{4.58}$$

Fig. 4.12(b) and (c) shows the directions of the closer condition by blue dashed arrows, which again agrees with the numerical results very well. These systems[Fig. 4.11 and Fig. 4.12] spontaneously break the rotational symmetry around the z-direction to make the Fermi surfaces of one conduction band and one valence band close together so that they can form the excitonic condensate while the other two bands remain normal.

4.6   Conclusion

In summary, we studied the electron-hole pair condensation in spatially separated bilayer systems. The population polarization and the subsequent Fermi surface mismatch leads to a unique ferromagnetism with SU(2)×SU(2) spin-rotational symmetry and the condensate and the normal state coexist in the system. The Rashba

SO interaction which arise naturally in two-dimensional systems with structural inversion asymmetry breaks the spin-rotational symmetry and leads to a fixed polar angle of the magnetization of each layer in the system. The relation between the magnetization direction and the system parameters such as density, density polarization between electrons and holes and the strength of the Rashba SO interaction is not clear yet. One of the reason for this seems to be that the magnetic anisotropy energy is very small compared to other energy scales so that the magnetization is very sensitive to the parameters. The in-plane component of the magnetization implies anisotropic energy spectra in SO systems, which will be interesting for the study of excited states.

Chapter 5

Fermion Pair Condensation in Magnetic Field

5.1 Introduction

In the previous chapter, we saw that the interplay of population polarization and fermion pair condensation leads to some interesting features, due to the Fermi surface mismatch. In this chapter and the following chapter, we study a different population polarized fermion system, a cold fermion atom system. Unlike the 4-component bilayer electron-hole systems where we can restore Fermi surface matching for one pair of bands, while leaving the other pair normal, the population imbalance in superconductors and cold fermion atom systems where we have only two components can lead to finite-momentum Cooper pair condensation. These states are called FFLO states [7, 8].

One of the most obvious signatures of superfluidity in fermionic cold-atom systems is the appearance of vortices and vortex lattices when the system is rotated [88]. Indeed recent experiments [32, 33] have observed vortex-lattice structures in fermionic cold-atom systems close to the BEC-BCS crossover region (see Fig. 5.1).
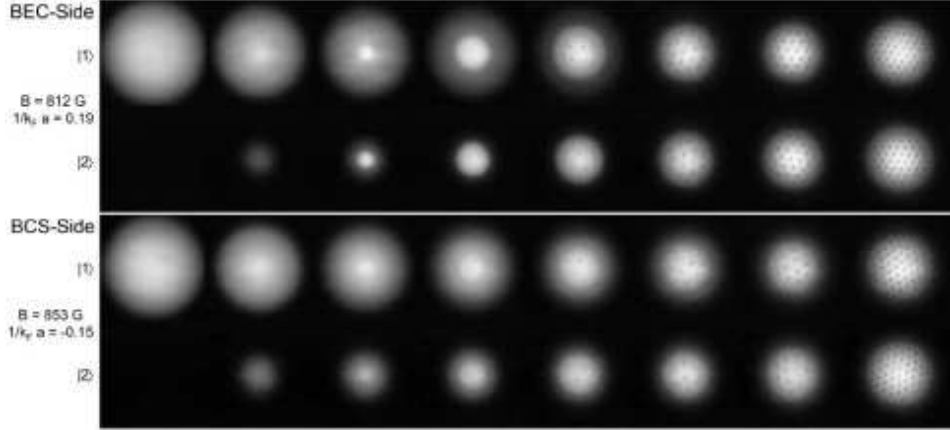
Figure 5.1: Vortex lattices observed in Ref. [33]. Population polarization is from 100% (left) to 0% (right). We can see the vortex lattices for both BEC and BCS sides of the crossover and at a critical polarization, the vortex structures disappear.

For this reason an obvious potential signature of an FFLO state is the appearance of the exotic vortex-lattice structures they are expected to form [89, 90, 91]. Rotation is essential for the realization of the vortex lattice structures. Working in the co-rotating reference frame, rotation is equivalent to an external magnetic field and a reduction in radial confinement strength due to the centripetal potential. From now on we use the language of the co-rotating frame so that the atoms experience an effective field with cyclotron frequency $\Omega_c = 2\Omega$ where Ω is the rotation frequency. In typical experiments the atomic Landau level splitting, equal to $2\hbar\Omega$, is much smaller than the Fermi energy. In this limit the Landau level index of the condensate could be determined by finding the optimal pairing wavevector on the BCS superfluid/normal phase boundary in the absence of rotation and using semi-classical quantization to add rotation to the condensate effective action. Here we use a fully quantum-mechanical approach, including Landau quantization even at the level of the underlying unpaired fermions. This approach is still relatively easy, partly because of the short-range of the atom-atom attractive effective interaction, and has of the advantage of determining the condensate Landau level index more

68
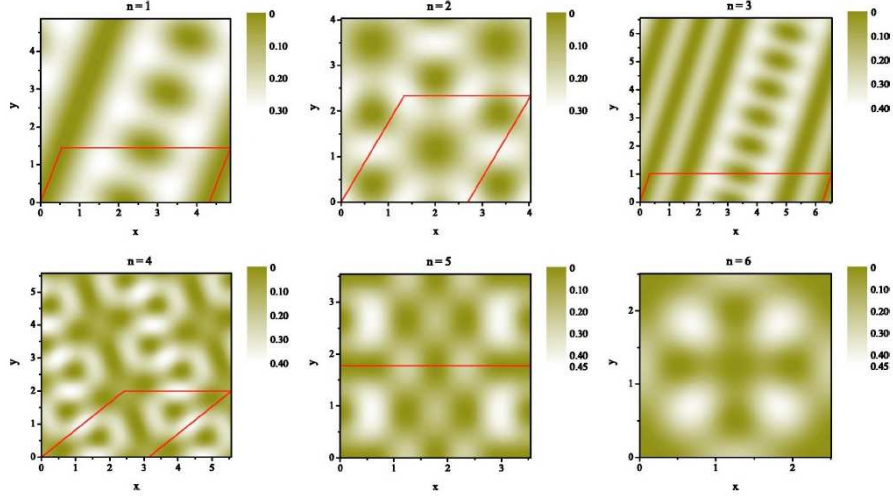
Figure 5.2: Vortex lattices of FFLO states for COM LL $n = 0$ to $n = 6$ reported in Ref. [91]. Lines indicate the unit cells.

accurately, and allows us to comment on the rapid rotation regime which might be approached experimentally in the future. FFLO vortex lattices (see Fig. 5.2) can be wildly different from the usual hexagonal Abrikosov vortex lattice. The structure of the vortex lattice is determined mainly [89, 90, 91] by the Landau level index of its condensed fermion pairs; the Abrikosov lattice forms when the Landau level index $j = 0$, which is the closest approximation to zero-total-momentum pairing allowed in a system that has come to equilibrium in a rotating frame. FFLO states in the absence of rotation can imply $j > 0$ Fermion pair condensation in rotated systems. Vortices have been observed in systems with population imbalance [33], but so far no unusual vortex structures have been observed (This could be due to the fact that these experiments realize the gapless Sarma phase [51] and another reason could be that the FFLO state is predicted by weak-coupling theory while all experiments are in the unitary limit).

In this chapter we develop a mean-field theory for rotating atom clouds. We derive an implicit equation for the critical temperature including the Landau quan-

tization effect due to the effective magnetic field. The non-zero pairing momentum in FFLO states then corresponds to higher center-of-mass(COM) Landau level (LL) and the implicit T_c equation gives the critical temperature for each COM LL pairing. We consider three-dimensional systems for the sake of definiteness, although two-dimensional systems could also be interesting experimentally. All our explicit calculations are for a uniform three-dimensional system and do not account for confinement. In Sec. 5.2 we introduce the FFLO states for spin-polarized fermion systems and describe the relation with Landau level quantization. In Sec. 5.3 we consider the transformation between individual particle and COM and relative states for two rotating atoms and derive the Bethe-Salpeter equation whose instability gives an implicit T_c equation. In Sec. 5.4 we derive COM Landau level index dependent linearized gap equations for the critical temperature of the rotating system.

5.2   FFLO States in Orbital Magnetic Field

Pairing is most effective when the states to be paired are as close to the Fermi energy as possible. When there is no population imbalance, pairs formed from electrons with opposite momentum (zero total momentum) are abundant at low energies as illustrated schematically in Fig. 5.3. For unbalanced populations the lowest energy pairs have total momentum equal to the difference between Fermi wavevectors. In systems with an orbital magnetic field linear momentum is not a good quantum number, but the motion of a pair can still be separated into center-of-mass and relative motion degrees-of-freedom. In a magnetic field, momentum space collapses into Landau levels whose degeneracy is illustrated in Fig. 5.4 by partitioning of momentum space into equal area segments centered on $\hbar\Omega_c(N + 1/2)$. A pair of electrons with given Landau level indices N and N' has finite quantum amplitudes for all center of mass Landau level indices from 0 to $N + N'$ which correspond closely to the distribution of center of mass (COM) kinetic energy values that would be

$$k_{F\uparrow} = k_{F\downarrow}, \quad Q = 0 \qquad k_{F\uparrow} \neq k_{F\downarrow}, \quad Q = k_{F\uparrow} - k_{F\downarrow}$$
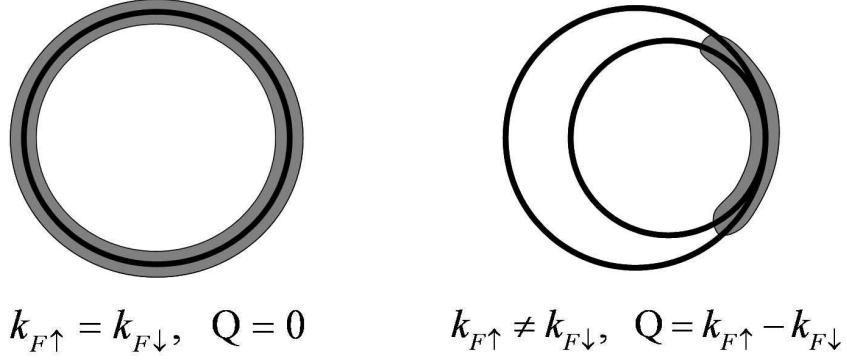
Figure 5.3: Low energy pairings for population balanced and unbalanced systems. Shaded regions indicate participating states for the low energy pairings in k-space. Q is the total momentum of the pairs, which is 0 for balanced systems and equal to the difference between Fermi wavevectors in unbalanced systems.
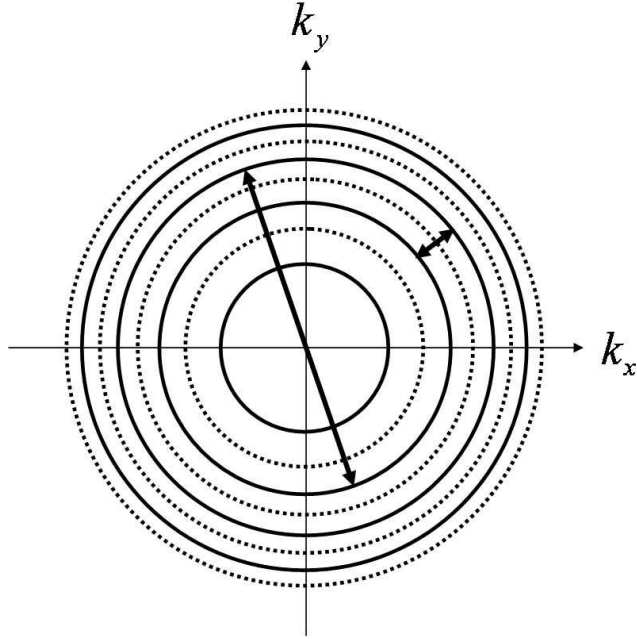
Figure 5.4: Degeneracy of Landau levels. States between two dotted circles collapse into the solid circle. All the areas between two adjacent dotted circles are the same and solid circles have radii given by $\hbar^2 k^2 / 2m = \hbar \Omega_c (N + 1/2)$. The arrows show the maximum and minimum momentum differences between particles in LL $N = 1$ and $N = 2$, which correspond qualitatively to the maximum and minimum of the COM momentum.
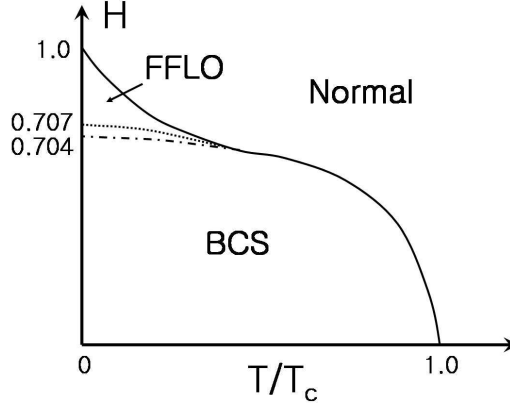
Figure 5.5: BCS theory phase diagram for FFLO and BCS states as calculated, for example, in Ref. [92]. Here, H is the ratio of the Zeeman energy (or normal state chemical potential difference) to the zero-field energy gap. The dotted line marks the Clogston limit where the energies of normal and the zero-pairing momentum BCS state are identical. The FFLO state occurs near the boundary between normal and BCS states.

obtained by averaging over the corresponding regions of momentum space illustrated in Fig. 5.4. These quantum probability amplitudes are the key ingredient in the linearized gap equations discussed below. We derive linearized gap equations which implicitly define the critical temperature for a phase transition from the normal to the superfluid state for each COM LL and determine the phase boundaries in parameter space. If excited COM LL's have a higher critical temperature than the lowest-lying COM LL, this signals the occurrence of exotic vortex lattice states and of FFLO states in the unrotated system. In Fig. 5.5 the phase diagram is shown for a non-rotating homogeneous system. The maximum value of the exchange field (or difference between normal state chemical potentials) for which pairing still occurs is given approximately by $H = \Delta_0/\sqrt{2}$, where Δ_0 is the BCS gap parameter at zero exchange field and zero temperature. Beyond this so-called Clogston limit [93] the BCS state is no longer stable. The FFLO state is expected to occur in this region of the phase diagram.

72

5.3   Bethe-Salpeter Equations

In this section we first consider the transformation between individual particle and COM and relative states for two rotating atoms and then use this to derive the Bethe-Salpeter equation.

To consider the pairing instability of a normal Fermi gas, we first turn our attention to the description of scattering between two atoms in a rotating reference frame. The rotation is represented by considering the atoms to be particles with unit charge in an effective homogeneous orbital magnetic field. The Hamiltonian for two particles is

$$
\begin{aligned}
\widehat{h} &= \frac{1}{2m} \left(-i\hbar \boldsymbol{\nabla}_{\mathbf{r}_1} - \mathbf{A}(\mathbf{r}_1) \right)^2 + \frac{1}{2m} \left(-i\hbar \boldsymbol{\nabla}_{\mathbf{r}_2} - \mathbf{A}(\mathbf{r}_2) \right)^2 \\
&= \frac{1}{2M} \left(-i\hbar \boldsymbol{\nabla}_{\mathbf{R}} - 2\mathbf{A}(\mathbf{R}) \right)^2 + \frac{1}{2\mu} \left(-i\hbar \boldsymbol{\nabla}_{\mathbf{r}} - \frac{\mathbf{A}(\mathbf{r})}{2} \right)^2 ,
\end{aligned}
$$

(5.1)

where $M = 2m$, $\mu = m/2$, $\mathbf{R} = (\mathbf{r}_1 + \mathbf{r}_2)/2$ and $\mathbf{r} = \mathbf{r}_1 - \mathbf{r}_2$. The vector potential $\mathbf{A}(\mathbf{r})$ is defined by $\boldsymbol{\nabla} \times \mathbf{A}(\mathbf{r}) = 2m\Omega\,\hat{\mathbf{z}}$ where Ω is the angular rotation frequency of the system and we assume that the rotation is around the z-axis. In the Landau gauge, $\mathbf{A}(\mathbf{r}) = (0, 2m\Omega x, 0)$ and the individual atom eigenfunctions with eigenvalues $\hbar\Omega(2N + 1)$ are given by

$$
\begin{aligned}
\psi_{N,k_{i,y},k_{i,z}}(\mathbf{r}_i) &= \langle \mathbf{r}_i | N, k_{i,y}, k_{i,z} \rangle \\
&= e^{i(k_{i,y}y_i + k_{i,z}z_i)} \phi_N(x_i + k_{i,y}l_B^2)/(L_y L_z)^{1/2} ,
\end{aligned}
$$

(5.2)

where $\phi_N(\mathbf{r})$ is the one-dimensional harmonic oscillator eigenfunction and the effective magnetic length l_B is defined by $\hbar^2/ml_B^2 = 2\hbar\Omega$. The eigenfunctions are labeled by the momenta in y and z directions, and by the LL index N. The eigenfunctions for the COM and relative coordinates are the same, except that the effective mag-

netic lengths are now $l_R = l_B/\sqrt{2}$ and $l_r = \sqrt{2}l_B$. In terms of ladder operators,

$$\widehat{h} = \hbar\Omega_c(a_1^\dagger a_1 + a_2^\dagger a_2 + 1) = \hbar\Omega_c(a_R^\dagger a_R + a_r^\dagger a_r + 1) \ , \tag{5.3}$$

where $a_i = (l_B/\sqrt{2}\hbar)(\pi_{i,x} - i\pi_{i,y})$, $\boldsymbol{\pi}_i = i\hbar\boldsymbol{\nabla}_i - \mathbf{A}(\mathbf{r}_i)$, $a_R = (a_1 + a_2)/\sqrt{2}$, $a_r = (a_1 - a_2)/\sqrt{2}$, and $\hbar\Omega_c = \hbar^2/ml_B^2 = 2\hbar\Omega$. The ladder operators can then be used to derive [94] an explicit expression for the unitary transformation between individual particle and COM and relative two-atom states:

$$\langle\mathbf{r_1}, \mathbf{r_2}|N, k_{1,y}, k_{1,z}; M, k_{2,y}, k_{2,z}\rangle = \sum_{j=0}^{N+M} B_j^{NM}\langle\mathbf{R}, \mathbf{r}|j, K_y, K_z; N + M - j, k_y, k_z\rangle \ , \tag{5.4}$$

where

$$K_y = k_{1,y} + k_{2,y} \ , \ \ K_z = k_{1,z} + k_{2,z} \ , \tag{5.5}$$

$$k_y = (k_{1,y} - k_{2,y})/2 \ , \ \ k_z = (k_{1,z} - k_{2,z})/2 \ , \tag{5.6}$$

and

$$B_j^{NM} = \left[\frac{j!(N + M - j)!N!M!}{2^{N+M}}\right]^{1/2} \sum_{m=0}^{j} \frac{(-)^{M-m}}{(j-m)!(N + m - j)!(M - m)!m!} \ . \tag{5.7}$$

It follows that B_j^{NM} is the probability amplitude for two atoms in LLs N and M, respectively to have COM LL j and the relative motion LL $N + M - j$. When $N = M$, $|B_j^{NM}|^2$ has maxima for $j = 0$ and $j = N + M$. However, if $N \neq M$, $|B_j^{NM}|^2$ can have a maximum for intermediate j, which means that for two atoms in different LLs, the most probable COM LL can be different from zero or $N + M$ as shown in Fig. 5.6. The smooth envelope apparent in these figures is simply the zero-field probability distribution of the COM kinetic energies given the Fermi momenta of two individual particles. The COM energy is maximum for parallel momentum
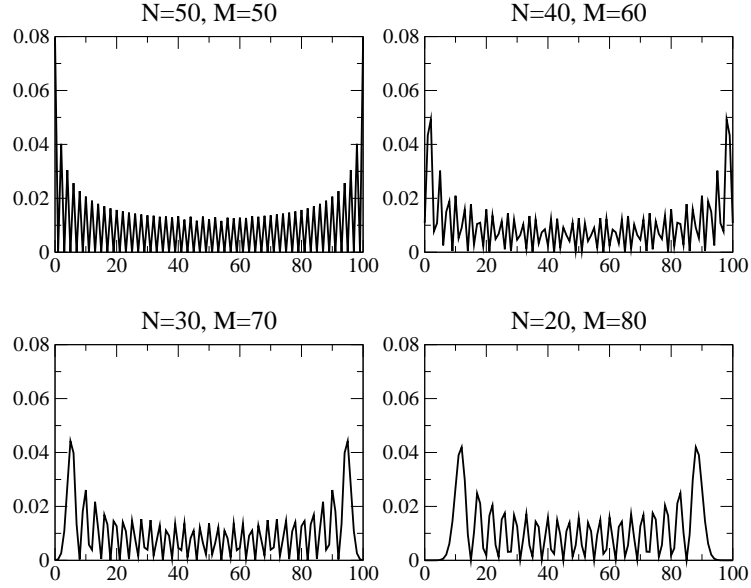
Figure 5.6: $|B_j^{NM}|^2$ vs j with $N + M = 100$ for different N's. The horizontal axes are j and the vertical axes are $|B_j^{NM}|^2$.

and minimum for oppositely oriented individual particle momenta. This coefficient plays an important role in determining the pairing COM LL in condensed states.

The pairing instability in a Fermi gas is signaled by a divergence of the many-body scattering function [62], which we approximate using the Bethe-Salpeter equation summarized by the finite-temperature Feynman diagrams illustrated in Fig. 5.7. We consider a system consisting of two hyperfine species denoted by $\uparrow$ and $\downarrow$. For definiteness we assume that the two species have the same energy spectrum but allow for different densities and therefore different chemical potentials. Population imbalance is relatively easy to achieve experimentally and the life-time of each hyperfine state is long enough compared to experimental time scales to justify the use of equilibrium statistical mechanics with separate particle reservoirs for the two species. The many-body scattering function is calculated by summing the ladder diagrams [95, 94](see Fig. 5.7). Generalizing the calculations of Ref. [94] to three dimensions from two we find that the total two-particle scattering function
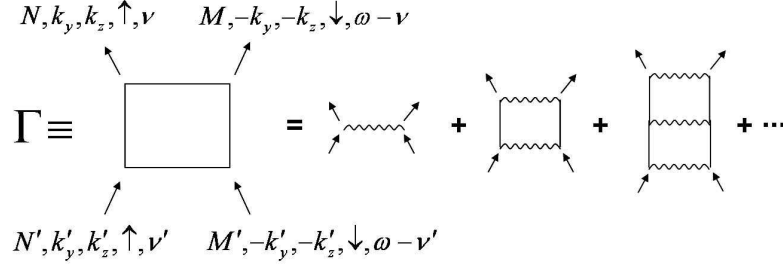
Figure 5.7: Ladder diagrams to be summed for scattering function Γ.

can be written as a sum over different COM Landau level index channels:

$$\Gamma(N, M, k_y, k_z; N', M', k'_y, k'_z; i\omega)$$
$$= \sum_j B_j^{NM} B_j^{N'M'} \gamma_j(N, M, k_y, k_z, N', M', k'_y, k'_z; i\omega). \tag{5.8}$$

where the partial scattering function for COM LL j

$$\gamma_j(N, M, k_y, k_z; N', M', k'_y, k'_z; i\omega)$$
$$= \langle N + M - j, k_y, k_z | \widehat{V} | N' + M' - j, k'_y, k'_z \rangle$$
$$+ \sum_{N'', M''} \sum_{k''_y, k''_z} \left| B_j^{N''M''} \right|^2 \langle N + M - j, k_y, k_z | \widehat{V} | N'' + M'' - j, k''_y, k''_z \rangle$$
$$\times K_{N'', M'', k''_z}(i\omega) \gamma_j(N'', M'', k''_y, k''_z; N', M', k'_y, k'_z; i\omega) . \tag{5.9}$$

In Eq. (5.9)

$$K_{N,M,k_z}(i\omega) = \frac{1 - f(\xi_{N,k_z,\uparrow}) - f(\xi_{M,-k_z,\downarrow})}{i\hbar\omega - \xi_{N,k_z,\uparrow} - \xi_{M,-k_z,\downarrow}} ; \tag{5.10}$$

$$\xi_{N,k_z,\sigma} = \varepsilon_{N,k_z} - \mu_\sigma ; \tag{5.11}$$

$$\varepsilon_{N,k_z} = \hbar\Omega_c \left(N + \frac{1}{2} \right) + \frac{\hbar^2 k_z^2}{2m} , \tag{5.12}$$

and $f(\xi)$ is the Fermi distribution function. In the case of a delta-function interaction

76

$V(\mathbf{r}) = -V_0\delta(\mathbf{r})$ we have that

$$\langle N + M - j, k_y, k_z | \widehat{V} | N' + M' - j, k'_y, k'_z \rangle$$
$$= -V_0 \phi^r_{N+M-j}(k_y l_r^2) \phi^r_{N'+M'-j}(k'_y l_r^2)(1/L_y L_z) , \qquad (5.13)$$

where ϕ^r_N is the one-dimensional harmonic oscillator eigenfunction in relative coordinates. Using this property and the orthogonality of the relative motion harmonic oscillator wavefunctions we find that

$$\gamma_j(N, M, k_y, k_z; N', M', k'_y, k'_z; i\omega)$$
$$= \frac{-V_0}{L_y L_z} \phi^r_{N+M-j}(k_y l_r^2) \phi^r_{N'+M'-j}(k'_y l_r^2)$$
$$\times \left(1 + \frac{V_0}{4\pi l_B^2 L_z} \sum_{N'', M'', k''_z} K_{N'', M'', k''_z}(i\omega) \left| B_j^{N''M''} \right|^2 \right)^{-1} . \qquad (5.14)$$

5.4   Linearized Gap Equations

In this section we derive the linearized gap equation for condensation of Fermion pairs with a definite COM Landau Level (LL) index. First we derive a relation between the scattering length and the two-body transition matrix which is used to remove the ultraviolet divergence of the T_c equation. Then we derive the implicit equations for the critical temperatures of each COM LL channel.

5.4.1   Two-Body Transition Matrix and Scattering Length in Systems with Orbital Magnetic Field

In this subsection we derive the relation between the scattering length and the strength of the delta-function like particle-particle interaction in a system with orbital magnetic field. The two-body transition operator for scattering at energy z is

defined by

$$\begin{aligned}
\widehat{T}^{2B}(z) &\equiv \widehat{V} + \widehat{V}\frac{1}{z-\widehat{H}_0}\widehat{V} + \cdots \\
&= \widehat{V} + \widehat{V}\frac{1}{z-\widehat{H}_0}\widehat{T}^{2B}(z) ,
\end{aligned} \tag{5.15}$$

where $\widehat{V}$ is the particle-particle interaction and $\widehat{H}_0$ is the non-interacting part of the two-body Hamiltonian. The matrix elements of this transition operator satisfy the Lippman-Schwinger equation. Noting that scattering conserves the COM motion, we calculate the T-matrix elements in relative motion Hilbert space with COM LL j and COM momenta K_y and K_z. Notice that the relative motion T-matrix does not depend on the y-component of the total momentum K_y in the Landau gauge.

$$\begin{aligned}
&\langle N + M - j, k_y, k_z|\,\widehat{T}^{2B}(j, K_z; z)\,|N' + M' - j, k_y', k_z'\rangle \\
&= \langle N + M - j, k_y, k_z|\widehat{V}|N' + M' - j, k_y', k_z'\rangle \\
&+ \sum_{N'',M''}\sum_{k_y'',k_z''}\langle N + M - j, k_y, k_z|\widehat{V}|N'' + M'' - j, k_y'', k_z''\rangle \\
&\quad \times \frac{|B_j^{N''M''}|^2}{z - \varepsilon_{N'',K_z/2+k_z''} - \varepsilon_{M'',K_z/2-k_z''}}\langle N'' + M'' - j, k_y'', k_z''|\widehat{V}|N' + M' - j, k_y', k_z'\rangle \\
&+ \cdots .
\end{aligned} \tag{5.16}$$

Using Eq. (5.13) we have that,

$$\langle N + M - j, k_y, k_z | \, \widehat{T}^{2B}(j, K_z; z) \, | N' + M' - j, k_y', k_z' \rangle$$

$$= \frac{-V_0}{L_y L_z} \phi_{N+M-j}^r(k_y l_r^2) \phi_{N'+M'-j}^r(k_y' l_r^2)$$

$$\times \left[1 + \frac{-V_0}{4\pi l_B^2 L_z} \sum_{N'', M'', k_z''} \frac{|B_j^{N'' M''}|^2}{z - \varepsilon_{N'', K_z/2+k_z''} - \varepsilon_{M'', K_z/2-k_z''}} + \cdots \right]$$

$$= \frac{-V_0}{L_y L_z} \phi_{N+M-j}^r(k_y l_r^2) \phi_{N'+M'-j}^r(k_y' l_r^2)$$

$$\times \left[1 - \frac{-V_0}{4\pi l_B^2 L_z} \sum_{N'', M'', k_z''} \frac{|B_j^{N'' M''}|^2}{z - \varepsilon_{N'', K_z/2+k_z''} - \varepsilon_{M'', K_z/2-k_z''}} \right]^{-1} . \quad (5.17)$$

For a dilute atomic gas, all the relevant energies are small compared to $\hbar^2/mr_V^2$ where r_V is the interaction range. We are therefore allowed to neglect the energy dependence of the two-body T-matrix [95]. (Note that the energy does not depend on k_y.) Hence we have that

$$\langle N + M - j, k_y, k_z | \, \widehat{T}^{2B}(j, K_z; z) \, | N' + M' - j, k_y', k_z' \rangle$$

$$\approx \langle 0, k_y, 0 | \, \widehat{T}^{2B}(j = 0, K_z = 0; z = 0) \, | 0, k_y', 0 \rangle$$

$$= \frac{-V_0}{L_y L_z} \phi_0^r(k_y l_r^2) \phi_0^r(k_y' l_r^2) \left[1 + \frac{-V_0}{4\pi l_B^2 L_z} \sum_{N'', M'', k_z''} \frac{|B_0^{N'' M''}|^2}{\varepsilon_{N'', k_z''} + \varepsilon_{M'', -k_z''}} \right]^{-1} \quad (5.18)$$

To extract an expression for the scattering length we put the above matrix element equal to the matrix element $\langle N + M - j, k_y, k_z | \, V_{\mathrm{pp}} \, | N' + M' - j, k_y', k_z' \rangle$ of the pseudo-potential $V_{\mathrm{pp}}(\mathbf{r}) = 4\pi a_{\mathrm{sc}} \hbar^2 \delta(\mathbf{r})/m$. From this we find that

$$\frac{m}{4\pi \hbar^2 a_{\mathrm{sc}}} = -\frac{1}{V_0} + \frac{1}{4\pi l_B^2 L_z} \sum_{N, M, k_z} \frac{|B_0^{NM}|^2}{\varepsilon_{N, k_z} + \varepsilon_{M, -k_z}} . \quad (5.19)$$

79

5.4.2 T_c Equation

As mentioned before, the instability of the normal state due to pairing is signaled by the divergence of the many body scattering function $\Gamma(i\omega = 0)$, and therefore a diverging $\gamma_j(i\omega = 0)$ means that pairs with COM LL j are unstable to condensation. This instability condition for the scattering function is equivalent to the linearized gap equation which defines the critical temperature [62] in mean-field theory. (In the mean-field-theory for the ordered state [96, 97] the order parameter can be expressed in terms of partial contributions from each COM LL channel. When the order parameter is small the various channels decouple and the partial contribution from a given channel vanishes at the same point at which the normal state partial scattering function diverges.) From Eq. (5.14), we get an implicit equation for the critical temperature T_c^j for each COM LL j, which reads

$$\frac{1}{V_0} = \frac{1}{4\pi l_B^2 L_z} \sum_{N,M,k_z} \frac{1 - f(\xi_{N,k_z,\uparrow}) - f(\xi_{M,-k_z,\downarrow})}{\xi_{N,k_z,\uparrow} + \xi_{M,-k_z,\downarrow}} \left| B_j^{NM} \right|^2 \ . \tag{5.20}$$

Unlike the BCS superconductors, for which retarded phonon-mediated attractive interactions have a natural ultraviolet cut-off, there is no cut-off in this equation and the summation is over all states. Hence, as it stands, this equation diverges, because of the assumption of a δ-function interaction. To remove this divergence, we need to recognize that the true atom-atom interaction is short-ranged compared to relevant atomic wavelengths but not a δ-function. Using the exact relation between scattering length and interaction strength Eq. (5.19), we remove the interaction strength V_0 by renormalizing to the scattering length [95] in the T_c^j equation and obtain convergent sums over intermediate states. The equation for T_c^j

then becomes

$$
-\frac{1}{k_{F0}a_{\mathrm{sc}}} = \frac{\hbar\Omega_c}{2\pi k_{F0}} \sum_{N,M} \int dk_z \left[\frac{1 - f(\xi_{N,k_z,\uparrow}) - f(\xi_{M,-k_z,\downarrow})}{\xi_{N,k_z,\uparrow} + \xi_{M,-k_z,\downarrow}} \left| B_j^{NM} \right|^2 \right.
$$
$$
\left. - \frac{1}{\varepsilon_{N,k_z} + \varepsilon_{M,-k_z}} \left| B_0^{NM} \right|^2 \right] , \qquad (5.21)
$$

where k_{F0} is the Fermi wavevector of the unpolarized system without rotation. The left-hand side of Eq. (5.21) is experimentally measurable. We determine T_c as a function of $1/k_{F0}a_{\mathrm{sc}}$ by solving this implicit equation combined with implicit equations for the temperature-dependent chemical potentials μ_σ

$$
n_\sigma = \frac{1}{V} \sum_{N,k_y,k_z} f(\varepsilon_{N,k_z} - \mu_\sigma) , \qquad (5.22)
$$

where n_σ is the density of atoms in hyperfine state σ, and V is the total volume of the system. In summary, we have derived an equation for the superfluid critical temperature in rotating fermionic cold-atom systems, incorporating Landau level quantization effects. In the next chapter we present numerical results obtained by solving these equations.

Chapter 6

Rotating Polarized Cold Fermion Atom Systems

6.1   Introduction

In this chapter we present the numerical solution of the T_c equations derived in the previous chapter. We study the polarization and interaction strength regime over which non-zero j pairing is expected in a rotating two-component Fermion system. We consider only the BCS side of the Feshbach resonance, on which FFLO physics occurs. In Sec. 6.2 we calculate the critical temperature as a function of the scattering length for various polarizations. In Sec. 6.3 we show the phase diagrams in a parameter space of the polarization and the scattering length. We finish in Sec. 6.4 with a discussion of our results, and present our conclusions. We postpone to this section a discussion of the competition between phase separated states and FFLO states, which is an issue for cold atoms but not for electrons in a solid because of long-range repulsive Coulomb interactions.

6.2   Numerical Determination of T_c

In this section we calculate T_c^j for each COM LL j for various rotation frequencies, interaction strengths and polarizations. We fix the total density of the system n_{tot} and used the polarization p as a parameter. The polarization is defined by

$$p = \frac{n_\uparrow - n_\downarrow}{n_\uparrow + n_\downarrow} \ , \tag{6.1}$$

where $n_\uparrow$ is the density of the majority species and $n_\downarrow$ is the density of the minority species. Hence, the density of atoms in species σ [$\sigma = +1$ (-1) corresponds to $\uparrow$ $(\downarrow)$] is given by

$$n_\sigma = \frac{1 + \sigma p}{2} \cdot n_{tot} \ . \tag{6.2}$$

The relationship between T_c^j and interaction strength is illustrated in Fig. 6.1. The true critical temperature for the system is the largest value of T_c^j.

$$T_c = \max\left\{T_c^j\right\} \ . \tag{6.3}$$

At weak rotation [Fig. 6.1 (a)], the transition temperature T_c for zero polarization shows the usual behavior [98] $T_c \propto \exp(-1/k_{F0}a_{sc})$ and the highest T_c^j is for the $j = 0$ channel regardless of the interaction strength. In this circumstance we expect the system will have a standard Abrikosov vortex lattice. The critical temperature decreases as polarization increases and superfluidity is suppressed above some critical polarization. It is more easily suppressed at weak interaction. FFLO states, which correspond to nonzero j, occur at strong interaction and high polarization. We emphasize that these states will have very distinct [91] vortex lattices, more open than the hexagonal Abrikosov lattices and qualitatively different for each value of j. It should be quite obvious experimentally when a $j \neq 0$ vortex lattice occurs. We caution, however, that as the temperature drops below the critical temperature,

83

different values of j will mix in the condensate [94, 96, 97], the $j = 0$ component will grow in weight even if it doesn't have the maximum T_c. We speculate that the phase transition between finite momentum FFLO states and zero-momentum BCS states, which occurs at zero field, is replaced in a field by a smooth crossover between open and close-packed hexagonal lattices. The best place to search experimentally for an exotic vortex lattice is close to the superfluid/normal phase boundary as possible by varying either temperature or interaction strength. Indeed it appears advisable to conduct experiments in systems with the smallest order parameter strength for which it is possible to reliably visualize the vortex lattice. Both the relatively large polarizations and strong interactions required for the appearance of $j \neq 0$ solutions, and the ability to tune parameters over wide ranges in atomic systems, demonstrate the exceptional potential of tunable cold atom systems in the hunt for FFLO vortex latices. The greatest obstacle to realization of the FFLO state is likely competition with phase separated states. We return to this point again later.

The results reported in Fig. 6.1 (a) can be understood qualitatively using quite simple considerations. When the temperature is low, weak pairing is expected to be dominated by states at the Fermi energy. For that reason, the zero-field pairing wavevector on the phase boundary is expected to be close to $k_{F\uparrow} - k_{F\downarrow}$ when $T_c \to 0$, i.e. when the interactions are just strong enough to cause pairing. Using a small p approximation it follows that the pairing wavevector for $T_c \to 0$ is given approximately by

$$Q = \frac{2k_{F0}p}{3}. \tag{6.4}$$

The Landau level index at finite fields can be estimated by quantizing the pairing wavevector. This gives

$$j \approx \frac{(\hbar^2 Q^2)/4m}{\hbar\Omega_c} \simeq \frac{\varepsilon_{F0}}{\hbar\Omega_c}\frac{2p^2}{9}. \tag{6.5}$$

It is easy to check that this equation is quite consistent with the numerical results
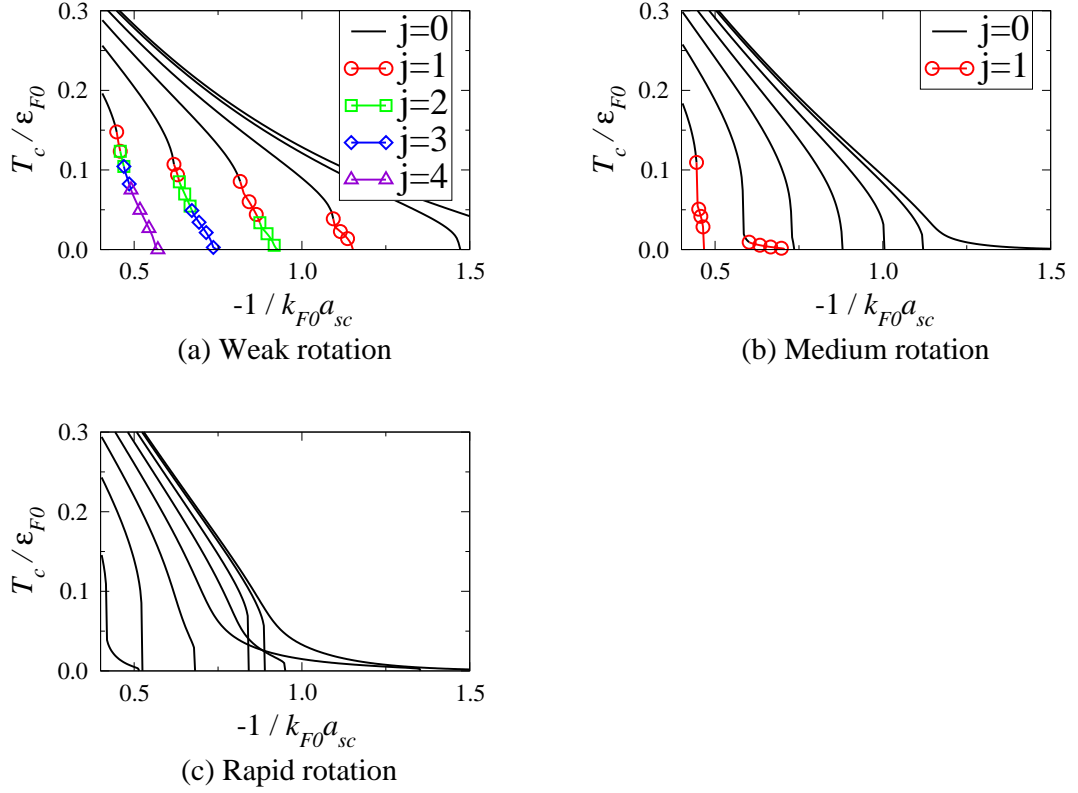
Figure 6.1: Critical T_c vs $-1/k_{F0}a_{\text{sc}}$. (a) $\hbar\Omega_c/\varepsilon_{F0} = 0.02$. The curves are for different polarizations 0.0, 0.1, 0.2, 0.3, 0.4, 0.5 from top to bottom. (b) $\hbar\Omega_c/\varepsilon_{F0} = 0.17$. Polarizations are from 0.0 to 0.6. (c) $\hbar\Omega_c/\varepsilon_{F0} = 0.50$. Polarizations are from 0.0 to 0.7.

we have obtained. For smaller values of $\hbar\Omega_c$ we therefore are confident that even larger values of j should occur, although exotic vortex lattice may again be confined even more strongly to the region close to the phase boundary. For a given value of polarization, the value of j decreases with increasing interaction strength because T_c moves to higher temperatures, reemphasizing the importance of pairing precisely at the Fermi energy.

Fig. 6.1 (b) and (c) show results for systems with larger values of $\hbar\Omega_c$ than have been reported in experiments to date. One observation is that non-zero j states are less likely to occur at large $\hbar\Omega_c$ and appear only at very high polarization and strong interactions. This property is explained by Eq. (6.5). Indeed one can check that the appearance of non-zero j values is again consistent with this esti- mate. Other new features that emerge in these figures are due mainly to large LL quantization effects. At very high rotation frequency [Fig. 6.1 (c)], only the $j = 0$ COM LL is realized. Note that at high temperature, all the graphs look similar.(T_c decreases monotonically as the polarization increases and as the interaction strength decreases.) T_c is more weakly dependent on the rotation frequency. This is because the thermal energy is comparable to or larger than the energy quantization due to rotation. On the other hand, at low temperatures, the LL quantization effects become important because the particles have one-dimensional densities-of-states for each Landau level leading to peaks in pairing (at least in this mean-field-theory calculation) when any Landau level is just slightly occupied. The non-monotonic density of states becomes important when the LL spacing is much bigger than the temperature. In this case, we expect non-monotonic behavior that is sensitive to the density of both hyperfine species; we expect non-monotonic dependence on polariza- tion and the occasional appearance of strong condensates at very large polarizations. Some of this non-monotonic behavior is evident in Fig. 6.1 (c).

(a) Weak rotation

(b) Medium rotation

(c) Rapid rotation
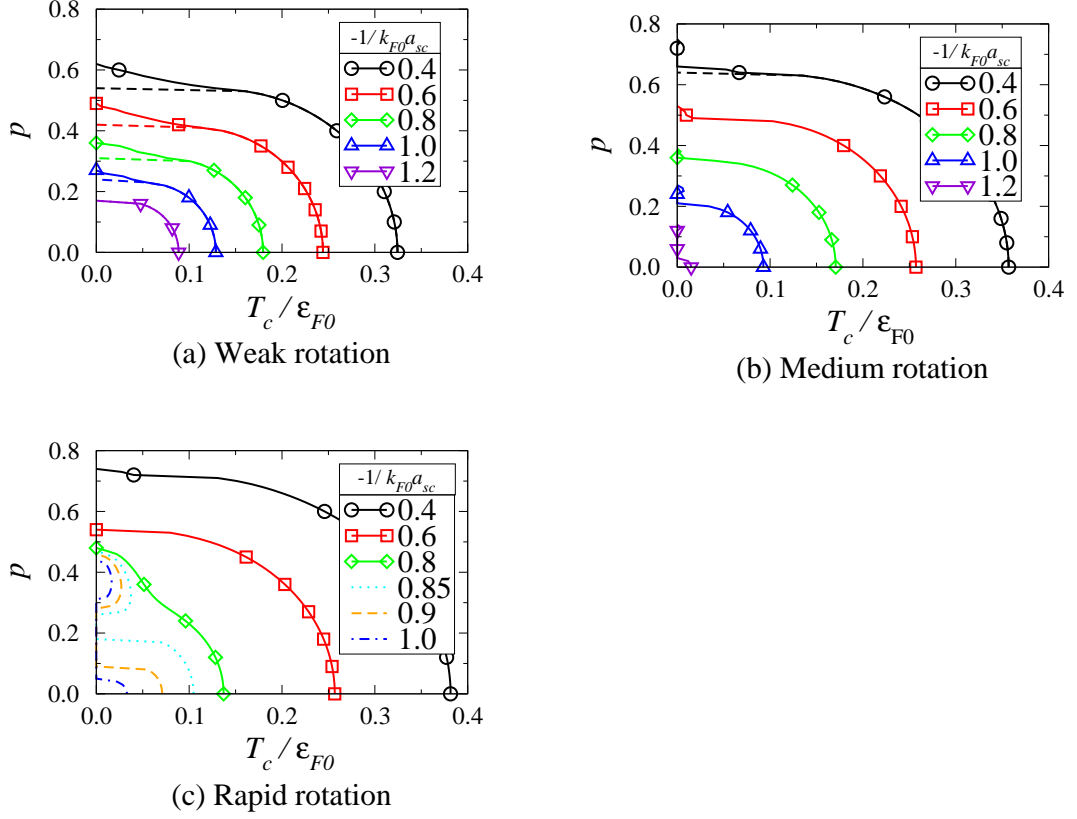
Figure 6.2: Polarization vs T_c/ε_{F0}. (a) $\hbar\Omega_c/\varepsilon_{F0} = 0.02$. Curves are for different values of $-1/k_{F0}a_{sc}$. (b) is for $\hbar\Omega_c/\varepsilon_{F0} = 0.17$ and (c) is for $\hbar\Omega_c/\varepsilon_{F0} = 0.50$. Dashed lines in (a) and (b) shows the T_c curves for $j = 0$ and all the curves in (c) corresponds to $j = 0$.

6.3 Phase Diagrams in Parameter Space

By using the critical temperature determined in the previous section, we determine the phase boundaries in the parameter space spanned by $\hbar\Omega_c$, a_{sc} and the polarization.

In Fig. 6.2 we show the phase boundaries *vs.* polarization and temperature for a series of interaction strengths. For slow rotation [Fig. 6.2 (a)] it is similar to the usual BCS-FFLO phase diagram (compare with Fig. 5.5). At higher rotation fre-
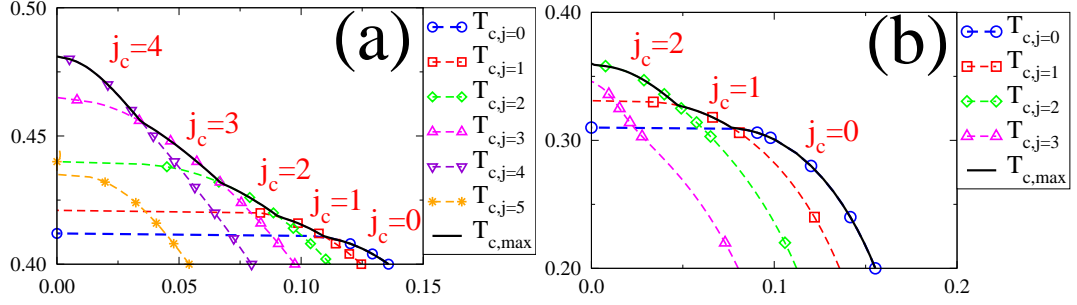
Figure 6.3: Enlarged figures of Fig. 6.2 (a) for $-1/k_{F0}a_{\mathrm{sc}}=$ (a) 0.6 and (b) 0.8 near the phase boundaries between FFLO states and normal fluid. The horizontal axis shows T_c/ε_{F0} and the vertical axis is polarization. We calculate T_c for different j's and determine the optimal j that gives the highest T_c.

quencies, shown in Fig. 6.2 (b), FFLO states are less likely to occur. The transition temperature still decreases monotonically as the polarization increases and above some critical polarization, the normal state prevails. At very high rotation frequencies, shown in Fig. 6.2 (c), the LL quantization effects become more important and we observe reemergence of condensed states at around $p = 0.4$. The difference of the Fermi energies at this polarization is exactly equal to the LL spacing and the dominant pairing occurs between individual particles whose Landau level indices differ by one.

In Fig. 6.3 we show an enlargement of the phase diagram for the FFLO state, showing also the critical temperatures for a number of different COM LL index channels j in addition to the one with the largest T_c. When the polarization is small, $j = 0$ pairing leads to the highest T_c; that is $j = 0$ is the optimal pairing channel for condensation which we denote as j_c. As the polarization increases, T_c^j for nonzero j is larger than $T_c^{j=0}$ and j_c increases with the polarization. This is analogous to having an increasing pairing COM momentum with increasing polarization field in the zero-field case. For a given value of $\hbar\Omega_c$, non-zero values of j_c are more likely when interactions are stronger, because the superfluid has to be able to withstand the ill effects of polarization out to a sufficiently large value of p. If the interaction
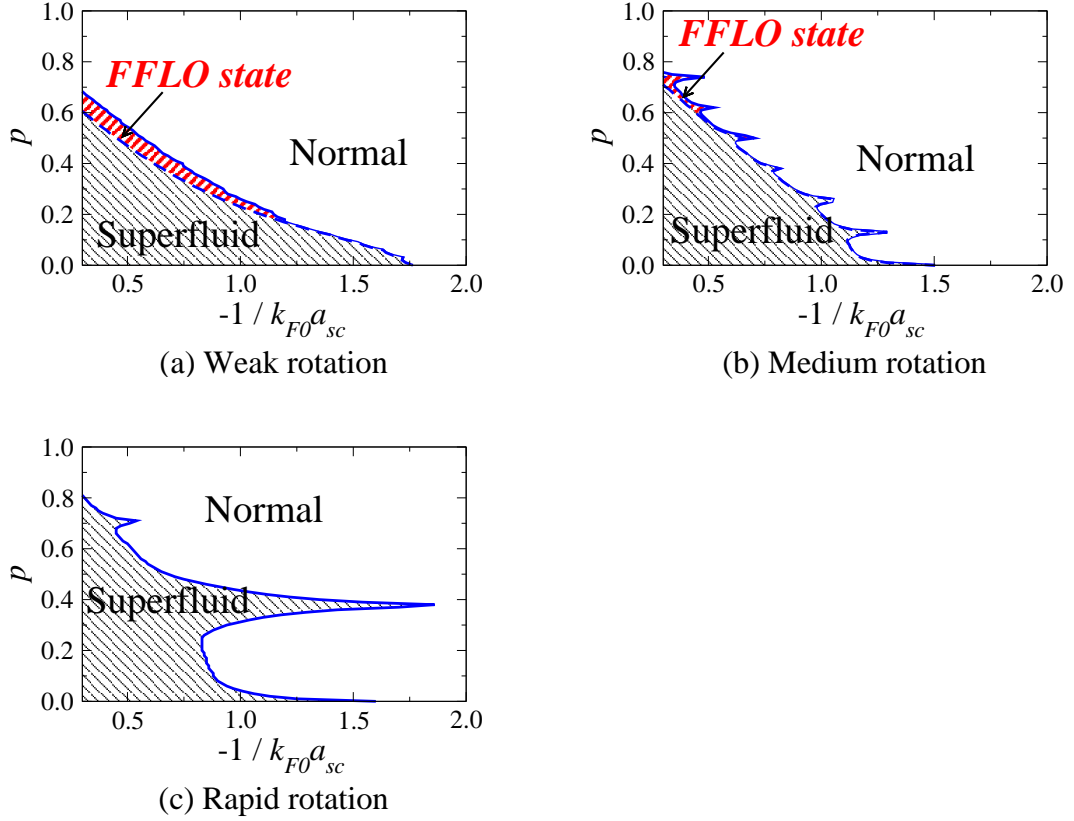
Figure 6.4: Polarization vs $-1/k_{F0}a_{sc}$. We calculate T_c for polarizations from 0 to 1 with increment 0.01 and choose the largest one that has a finite T_c. (a) $\hbar\Omega_c/\varepsilon_{F0} = 0.02$ (b) $\hbar\Omega_c/\varepsilon_{F0} = 0.17$ and (c) $\hbar\Omega_c/\varepsilon_{F0} = 0.50$. Solid blue curves show phase boundary between normal fluid and superfluid and dashed blue curves in (a) and (b) show phase boundary for COM LL $j = 0$.

is too weak, no non-zero j pairing can occur and j_c is zero.

In Fig. 6.4 we plot the phase diagram *vs.* polarization and effective interaction space for slow, intermediate, and rapid rotations. The critical polarization decreases as the interaction strength decreases for weak rotations [Fig. 6.4 (a)], as seen in experiment [33]. The regions labeled FFLO in this figure have $j \neq 0$ condensates at the normal superfluid boundary. Quite generally this behavior occurs only in a small region along the boundary between the superfluid and normal state in the regime of large polarization and strong interactions. Faster rotation gener-

ally suppresses FFLO states, as emphasized earlier, but the superfluid phase can be realized at high polarization and weak interaction by tuning the system such that the Fermi energy mismatch between majority and minority species is an integer times the LL spacing, and the Fermi energies are close to a quantized LL energy. In Fig. 6.4 (c), we see that big peaks occur if these conditions are met. At zero polarization $\varepsilon_{F\uparrow} = \varepsilon_{F\downarrow} = 1.96$, in units of LL spacing, and the lowest LL is at 0.5. For $p = 0.41$, $\varepsilon_{F\uparrow} = 2.52$ and $\varepsilon_{F\downarrow} = 1.52$ so that the Fermi energy difference is exactly the LL spacing and each Fermi energy is very close to the LLs. For $p = 0.72$, $\varepsilon_{F\uparrow} = 2.80$ and $\varepsilon_{F\downarrow} = 0.80$.

6.4   Discussion and Conclusions

In summary, using the T_c equation we have calculated the phase boundary between the normal and superfluid phase considering pairing in different center-of-mass Landau levels. We find that states with higher Landau level condensates can occur on the boundary between the normal and superfluid phase regions in a parameter space that can in principle be explored systematically by taking advantage of Feshbach resonances and of the ability to create arbitrary degrees of hyperfine state polarization in an atom cloud. These FFLO vortex lattice states will have distinct vortex lattices [89, 90, 91] which should aid their identification. High polarization and strong interactions are required to realize the FFLO state. At high rotation frequency, features that originate from rotational quantization effects play an important role and we find that for certain parameters the superfluid phase persists to high polarization.

The regime where the FFLO state occurs in rotating systems seems accessible to experiment, and hence we believe that these exotic vortex structures are observable. The greatest obstacle to their observation may be competition with states in which the atoms phase separate into regions with condensation but no polarization

and regions with polarization but no condensation. We believe that FFLO physics would almost certainly occur if phase separation could be suppressed. Phase separation does not occur for electrons in a superconducting metal, and cannot because of the large Coulomb energy price that would have to be paid. One possibility for suppressing phase separation in atomic systems with attractive interactions, is to artificially create the necessary weak but long range repulsive interactions by electrically inducing dipoles [99] in a pancake shaped [100], but not necessarily quasi-two-dimensional trapped atom system. The typical dipole-dipole interaction energy is $p^2/R^3 \sim p^2 n \sim \alpha^2 E^2 n$ where p is the dipole moment induced by the external electric field E, R is the average inter-atom distance, n is the density of the atoms and α is the polarizability of the atom. If this energy is much smaller than the typical atom-atom interaction energy $\varepsilon_{F0}(k_{F0}|a_{sc}|)$, then the physics on short length scales does not change much. On the other hand, if the energy cost of the whole system due to the long range dipole interaction when the system is phase separated is much larger than the condensation energy gain, phase separation can be suppressed. Thus, $p^2 n^2 V \gg D(0)\Delta_0^2 \sim N\varepsilon_{F0}e^{-\pi/k_{F0}|a_{sc}|}$ where $D(0)$ is the density of states at the Fermi level, N is the number of atoms and V is the volume of the system. These conditions lead to a condition for the external electric field

$$e^{-\pi/k_{F0}|a_{sc}|} \ll \frac{\alpha^2 n E^2}{\varepsilon_{F0}} \ll k_{F0}|a_{sc}| \tag{6.6}$$

which can be easily satisfied for small $k_{F0}|a_{sc}|$. FFLO states are most likely expected to occur near the critical temperature T_c while experimentally observed phase-separated states are well below T_c. It is known that phase separation is less likely at higher temperatures so it could be possible to observe FFLO states near T_c without explicitly suppressing phase separation.

Finally we mention that peculiar additional interesting effects occur because of Landau level quantization if the rotation frequency is sufficiently large. Very large

rotation frequencies have been achieved in experiments with bosonic atoms [101]. We believe, therefore, that there is no fundamental obstacle to approaching the rapid-rotation limit with Fermions. Although we have used mean-field-theory here to study this regime, there is every reason to expect unanticipated properties to emerge from strong quantum fluctuations and correlations. At sufficiently rapid rotations, it should be possible to for the first time study the fractional quantum Hall effect in fermion systems with attractive interactions [102].

Chapter 7

Summary

We have studied two different polarized fermion systems focusing on how the pairing mechanism adapts to a finite polarization. Our calculations use a generalized BCS mean-field-theory approach to describe the superconducting state and are therefore most reliable in the weak coupling limit. When there is spin degeneracy for each constituent of the Cooper pair as in bilayer electron-hole systems, the Fermi surface mismatch caused by the polarization gives rise to the spontaneous spin-polarization of each species to maximize the energy gain obtained by condensation. This leads to the uniformly mixed state of the condensate and the normal fluid. In this case the Cooper pairs have zero total momentum since they are formed from the components that now have the same Fermi surfaces due to spin-polarization. The SO coupling lifts the spin degeneracy and can lead to the deformation of the energy spectrum. The interplay between the ferromagnetic order parameter and the condensate order parameter appears to be complicated in the presence of SO coupling and has not yet been fully resolved. This is an important direction for future work. In addition to the ground state characteristics we have studied, experimental evidence for the excitonic condensation will most likely be the transport properties of separately contacted bilayer systems. Once the system forms a condensate, the transport of each layer will

be highly coherent, and the effect of SO interaction on the coherent transport will be also interesting from a spintronics point of view. We considered only uniform order parameters in this work. In principle FFLO-like pairing is also possible in polarized electron-hole systems. We expect ferromagnetic phase is energetically favorable but more careful consideration is required to exclude this possibility.

In atomic systems, there is no spin-degeneracy as in the bilayer systems. The Cooper pairs then can have finite total momenta as the lowest energy state. In view of the extreme controllability of the parameters in cold atom systems, the observation of the FFLO state seems highly plausible. We have developed a mean-field theory for the critical temperature of the rotating fermion atom systems and the phase boundary determined by solving the implicit T_c equation suggests that FFLO states are experimentally accessible. Even though the qualitative pictures of the phase diagram may be also good for the confined systems, spatially nonuniform theory is required to describe the effects of the confining potential.

Appendix A

Derivation of the Rashba Spin-Orbit Interaction in Zinc-blende Semiconductors

In this appendix, we briefly review the Löwdin partitioning method [85, 86] and the Luttinger Hamiltonian [103] for semiconductors and then explicitly derive the Rashba Spin-orbit interaction Hamiltonian for two-dimensional electron and hole systems. Using Löwdin partitioning technique, we can derive the effective Hamiltonian for a subspace with the effects from outside the subspace treated as perturbations. The Rashba SO interaction for the conduction band comes from the third order terms of the $\mathbf{k} \cdot \mathbf{p}$ interaction that couples the conduction band states and the valence band states, and the Rashba SO for the heavy-hole valence band comes from the off-diagonal terms in the 4×4 Luttinger Hamiltonian that describes the valence bands.

A.1 Partitioning Method

Consider an eigenvalue problem that can be represented in a matrix form

$$Hc = \varepsilon c \ . \tag{A.1}$$

Assuming that the system can be divided into two subspaces A and B,

$$\begin{pmatrix} H_{AA} & H_{AB} \\ H_{BA} & H_{BB} \end{pmatrix} \begin{pmatrix} c_A \\ c_B \end{pmatrix} = \varepsilon \begin{pmatrix} c_A \\ c_B \end{pmatrix} , \tag{A.2}$$

we obtain two matrix equations,

$$\begin{cases} H_{AA}c_A + H_{AB}c_B = \varepsilon c_A \\ H_{BA}c_A + H_{BB}c_B = \varepsilon c_B \end{cases} . \tag{A.3}$$

Solving c_B from the second equation and then substitute in the first equation, we obtain

$$c_B = \frac{1}{\varepsilon - H_{BB}} H_{BA}c_A \tag{A.4}$$

$$\left(H_{AA} + H_{AB}\frac{1}{\varepsilon - H_{BB}} H_{BA} \right) c_A = \varepsilon c_A$$

$$\Rightarrow \quad U_{AA}c_A = \varepsilon c_A \ , \tag{A.5}$$

where

$$U_{AA} \equiv H_{AA} + H_{AB}\frac{1}{\varepsilon - H_{BB}} H_{BA} \ . \tag{A.6}$$

Eq. (A.5) is the reduced eigenvalue equation in subspace A. If we can divide H_{BB} into diagonal part H_{BB}^d and off-diagonal part H_{BB}', assuming H_{BB}' is small, we can

96

expand U_{AA} in a power series in H'_{BB}.

$$U_{AA} = H_{AA} + H_{AB} \frac{1}{\varepsilon - H_{BB}^d} H_{BA} + H_{AB} \frac{1}{\varepsilon - H_{BB}^d} H'_{BB} \frac{1}{\varepsilon - H_{BB}^d} H_{BA} + \cdots . \quad \text{(A.7)}$$

The eigenvalue ε and the eigenvector c_A can be evaluated by solving Eq. (A.5) iteratively using Eq. (A.7) up to some finite order.

A.2 Luttinger Hamiltonian

Semiconductors with diamond- or zinc-blende-type structures can be described by the Luttinger Hamiltonian [103] which can be derived from the $\mathbf{k} \cdot \mathbf{p}$ Hamiltonian using the partitioning method. If there is a confining potential as in quantum wells, we can use the envelope function approximation making use of the long length scale of the confining potential. In this section, we derive the Luttinger Hamiltonian for the conduction bands and the valence bands, and use the envelope function approximation for the subbands in the presence of the confining potential. The Rashba SO interaction will be derived in the next section using the subband states of the envelope function approximation as basis states.

The Hamiltonian for an electron in a crystal in the presence of a confining potential is given by

$$\widehat{H} = \widehat{H}_0 + V_{\text{conf}}(\mathbf{r}) \quad \text{(A.8)}$$

with

$$\widehat{H}_0 = \frac{p^2}{2m} + V_{\text{cr}}(\mathbf{r}) + V_{SO} \quad \text{(A.9)}$$

where $V_{\text{cr}}(\mathbf{r})$ is the crystal field, $V_{\text{conf}}(\mathbf{r})$ is the confining potential and the atomic spin-orbit interaction V_{SO} is

$$V_{SO} = \frac{\hbar}{4m^2c^2} (\boldsymbol{\nabla} V_{\text{cr}} \times \mathbf{p}) \cdot \boldsymbol{\sigma} . \quad \text{(A.10)}$$

97

We will use a complete orthonormal basis defined by

$$\langle \mathbf{r} | n\mathbf{k} \rangle = e^{i\mathbf{k} \cdot \mathbf{r}} u_{n0}(\mathbf{r}) \tag{A.11}$$

where $u_{n0}(\mathbf{r})$ is related to the Bloch state $\psi_{n\mathbf{k}}$,which is the eigenstate of the Hamiltonian in the absence of the confining potential, by

$$\psi_{n\mathbf{k}}(\mathbf{r}) = e^{i\mathbf{k} \cdot \mathbf{r}} u_{n\mathbf{k}}(\mathbf{r}) \ . \tag{A.12}$$

$u_{n0}(\mathbf{r})$ is an eigenstate of $\widehat{H}_0$ with eigenvalue ε_{n0} and has the same periodic properties as the crystal. n is the band index and $\mathbf{k}$ is the wavevector in the first Brillouin zone. Once we know the band edge ε_{n0} for $\mathbf{k} = 0$, we can calculate the energy for small $\mathbf{k}$ using the perturbation method. The matrix elements of $\widehat{H}_0$ in this basis are given by

$$
\begin{aligned}
\langle n\mathbf{k} | \widehat{H}_0 | n'\mathbf{k}' \rangle &= \int_V d\mathbf{r} e^{-i(\mathbf{k}-\mathbf{k}') \cdot \mathbf{r}} \underbrace{u_{n0}^\dagger(\mathbf{r}) \left(\widehat{H}_0 + \frac{\hbar}{m} \mathbf{k} \cdot \boldsymbol{\pi} + \frac{\hbar^2 k^2}{2m} \right) u_{n'0}(\mathbf{r})}_{\equiv f(\mathbf{r})} \\
&= \left(\varepsilon_{n0} + \frac{\hbar^2 k^2}{2m} \right) \delta_{nn'} \delta_{\mathbf{k}\mathbf{k}'} + \frac{\hbar}{m} (\mathbf{k} \cdot \boldsymbol{\pi})_{nn'} \delta_{\mathbf{k}\mathbf{k}'}
\end{aligned}
\tag{A.13}
$$

where $\boldsymbol{\pi} = \mathbf{p} + \hbar(\boldsymbol{\sigma} \times \boldsymbol{\nabla} V_{\mathbf{cr}})/4mc^2$ and $(\mathbf{k} \cdot \boldsymbol{\pi})_{nn'} = \langle n0 | \mathbf{k} \cdot \boldsymbol{\pi} | n'0 \rangle$. We assume that the spin-dependent part of $\boldsymbol{\pi}$ gives negligible contribution so that $\mathbf{k} \cdot \boldsymbol{\pi} \simeq \mathbf{k} \cdot \mathbf{p}$. Here we used a property that for the periodic function $f(\mathbf{r})$, it can be expanded as a sum

$\sum_{\mathbf{K}} e^{i\mathbf{K}\cdot\mathbf{r}} \tilde{f}(\mathbf{K})$ where $\mathbf{K}$ is a reciprocal lattice vector and then

$$
\begin{aligned}
\int_V d\mathbf{r} e^{-i(\mathbf{k}-\mathbf{k}')\cdot\mathbf{r}} f(\mathbf{r}) &= \int_V d\mathbf{r} e^{-i(\mathbf{k}-\mathbf{k}')\cdot\mathbf{r}} \sum_{\mathbf{K}} e^{i\mathbf{K}\cdot\mathbf{r}} \tilde{f}(\mathbf{K}) \\
&= \sum_{\mathbf{K}} \tilde{f}(\mathbf{K}) \int_V d\mathbf{r} e^{-i(\mathbf{k}-\mathbf{k}'-\mathbf{K})\cdot\mathbf{r}} \\
&= \sum_{\mathbf{K}} \tilde{f}(\mathbf{K}) \delta_{\mathbf{k}-\mathbf{k}',\mathbf{K}} \\
&= \tilde{f}(0) \delta_{\mathbf{k}\mathbf{k}'} \\
&= \int_V d\mathbf{r} f(\mathbf{r}) \delta_{\mathbf{k}\mathbf{k}'}
\end{aligned}
\tag{A.14}
$$

because, for $\mathbf{k}$ and $\mathbf{k}'$ both in the first Brillouin zone, $\mathbf{k} - \mathbf{k}' = \mathbf{K}$ is only possible for $\mathbf{K} = 0$. The matrix elements of V_{conf} are

$$
\begin{aligned}
\langle n\mathbf{k}|V_{\mathrm{conf}}|n'\mathbf{k}'\rangle &= \int_V d\mathbf{r} e^{-i(\mathbf{k}-\mathbf{k}')\cdot\mathbf{r}} u_{n0}^\dagger(\mathbf{r}) V_{\mathrm{conf}}(\mathbf{r}) u_{n'0}(\mathbf{r}) \\
&= \int_V d\mathbf{r} e^{-i(\mathbf{k}-\mathbf{k}')\cdot\mathbf{r}} \sum_{\mathbf{K}} e^{i\mathbf{K}\cdot\mathbf{r}} c_{nn'}(\mathbf{K}) V_{\mathrm{conf}}(\mathbf{r}) \\
&= V \sum_{\mathbf{K}} c_{nn'}(\mathbf{K}) \tilde{V}_{\mathrm{conf}}(\mathbf{k}-\mathbf{k}'-\mathbf{K}) ,
\end{aligned}
\tag{A.15}
$$

where

$$
c_{nn'}(\mathbf{K}) = \frac{1}{V} \int_V d\mathbf{r} e^{-i\mathbf{K}\cdot\mathbf{r}} u_{n0}^\dagger(\mathbf{r}) u_{n'0}(\mathbf{r}) .
\tag{A.16}
$$

For a slowly varying confining potential, $\tilde{V}_{\mathrm{conf}}(\mathbf{k}-\mathbf{k}'-\mathbf{K})$ is negligible for nonzero $\mathbf{K}$. Then

$$
\begin{aligned}
\langle n\mathbf{k}|V_{\mathrm{conf}}|n'\mathbf{k}'\rangle &= \tilde{V}_{\mathrm{conf}}(\mathbf{k}-\mathbf{k}') c_{nn'}(0) \\
&= \tilde{V}_{\mathrm{conf}}(\mathbf{k}-\mathbf{k}') \delta_{nn'} .
\end{aligned}
\tag{A.17}
$$
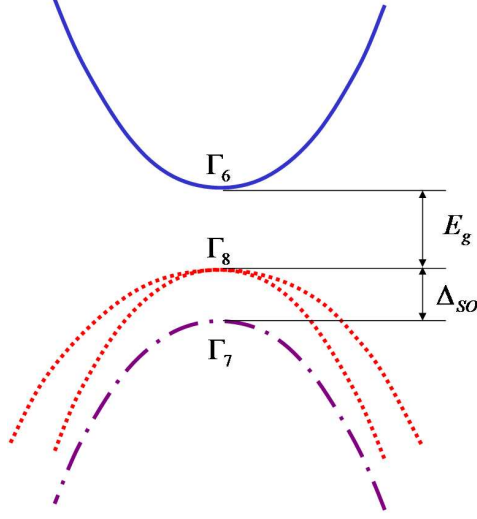
Figure A.1: Illustration of the band structure of bulk GaAs. The conduction band(blue solid curve) edge has Γ_6 symmetry and the valence band edge has Γ_8 symmetry for heavy-hole and light-hole bands(red dotted curves) and Γ_7 symmetry for split-off bands(violet dot-dashed curve).

Combining Eq. (A.13) and Eq. (A.17) we obtain

$$\langle n\mathbf{k}|\widehat{H}|n'\mathbf{k}'\rangle = \left(\varepsilon_{n0} + \frac{\hbar^2 k^2}{2m}\right)\delta_{nn'}\delta_{\mathbf{k}\mathbf{k}'} + \frac{\hbar}{m}(\mathbf{k}\cdot\mathbf{p})_{nn'}\delta_{\mathbf{k}\mathbf{k}'} + \tilde{V}_{\mathrm{conf}}(\mathbf{k}-\mathbf{k}')\delta_{nn'} . \quad (A.18)$$

We will use the partitioning method with Eq. (A.18) to find effective Hamiltonian for the conduction and valence band subspaces.

The band structure and the band edge near Γ point for bulk GaAs are illustrated in Fig. A.1. The conduction band is doubly degenerate and has Γ_6 symmetry, so that the band edge states are

$$u_{c\alpha}(\mathbf{r}) = u_{c0}(\mathrm{r})\alpha \quad (A.19)$$

$$u_{c\beta}(\mathbf{r}) = u_{c0}(\mathrm{r})\beta \quad (A.20)$$

where $u_{c0}(\mathrm{r})$ has s-orbital-like symmetry, and $\alpha(\beta)$ is spin up(down) state. The

100

valence band edge states have $j = 3/2$-like symmetry and can be represented as

$$u_{v1}(\mathbf{r}) = \langle\mathbf{r}|\frac{3}{2},\frac{3}{2}\rangle = -\frac{1}{\sqrt{2}}(X + iY)\alpha \tag{A.21}$$

$$u_{v2}(\mathbf{r}) = \langle\mathbf{r}|\frac{3}{2},\frac{1}{2}\rangle = -\frac{1}{\sqrt{6}}((X + iY)\beta - 2Z\alpha) \tag{A.22}$$

$$u_{v3}(\mathbf{r}) = \langle\mathbf{r}|\frac{3}{2},-\frac{1}{2}\rangle = \frac{1}{\sqrt{6}}((X - iY)\alpha + 2Z\beta) \tag{A.23}$$

$$u_{v4}(\mathbf{r}) = \langle\mathbf{r}|\frac{3}{2},-\frac{3}{2}\rangle = \frac{1}{\sqrt{2}}(X - iY)\beta \tag{A.24}$$

$$u_{v5}(\mathbf{r}) = \langle\mathbf{r}|\frac{1}{2},\frac{1}{2}\rangle = \frac{1}{\sqrt{3}}((X + iY)\beta + Z\alpha) \tag{A.25}$$

$$u_{v6}(\mathbf{r}) = \langle\mathbf{r}|\frac{1}{2},-\frac{1}{2}\rangle = -\frac{1}{\sqrt{3}}((X - iY)\alpha - Z\beta) \tag{A.26}$$

where X, Y and Z are p-like states

$$X \propto xf(r) \tag{A.27}$$

$$Y \propto yf(r) \tag{A.28}$$

$$Z \propto zf(r) , \tag{A.29}$$

and u_{v1} and u_{v4} form the heavy hole bands, u_{v2} and u_{v3} form the light hole bands and u_{v5} and v_{v6} form the split-off bands. Now we can calculate the matrix elements of $\mathbf{k}\cdot\boldsymbol{\pi}$. Due to the symmetry and the selection rule, the matrix elements of $\mathbf{k}\cdot\mathbf{p}$ between conduction band states are zero. While the matrix elements between valence band states give linear terms in $\mathbf{k}$ for systems without inversion symmetry, these linear terms are relatively unimportant for valence bands so we will not consider these terms further. The matrix elements we consider for $\mathbf{k} \cdot \mathbf{p}$ is therefore between the conduction band states and the valence band states. Using Eq. (A.7) the effective

Hamiltonian matrix elements for a subspace $\mathbb{D}_A$ become

$$
\begin{aligned}
\langle n\mathbf{k}|\widehat{H}_A|n'\mathbf{k}'\rangle &= \left(\varepsilon_{n0} + \frac{\hbar^2 k^2}{2m}\right)\delta_{nn'}\delta_{\mathbf{k}\mathbf{k}'} + \tilde{V}_{\mathrm{conf}}(\mathbf{k} - \mathbf{k}')\delta_{nn'} \\
&\quad + \sum_{m\notin\mathbb{D}_A}\left(\frac{\hbar}{m}\right)^2 \frac{(\mathbf{k}\cdot\mathbf{p})_{nm}(\mathbf{k}\cdot\mathbf{p})_{mn'}}{\varepsilon - \varepsilon_{m0}}\delta_{\mathbf{k}\mathbf{k}'} \\
&\equiv D_{nn'}(\mathbf{k})\delta_{\mathbf{k}\mathbf{k}'} + \tilde{V}_{\mathrm{conf}}(\mathbf{k} - \mathbf{k}')\delta_{nn'}
\end{aligned}
\tag{A.30}
$$

up to second order. The eigenvalue ε is evaluated by solving

$$
\sum_{n'\mathbf{k}'\in\mathbb{D}_c}\langle n\mathbf{k}|\widehat{H}|n'\mathbf{k}'\rangle c_{n'\mathbf{k}'} = \varepsilon c_{n\mathbf{k}} \ .
\tag{A.31}
$$

Multiplying $e^{i\mathbf{k}\cdot\mathbf{r}}$ and then summing over all $\mathbf{k}$ in the first Brillouin zone,

$$
\sum_{nn'} D_{nn'}(-i\boldsymbol{\nabla})F_{n'}(\mathbf{r}) + \sum_{\mathbf{k},\mathbf{k}'}\tilde{V}_{\mathrm{conf}}(\mathbf{k} - \mathbf{k}')e^{i\mathbf{k}\cdot\mathbf{r}}c_{n\mathbf{k}'} = \varepsilon F_n(\mathbf{r})
\tag{A.32}
$$

where

$$
F_n(\mathbf{r}) \equiv \sum_{\mathbf{k}} e^{i\mathbf{k}\cdot\mathbf{r}}c_{n\mathbf{k}} \ .
\tag{A.33}
$$

The second term can be simplified using

$$
\begin{aligned}
\sum_{\mathbf{k},\mathbf{k}'}\tilde{V}_{\mathrm{conf}}(\mathbf{k} - \mathbf{k}')e^{i\mathbf{k}\cdot\mathbf{r}}c_{n\mathbf{k}} &= \sum_{\mathbf{q}} e^{i\mathbf{q}\cdot\mathbf{r}}\tilde{V}_{\mathrm{conf}}(\mathbf{q})\sum \mathbf{k}'e^{i\mathbf{k}'\cdot\mathbf{r}}c_{n\mathbf{k}'} \tag{A.34} \\
&\simeq V_{\mathrm{conf}}(\mathbf{r})F_n(\mathbf{r}) \tag{A.35}
\end{aligned}
$$

because $\tilde{V}_{\mathrm{conf}}(\mathbf{q})$ is negligible for large q. Thus, we obtainthe Schrödinger equation for the *envelope function* $F_n(\mathbf{r})$,

$$
\sum_{nn'} D_{nn'}(-i\boldsymbol{\nabla})F_{n'}(\mathbf{r}) + V_{\mathrm{conf}}(\mathbf{r})F_n(\mathbf{r}) = \varepsilon F_n(\mathbf{r}) \ .
\tag{A.36}
$$

$D_{nn'}(\mathbf{k})$ itself depends on the eigenvalue ε, but we can replace ε with ε_{n0} since the

term containing ε dependence is already second order. Therefore, $D_{nn'}(\mathbf{k})$ determines the bulk band structure up to second order, which is equivalent to the effective mass approximation. In the presence of the confining potential, the j-th subband eigenstate can be obtained by solving Eq. (A.36) and then by multiplying the band edge states u_{n0}:

$$
\begin{aligned}
\psi_n^j(\mathbf{r}) &= \sum_{n\mathbf{k}} c_{n\mathbf{k}} \langle \mathbf{r}|n\mathbf{k}\rangle \\
&= \sum_{n\mathbf{k}} e^{i\mathbf{k}\cdot\mathbf{r}} c_{n\mathbf{k}} u_{n0}(\mathbf{r}) \tag{A.37} \\
&= \sum_n F_n(\mathbf{r}) u_{n0}(\mathbf{r}) \ . \tag{A.38}
\end{aligned}
$$

For the conduction bands for bulk systems, $D_{nn'}(\mathbf{k})$ is diagonal and we obtain

$$
\begin{aligned}
\varepsilon_{c\mathbf{k}} &= \varepsilon_{c0} + \frac{\hbar^2 k^2}{2m} + \sum_{m\notin\mathbb{D}_c} \frac{\hbar^2}{m^2} \frac{|(\mathbf{k}\cdot\mathbf{p})_{c,m}|^2}{\varepsilon_{c0}-\varepsilon_{m0}} \tag{A.39} \\
&= \varepsilon_{c0} + \frac{\hbar^2 k^2}{2m_c^*} \tag{A.40}
\end{aligned}
$$

where m_c^* is the effective mass for the conduction bands. In the presence of the confining potential, the wavevector in the direction of the confining potential is quantized and the conduction band split into several subbands, but each subband is still doubly spin-degenerate. The envelope function for the j-th subband is given by solving

$$
\left(\varepsilon_{c0} - \frac{\hbar^2}{2m_c^*}\nabla^2 + V_{\mathrm{conf}}(\mathbf{r}) \right) F_c^j(\mathbf{r}) = \varepsilon_{cj} F_c^j(\mathbf{r}) \ . \tag{A.41}
$$

The situation is more complicated for the valence bands due to the 4-fold degeneracy at the valence band edge. $D_{nn'}(\mathbf{k})$ is not diagonal and it is given by 4×4 Luttinger Hamiltonian if we consider only the heavy hole and light hole bands, and 6×6

Luttinger Hamiltonian if we include the split-off bands.

$$
H_L = \left(
\begin{array}{cccc|cc}
H_{hh} & -iL & -M & 0 & -\frac{iL}{\sqrt{2}} & \sqrt{2}M \\[4pt]
iL^* & H_{lh} & 0 & -M & -\frac{(P-2Q)}{3\sqrt{2}} & -i\frac{\sqrt{3}L}{\sqrt{2}} \\[4pt]
-M^* & 0 & H_{lh} & iL & -i\frac{\sqrt{3}L^*}{\sqrt{2}} & -\frac{(P-2Q)}{3\sqrt{2}} \\[4pt]
0 & -M^* & -iL^* & H_{hh} & \sqrt{2}M^* & -\frac{iL^*}{\sqrt{2}} \\[4pt]
\hline
\frac{iL^*}{\sqrt{2}} & -\frac{(P-2Q)}{3\sqrt{2}} & i\frac{\sqrt{3}L}{\sqrt{2}} & \sqrt{2}M & \frac{P+Q}{3}-\Delta_{SO} & 0 \\[4pt]
\sqrt{2}M^* & i\frac{\sqrt{3}L^*}{\sqrt{2}} & -\frac{(P-2Q)}{3\sqrt{2}} & \frac{iL}{\sqrt{2}} & 0 & \frac{P+Q}{3}-\Delta_{SO}
\end{array}
\right)
\tag{A.42}
$$

where

$$
H_{hh} = -\frac{\hbar^2 k_z^2}{2m}(\gamma_1 - 2\gamma_2) - \frac{\hbar^2}{2m}(\gamma_1 + \gamma_2)(k_x^2 + k_y^2) \tag{A.43}
$$

$$
H_{lh} = -\frac{\hbar^2 k_z^2}{2m}(\gamma_1 + 2\gamma_2) - \frac{\hbar^2}{2m}(\gamma_1 - \gamma_2)(k_x^2 + k_y^2) \tag{A.44}
$$

$$
L = \frac{i\sqrt{3}\hbar^2}{m}\gamma_3 k_z(k_x - ik_y) \tag{A.45}
$$

$$
M = -\frac{\sqrt{3}\hbar^2}{2m}\left(\gamma_2(k_x^2 - k_y^2) - 2i\gamma_3 k_x k_y\right) \tag{A.46}
$$

$$
P = -\frac{\hbar^2}{m}\left((\gamma_1 + \gamma_2)(k_x^2 + k_y^2) + (\gamma_1 - 2\gamma_2)k_z^2\right) \tag{A.47}
$$

$$
Q = -\frac{\hbar^2}{2m}\left((\gamma_1 - 2\gamma_2)(k_x^2 + k_y^2) + (\gamma_1 + 4\gamma_2)k_z^2\right) \tag{A.48}
$$

and γ's are the Luttinger parameters. For many materials, $\gamma_1 > \gamma_2 \simeq \gamma_3$, so we make an assumption that $\gamma_2 \simeq \gamma_3$ and replace γ_2 and γ_3 with the average value $\bar{\gamma} = (\gamma_2 + \gamma_3)/2$. In this axial approximation, the bulk band structure of the valence bands described by 4×4 Luttinger Hamiltonian is isotropic and parabolic with the effective masses

$$
m_{hh} = \frac{m}{\gamma_1 - 2\bar{\gamma}} \tag{A.49}
$$

$$
m_{lh} = \frac{m}{\gamma_1 + 2\bar{\gamma}} \tag{A.50}
$$

for heavy hole and light hole bands respectively, which is illustrated in Fig. A.1. Each band is doubly degenerate and 4-fold degenerate only at $\mathbf{k} = 0$. In the presence of a confining potential, the heavy hole and light hole bands are divided into several subbands respectively, and the degeneracy of the heavy hole and light hole bands at band edge $\mathbf{k} = 0$ is lifted due to the different effective masses.

A.3 Rashba SO Interaction

In this section, we use the subband states as a basis to derive the Rashba SO interaction in the presence of an external field. The Hamiltonian is

$$\widehat{H} = \widehat{H}_0 + V_{\text{conf}}(\mathbf{r}) + V_{\text{ext}}(\mathbf{r}) \tag{A.51}$$

where

$$\widehat{H}_0 = \frac{p^2}{2m} + V_{\text{cr}}(\mathbf{r}) + V_{SO} \tag{A.52}$$

and the j-th subband state of band n we obtained using the envelope function approximation for a system without the external field is

$$\psi_n^j(\mathbf{r}) = F_n^j(\mathbf{r}) u_{n0}(\mathbf{r}) \equiv \langle \mathbf{r} | n; j \rangle \; . \tag{A.53}$$

The envelope function $F_n^j(\mathbf{r})$ is slowly varying function and changes little on a length scale of the lattice vector, and the bulk band edge state $u_{n0}(\mathbf{r})$ is periodic function of the lattice vector. Making use of the two length scales, we calculate the matrix

105

elements of the Hamiltonian in this basis.

$$\langle n; j|\widehat{H}|n'; j'\rangle$$

$$= \int_V d\mathbf{r}\, u_{n0}^\dagger(\mathbf{r})F_n^{j*}(\mathbf{r})\left[\left(\frac{p^2}{2m}F_m^{j'}(\mathbf{r}) \right) u_{m0}(\mathbf{r}) \right.$$

$$+ F_m^{j'}(\mathbf{r})\left(\widehat{H}_0 u_{m0}(\mathbf{r}) \right)$$

$$+ \frac{1}{m}\left(\mathbf{p}F_m^{j'}(\mathbf{r}) \right) \cdot \left(\boldsymbol{\pi} u_{m0}(\mathbf{r}) \right)$$

$$\left. + \left(V_{\text{conf}}(\mathbf{r}) + V_{\text{ext}}(\mathbf{r}) \right) F_m^{j'}(\mathbf{r}) u_{m0}(\mathbf{r}) \right]$$

$$\simeq \sum_{\mathbf{R}} \left[F_n^{j*}(\mathbf{R})\frac{P^2}{2m}F_m^{j'}(\mathbf{R}) \int_{\Omega_{\text{cell}}} d\mathbf{r}\, u_{n0}^\dagger(\mathbf{r})u_{m0}(\mathbf{r}) \right.$$

$$+ F_n^{j*}(\mathbf{R})F_m^{j'}(\mathbf{R}) \int_{\Omega_{\text{cell}}} d\mathbf{r}\, u_{n0}^\dagger(\mathbf{r})\widehat{H}_0 u_{m0}(\mathbf{r})$$

$$+ \frac{1}{m}F_n^{j*}(\mathbf{R})\mathbf{P}F_m^{j'}(\mathbf{R}) \cdot \int_{\Omega_{\text{cell}}} d\mathbf{r}\, u_{n0}^\dagger(\mathbf{r})\boldsymbol{\pi} u_{m0}(\mathbf{r})$$

$$\left. + F_n^{j*}(\mathbf{R})\left(V_{\text{conf}}(\mathbf{R}) + V_{\text{ext}}(\mathbf{R}) \right)F_m^{j'}(\mathbf{R}) \int_{\Omega_{\text{cell}}} d\mathbf{r}\, u_{n0}^\dagger(\mathbf{r})u_{m0}(\mathbf{r}) \right]$$

$$\simeq \langle\langle n; j|\left(\frac{P^2}{2m} + V_{\text{conf}}(\mathbf{R}) \right)|n; j'\rangle\rangle\delta_{nm} + \varepsilon_{n0}\delta_{nm}\delta_{jj'}$$

$$+ \frac{\hbar}{m}\langle\langle n; j| - i\boldsymbol{\nabla}_{\mathbf{R}}|m; j'\rangle\rangle \cdot \mathbf{p}_{nm} + \langle\langle n; j|V_{\text{ext}}(\mathbf{R})|n; j'\rangle\rangle\delta_{nm} \qquad \text{(A.54)}$$

where Ω_{cell} is the volume of a unit cell and we assumed $\boldsymbol{\pi}_{nm} \simeq \mathbf{p}_{nm}$ with $\mathbf{p}_{nm} \equiv \langle n0|\mathbf{p}|m0\rangle$ as before. The double bracket means the expectation value with respect to the envelope functions, that is,

$$\langle\langle n; j|\widehat{O}|m; j'\rangle\rangle \equiv \frac{1}{V} \int_V d\mathbf{R}\, F_n^{j*}(\mathbf{R})\widehat{O}F_m^{j'}(\mathbf{R}) \qquad \text{(A.55)}$$

for any operator $\widehat{O}$. Eq. (A.54) is formally equivalent to Eq. (A.18) , but in the new basis. Note that $\mathbf{k}$ in Eq. (A.18) becomes an operator that acts on the envelope function.

Now we can use these matrix elements to apply the partitioning method [Eq. (A.7)]. We assume that the confining potential only depends on z and an even function of z, and the external potential is given by $V_{\text{ext}}(z) = eEz$ where $\mathbf{E} = E\hat{\mathbf{z}}$ is the effective electric field. Then all the envelope functions have a form

$$F_n^j(\mathbf{r}) = e^{i\mathbf{k}_\perp \cdot \mathbf{r}_\perp} F_n^j(z) \tag{A.56}$$

where $\mathbf{k}_\perp$ and $\mathbf{r}_\perp$ are the projections of $\mathbf{k}$ and $\mathbf{r}$, respectively, to a plane perpendicular to the z-direction. For a subspace $\mathbb{D}_{c;j=1}$ which is spanned by the lowest conduction subbands $|c\alpha; j = 1\rangle$ and $|c\beta; j = 1\rangle$, the effective 2×2 Hamiltonian up to second order is diagonal and reduces to the matrix form of the conduction band envelope function Schrödinger equation [Eq. (A.41)]. The lowest non-zero off-diagonal term comes form the third order term

$$
\begin{aligned}
\langle c\alpha; 1| \widehat{H}_{\mathbb{D}_{c;1}}^{(3)} |c\beta; 1\rangle &= \frac{\hbar^2}{m^2} \sum_{\substack{m \notin \mathbb{D}_c \\ j'j''}} \frac{\langle\langle c\alpha; 1| - i\boldsymbol{\nabla}_{\mathbf{R}}|m; j'\rangle\rangle \cdot \mathbf{p}_{c\alpha,m}}{\varepsilon_{c1} - \varepsilon_{mj'}} \\
&\times \ \langle\langle m; j'|V_{\text{ext}}(\mathbf{R})|m; j''\rangle\rangle \frac{\mathbf{p}_{m,c\beta} \cdot \langle\langle m; j''| - i\boldsymbol{\nabla}_{\mathbf{R}}|c\beta; 1\rangle\rangle}{\varepsilon_{c1} - \varepsilon_{mj''}} ,
\end{aligned}
\tag{A.57}
$$

where $\varepsilon_{\mu j}$ is the j-th subband energy of the conduction(c), heavy hole(h), light hole(l) and split-off(s) bands. We replaced ε with ε_{c1} as a good approximation. Since the envelope functions for α and β spin state conduction bands satisfy the same equation, we can drop the spin indices for the conduction band in the double bracket values. Considering the coupling with subbands from each valence bands

(heavy hole, light hole and split-off bands), after some algebra we obtain

$$
\begin{aligned}
\langle c\alpha; 1|\widehat{H}^{(3)}_{\mathbb{D}_{c;1}}|c\beta; 1\rangle &= i(k_x - ik_y)eEP^2 \sum_{j'j''} \left(\frac{A^{j'j''}_{cl}}{\Delta^{cl}_{1j'}\Delta^{cl}_{1j''}} - \frac{A^{j'j''}_{cs}}{\Delta^{cs}_{1j'}\Delta^{cs}_{1j''}} \right) \\
&= i\alpha_R E(k_x - ik_y) \\
&= \left[\alpha_R(\mathbf{k} \times \mathbf{E}) \cdot \boldsymbol{\sigma} \right]_{\alpha\beta}
\end{aligned}
\tag{A.58}
$$

where P is Kane's momentum matrix elements [104], $\Delta^{\mu\mu'}_{ij} = \varepsilon_{\mu i} - \varepsilon_{\mu' j}$ and

$$
A^{j'j''}_{cl} = \frac{2\hbar^2}{3m^2} \left(\langle\langle c; 1|\partial_z|l; j'\rangle\rangle\langle\langle l; j'|z|l; j''\rangle\rangle\langle\langle l; j''|c; 1\rangle\rangle \right)
\tag{A.59}
$$

$$
A^{j'j''}_{cs} = \frac{2\hbar^2}{3m^2} \left(\langle\langle c; 1|\partial_z|s; j'\rangle\rangle\langle\langle s; j'|z|s; j''\rangle\rangle\langle\langle s; j''|c; 1\rangle\rangle \right) ,
\tag{A.60}
$$

and the Rashba coefficient is

$$
\alpha_R = eP^2 \sum_{j'j''} \left(\frac{A^{j'j''}_{cl}}{\Delta^{cl}_{1j'}\Delta^{cl}_{1j''}} - \frac{A^{j'j''}_{cs}}{\Delta^{cs}_{1j'}\Delta^{cs}_{1j''}} \right) .
\tag{A.61}
$$

Due to the parity of the envelope functions, nonvanishing contributions come from only j'=even and j''=odd. The Rashba interaction for the conduction band is defined by

$$
\widehat{H}^R_c = \alpha_R(\mathbf{k} \times \mathbf{E}) \cdot \boldsymbol{\sigma} .
\tag{A.62}
$$

If the confining potential is a square well with infinite height, the envelope functions are the same for all bands for the same j. Then $A^{j'j''}_{cl} = A^{j'j''}_{cs} \equiv a_{j'j''}$ and we obtain

$$
\alpha_R = eP^2 \sum_{j'j''} a_{j'j''} \left(\frac{1}{\Delta^{cl}_{1j'}\Delta^{cl}_{1j''}} - \frac{1}{\Delta^{cs}_{1j'}\Delta^{cs}_{1j''}} \right) ,
\tag{A.63}
$$

which is given in Ref. [87] for the largest contribution from j'=2 and j''=1.

For the valence bands, the matrix elements of $\widehat{H}_0 + V_{\text{conf}}$ up to the second order are the Luttinger Hamiltonian H_L given by Eq. (A.42) if we treat the elements

of the Luttinger Hamiltonian as operators such as

$$\langle vi;j|(\widehat{H}_0 + V_{\text{conf}})|vi';j'\rangle = \langle\langle vi;j|H_L(-i\boldsymbol{\nabla})_{vi,vi'}|vi';j'\rangle\rangle \ . \tag{A.64}$$

For the subspace $\mathbb{D}_{h;1}$ which is spanned by the lowest heavy hole subband states $|v1;j=1\rangle$ and $|v4;j=1\rangle$, V_{ext} couples different subbands originating from the same band and the Luttinger Hamiltonian gives the coupling between the heavy hole and the light hole subbands. Then the third order off-diagonal term in $\mathbb{D}_{h;1}$ is

$$\begin{aligned}
&\langle v1;1|\widehat{H}^{(3)}_{\mathbb{D}_{h;1}}|v4;1\rangle \\
&= \sum_{\substack{i=2,3 \\ j'j''}} \frac{\langle\langle v1;1|(H_L)_{v1,vi}|vi;j'\rangle\rangle\langle\langle vi;j'|V_{\text{ext}}|vi;j''\rangle\rangle\langle\langle vi;j''|(H_L)_{vi,v4}|v4;1\rangle\rangle}{(\varepsilon_{h,1}-\varepsilon_{l,j'})(\varepsilon_{h,1}-\varepsilon_{l,j''})} \\
&+ \sum_{\substack{i=2,3 \\ j'j''}} \frac{\langle\langle v1;1|V_{\text{ext}}|v1;j'\rangle\rangle\langle\langle v1;j'|(H_L)_{v1,vi}|vi;j''\rangle\rangle\langle\langle vi;j''|(H_L)_{vi,v4}|v4;1\rangle\rangle}{(\varepsilon_{h,1}-\varepsilon_{h,j'})(\varepsilon_{h,1}-\varepsilon_{l,j''})} \\
&+ \sum_{\substack{i=2,3 \\ j'j''}} \frac{\langle\langle v1;1|(H_L)_{v1,vi}|vi;j'\rangle\rangle\langle\langle vi;j'|(H_L)_{vi,v4}|v4;j''\rangle\rangle\langle\langle v4;j''|V_{\text{ext}}|v4;1\rangle\rangle}{(\varepsilon_{h,1}-\varepsilon_{l,j'})(\varepsilon_{h,1}-\varepsilon_{h,j''})} \ .
\end{aligned} \tag{A.65}$$

Luttinger parameters γ_2 and γ_3 in the expression of M will be replaced with their average $\bar{\gamma}$ for the axial approximation. After some algebra we obtain

$$\begin{aligned}
\langle v1;1|\widehat{H}^{(3)}_{\mathbb{D}_{h;1}}|v4;1\rangle &= i(k_x-ik_y)^3 eE \sum_{j'j''}\left(\frac{A_1^{j'j''}}{\Delta_{1j'}^{hl}\Delta_{1j''}^{hl}} - \frac{A_2^{j'j''}}{\Delta_{1j'}^{hl}\Delta_{1j''}^{hh}} + \frac{A_3^{j'j''}}{\Delta_{1j'}^{hl}\Delta_{1j''}^{hh}}\right) \\
&= i\beta_{hh}E(k_x-ik_y)^3 \\
&= \left[i\beta_{hh}E(\sigma_+ k_-^3 + \sigma_- k_+^3)\right]_{v1,v4}
\end{aligned} \tag{A.66}$$

where $\sigma_\pm = 1/2(\sigma_x \pm i\sigma_y)$, $k_\pm = k_x \pm ik_y$ and

$$A_1^{j'j''} = \frac{3\hbar^4}{2m^2}\gamma_3(\gamma_2 + \gamma_3)\langle\langle h; 1|l; j'\rangle\rangle\langle\langle l; j'|z|l; j''\rangle\rangle\langle\langle l; j''|\partial_z|h; 1\rangle\rangle \qquad (A.67)$$

$$A_2^{j'j''} = \frac{3\hbar^4}{2m^2}\gamma_3(\gamma_2 + \gamma_3)\langle\langle h; 1|l; j'\rangle\rangle\langle\langle l; j'|\partial_z|h; j''\rangle\rangle\langle\langle h; j''|z|h; 1\rangle\rangle \qquad (A.68)$$

$$A_3^{j'j''} = \frac{3\hbar^4}{2m^2}\gamma_3(\gamma_2 + \gamma_3)\langle\langle h; 1|z|h; j'\rangle\rangle\langle\langle h; j'|l; j''\rangle\rangle\langle\langle l; j''|\partial_z|h; 1\rangle\rangle \ . \qquad (A.69)$$

Here h is $v1$ or $v4$, l is $v2$ or $v3$ in the double bracket. Due to the parity of the envelope functions, $A_1^{j'j''}$ and $A_2^{j'j''}$ are nonzero only for j'=odd and j''=even and $A_3^{j'j''}$ is nonzero only for j'=even and j''=even. The Rashba coefficient is

$$\beta_{hh} = e\sum_{j'j''}\left(\frac{A_1^{j'j''}}{\Delta_{1j'}^{hl}\Delta_{1j''}^{hl}} - \frac{A_2^{j'j''}}{\Delta_{1j'}^{hl}\Delta_{1j''}^{hh}} + \frac{A_3^{j'j''}}{\Delta_{1j'}^{hl}\Delta_{1j''}^{hh}}\right) \ . \qquad (A.70)$$

Therefore the Rashba SO interaction for the heavy hole subbands is

$$\widehat{H}_{hh}^R = i\beta_{hh}E(\sigma_+ k_-^3 + \sigma_- k_+^3) \ . \qquad (A.71)$$

Bibliography

[1] H. K. Onnes. *Comm. Phys. Lab. Univ. Leiden*, 120b, 122b, 124c, 1911.

[2] J. Bardeen, L. N. Cooper, and J. R. Schrieffer. *Phys. Rev.*, 108:1175, 1957.

[3] M. R. Norman. e-print cond-mat/0609559.

[4] P. A. Lee, N. Nagaosa, and X. -G. Wen. *Rev. Mod. Phys.*, 78:17, 2006.

[5] D. Fay and J. Appel. *Phys. Rev. B*, 22:3173, 1980.

[6] L. N. Cooper. *Phys. Rev.*, 104:1189, 1956.

[7] P. Fulde and R. A. Ferrell. *Phys. Rev.*, 135:A550, 1964.

[8] A. I. Larkin and Yu. N. Ovchinnikov. *Sov. Phys. JETP*, 20:762, 1965.

[9] H. A. Radovan, N. A. Fortune, T. P. Murphy, S. T. Hannahs, E. C. Palm, S. W. Tozer, and D. Hall. *Nature*, 425:51, 2003.

[10] K. Kakuyanagi, M. Saitoh, K. Kumagai, S. Takashima, M. Nohara, H. Takagi, and Y. Matsuda. *Phys. Rev. Lett.*, 94:047602, 2005.

[11] J. M. Blatt, K. W. Boer, and W. Brandt. *Phys. Rev.*, 126:1691, 1962.

[12] L. V. Keldysh and Y. V. Kopaev. *Sov. Phys. Solid State*, 6:2219, 1965.

[13] L. V. Keldysh and A. N. Kozlov. *Sov. Phys. JETP*, 27:521, 1968.

[14] A. N. Kozlov and L. A. Maksomov. *Sov. Phys. JETP*, 21:790, 1965.

[15] D. Jérome, T. M. Rice, and W. Kohn. *Phys. Rev.*, 158:462, 1967.

[16] Yu. E. Lozovik and V. I. Yudson. *JETP Lett.*, 22:271, 1975.

[17] S. I. Shevchenko, *Sov. J. Low Temp. Phys.*, 2:251, 1976.

[18] S. De Palo, F. Rapisarda, and G. Senatore. *Phys. Rev. Lett.*, 88:206401, 2002.

[19] L. V. Butov, A. L. Ivanov, A. Imamoglu, P. B. Littlewood, A. A. Shashkin, V. T. Dolgopolov, K. L. Campman, and A. C. Gossard. *Phys. Rev. Lett.*, 86:5608, 2001.

[20] A. V. Larinov, V. B. Timofeev, P. A. Ni, S. V. Dubonos, I. Hvam, and K. Soerensen. *JETP Lett.*, 75:570, 2002.

[21] L. V. Butov, C. W. Lai, A. L. Ivanov, A. C. Gossard, and D. S. Chemla. *Nature*, 417:47, 2002.

[22] L. V. Butov, A. C. Gossard, and D. S. Chemla. *Nature*, 418:751, 2002.

[23] D. Snoke, S. Denev, Y. Liu, L. Pfeiffer, and K. West. *Nature*, 418:754, 2002.

[24] D. Snoke. *Science*, 298:1368, 2002.

[25] J. Keeling, L. S. Levitov, and P. B. Littlewood. *Phys. Rev. Lett.*, 92:176402, 2004.

[26] J. P. Eisenstein, L. N. Pfeiffer, and K. W. West. *Appl. Phys. Lett.*, 57:2324, 1990.

[27] I. B. Spielman, J. P. Eisenstein, L. N. Pfeiffer, and K. W. West. *Phys. Rev. Lett.*, 84:5808, 2000.

[28] M. Kellogg, J. P. Eisenstein, L. N. Pfeiffer, and K. W. West. *Phys. Rev. Lett.*, 93:036801, 2004.

[29] J. P. Eisenstein and A. H. MacDonald. *Nature*, 432:691, 2004.

[30] B. A. Volkov, Yu. V. Kopaev, and A. I. Rusinov. *Sov. Phys. JETP*, 41:952, 1975.

[31] B. A. Volkov, A. I. Rusinov, and R. Kh. Timerov. *Sov. Phys. JETP*, 43:589, 1976.

[32] M. W. Zwierlein, J. R. Abo-Shaeer, A. Schirotzek, C.H. Schunck, and W. Ketterle. *Nature*, 435:1047, 2005.

[33] M. W. Zwierlein, A. Schirotzek, C. H. Schunck, and W. Ketterle. *Science*, 311:492, 2006.

[34] M. W. Zwierlein, C. H. Schunck, A. Schirotzek, and W. Ketterle. *nature*, 442:54, 2006.

[35] G. B. Partridge, W. Li, R. I. Kamar, Y. A. Liao, and R. G. Hulet. *Science*, 311:503, 2006.

[36] G. Sarma. *J. Phys. Chem. Solids*, 24:1029, 1963.

[37] D. E. Sheehy and L. Radzihovsky. *Phys. Rev. Lett.*, 96:060401, 2006.

[38] J. Kinnunen, L. M. Jensen, and P. Törmä. *Phys. Rev. Lett.*, 96:110403, 2006.

[39] F. Chevy. *Phys. Rev. Lett.*, 96:130401, 2006; e-print cond-mat/0605751.

[40] P. Pieri and G. C. Strinati. *Phys. Rev. Lett.*, 96:150404, 2006.

[41] W. Yi and L.-M. Duan. *Phys. Rev. A*, 73:031604(R), 2006.

[42] T. N. De Silva and E. J. Mueller. *Phys. Rev. A*, 73:051602(R), 2006; *Phys. Rev. Lett.*, 97:070402, 2006.

[43] M. Haque and H. T. C. Stoof. *Phys. Rev. A*, 74:011602, 2006.

[44] T.-L. Ho and H. Zai. e-print cond-mat/0602568.

[45] A. Imambekov, C. J. Bolech, M. Lukin, and E. Demler. e-print cond-mat/0604423.

[46] K. Machida, T. Mizushima, and M. Ichioka. *Phys. Rev. Lett.*, 97:120407, 2006.

[47] J.-P. Martikainen. *Phys. Rev. A*, 74:013602, 2006.

[48] C.-C. Chien, Q. Chen, Y. He, and K. Levin. *Phys. Rev. Lett.*, 97:090402, 2006; *Phys. Rev. A*, 74:021602(R), 2006.

[49] M. M. Parish, F. M. Marchetti, A. Lamacraft, and B. D. Simons. e-print cond-mat/0605744.

[50] A. Bulgac and M. McNeil Forbes. e-print cond-mat/0606043.

[51] K. B. Gubbels, M. W. J. Romans, and H. T. C. Stoof. e-print cond-mat/0606330.

[52] W. C. Stwalley. *Phys. Rev. Lett.*, 37:1628, 1976.

[53] E. Tiesinga, B. J. Verhaar, and H.T.C. Stoof. *Phys. Rev. A*, 47:4114, 1993.

[54] D. M. Eagles. *Phys. Rev.*, 186:456, 1969.

[55] A. J. Leggett. *J. Phys. (Paris), Colloq.*, 41:7, 1980.

[56] P. Nozières and S. Schmitt-Rink. *J. Low. Temp. Phys.*, 59:195, 1985.

[57] E. Burovski, N. Prokof'ev, B. Svistunov, and M. Troyer. *New J. Phys.*, 8:153, 2006.

[58] E. I. Rashba. *Sov. Phys. Solid State*, 2:1109, 1960.

[59] Yu. A. Bychkov and E. I. Rashba. *JETP Lett.*, 39:78, 1984.

[60] V. L. Ginzburg and L. D. Landau. *Zh. Eksperim. i. Teor. Fiz.*, 20:1064, 1950.

[61] L. P. Gorkov. *Sov. Phys. JETP*, 9:1364, 1959.

[62] J. R. Schrieffer. *Theory of Superconductivity*, Perseus, Oxford, 1999.

[63] P. G. de Gennes. *Superconductivity of Metals and Alloys*, Addison-Wesley, Reading, MA., 1992.

[64] M. Tinkham. *Introduction to Superconductivity*, 2nd ed., McGraw-Hill, New York, 1996.

[65] W. Meissner and R. Ochsenfeld. *Naturwissenschaften*, 21:787, 1933.

[66] F. London and H. London. *Proc. Roy. Soc. (London)*, A149:71, 1935.

[67] F. London. *Superfluids*, 2nd ed., Dover, New York, 1961.

[68] Y. Nambu. *Phys. Rev.*, 117:648, 1960.

[69] L. P. Gorkov. *Sov. Phys. JETP*, 7:505, 1958.

[70] B. S. Deaver and W. M. Fairbank. *Phys. Rev. Lett.*, 7:43, 1961.

[71] R. Doll and M. Näbauer. *Phys. Rev. Lett.*, 7:51, 1961.

[72] A. A. Abrikosov. *Sov. Phys. JETP*, 6:489, 1957.

[73] W. H. Kleiner, L. M. Roth, and S. H. Autler. *Phys. Rev.*, 133:A1226, 1964.

[74] J. Nitta, T. Akazaki, H. Takayanagi, and T. Enoki. *Phys. Rev. Lett.*, 78:1335, 1997.

[75] J. P. Lu, J. B. Yau, S. P. Shukla, M. Shayegan, L. Wissinger, U. Rössler, and R. Winkler. *Phys. Rev. Lett.*, 81:1282, 1998.

[76] T. Schäpers, G. Engels, J. Lange, T. Klocke, M. Hollfelder, and H. Lüth. *J. Appl. Phys.*, 83:4324, 1998.

[77] D. Grundler. *Phys. Rev. Lett.*, 84:6074, 2000.

[78] X. Zhu, P. B. Littlewood, M. S. Hybersten, and T. M. Rice. *Phys. Rev. Lett.*, 74:1633, 1995.

[79] D. P. Young, D. Hall, M. E. Torelli, Z. Fisk, J. L. Sarao, J. D. Thompson, H. -R. Ott, S. B. Oseroff, R. G. Goodrich, and R. Zysler. *Nature*, 397:412, 1999.

[80] L. Balents and C. M. Varma. *Phys. Rev. Lett.*, 84:1264, 2000.

[81] M. Y. Veillette and L. Balents. *Phys. Rev. B*, 65:014428, 2001.

[82] E. Bascones, A. A. Burkov, and A. H. MacDonald. *Phys. Rev. Lett.*, 89:086401, 2002.

[83] G. Senatore, S. Moroni, and D. Varsano. *Solid State Comm.*, 119:333, 2001.

[84] B. I. Halperin and T. M. Rice. *Solid State Phys.*, 21:115, 1968.

[85] P. -O. Löwdin. *J. Chem. Phys.*, 19:1396, 1951.

[86] P. -O. Löwdin. The Calculation of Upper and Lower Bounds of Energy Eigenvalues in Perturbation Theory by Means of Partitioning Techniques. In Calvin H. Wilcox, editor, *Perturbation Theory and its Applications in Quantum Mechanics*, Wiley, New York, 1966.

[87] R. Winkler, H. Noh, E. Tutuc, and M. Shayegan. *Phys. Rev. B*, 65:155303, 2002.

[88] D. L. Feder. *Phys. Rev. Lett.*, 93:200406, 2004.

[89] H. Shimahara and D. Rainer. *J. Phys. Soc. Jpn.*, 66:3591, 1997.

[90] U. Klein. *Phys. Rev. B*, 69:134518, 2004.

[91] K. Yang and A. H. MacDonald. *Phys. Rev. B*, 70:094512, 2004.

[92] Q. Cui, C.-R. Hu, J. Y. T. Wei, and K. Yang. *Phys. Rev. B*, 73:214514, 2006.

[93] A. M. Clogston. *Phys. Rev. Lett.*, 9:266, 1962.

[94] A. H. MacDonald, H. Akera, and M. R. Norman. *Phys. Rev. B*, 45:10147, 1992.

[95] H. T. C. Stoof, M. Bijlsma, and M. Houbiers. *J. Res. Natl. Inst. Stand. Technol.*, 101:443, 1996.

[96] H. Akera, A. H. MacDonald, S. M. Girvin, and M. R. Norman. *Phys. Rev. Lett.*, 67:2375, 1991.

[97] M. R. Norman, A. H. MacDonald, and H. Akera. *Phys. Rev. B*, 51:5927, 1995.

[98] L. P. Gorkov and T. K. Melik-Barkhudarov. *Sov. Phys. JETP*, 13:1018, 1961.

[99] M. Marinescu and L. You. *Phys. Rev. Lett.*, 81:4596, 1998.

[100] M. Baranov, L. Dobrek, K. Gorall, L. Santos, and M. Lewenstein. *Phys. Scr.*, T102:74, 2002.

[101] V. Schweikhard, I. Coddington, P. Engels, V. P. Mogendorff, and E. A. Cornell. *Phys. Rev. Lett.*, 92:040404, 2004.

[102] N. Regnault and T. Jolicoeur. *Phys. Rev. B*, 70:241307(R), 2004.

[103] J. M. Luttinger and W. Kohn. *Phys. Rev.*, 97:869, 1955.

[104] H. -R. Trebin, U. Rössler, and R. Ranvaud. *Phys. Rev. B*, 20:686, 1979.

Vita

Yun-Pil Shim was born in Chungju, Korea on November 25, 1973, the son of Seung Jin Shim and Yang Ja Lee. He received the degree of Bachelor of Science in Physics from Seoul National University in February 2000. He began his graduate studies at the University of Texas at Austin in September 2000.

Permanent Address: 12166 Metric Blvd. Apt. 221

Austin, TX 78758

This dissertation was typeset with LaTeX 2_ε[1] by the author.

---

[1] LaTeX 2_ε is an extension of LaTeX. LaTeX is a collection of macros for TeX. TeX is a trademark of the American Mathematical Society. The macros used in formatting this dissertation were written by Dinesh Das, Department of Computer Sciences, The University of Texas at Austin, and extended by Bert Kay, James A. Bednar, and Ayman El-Khashab.